OCS Study
MMS 2008-001

Coastal Marine Institute

Deepwater Currents in the Eastern Gulf of Mexico: Observations at 25.5ºN and 87ºW

U.S. Department of the Interior
Minerals Management Service
Gulf of Mexico OCS Region

Cooperative Agreement
Coastal Marine Institute
Louisiana State University

OCS Study
MMS 2008-001

Coastal Marine Institute

Deepwater Currents in the Eastern Gulf of Mexico: Observations at 25.5ºN and 87ºW

Authors

Masamichi Inoue
Susan E. Welsh
Lawrence J. Rouse, Jr.
Eddie Weeks

May 2008

Prepared under MMS Contract
1435-01-99-CA-30951-16805
by
Louisiana State University
Coastal Marine Institute
Baton Rouge, Louisiana 70803

Published by

U.S. Department of the Interior
Minerals Management Service
Gulf of Mexico OCS Region

Cooperative Agreement
Coastal Marine Institute
Louisiana State University

DISCLAIMER

This report was prepared under contract between the Minerals Management Service (MMS) and Louisiana State University. This report has been technically reviewed by the MMS and approved for publication. Approval does not signify that the contents necessarily reflect the view and policies of the Service nor does mention of trade names or commercial products constitute endorsement or recommendation for use. It is, however, exempt from review and compliance with MMS editorial standards.

REPORT AVAILABILITY

Extra copies of the report may be obtained from the Public Information Office (MS 5034) at the following address:

U.S. Department of the Interior
Minerals Management Service
Public Information Office (MS 5034)
Gulf of Mexico OCS Region
1201 Elmwood Park Boulevard
New Orleans, Louisiana 70123-2394

Telephone Number: (504) 736-2519
1-800-200-GULF

CITATION

Suggested citation:

Inoue, M., S.E. Welsh, L.J. Rouse, Jr., and E. Weeks. 2008. Deepwater currents in the Eastern Gulf of Mexico: Observations at 25.5°N and 87°W. U.S. Dept. of the Interior, Minerals Management Service, Gulf of Mexico OCS Region, New Orleans, LA. OCS Study MMS 2008-001. 95 pp.

ABSTRACT

The first observations of deepwater manifestation of the Loop Current and the Loop Current rings in the eastern Gulf of Mexico have been completed using a deepwater mooring deployed at 25.5^{o}N and 87^{o}W at a water depth of 3356 m in a flat bottom area away from the slope water region. This location turns out to be an ideal location to monitor the Loop Current and deepwater currents in the eastern gulf because of its proximity to the Loop Current. The mooring data suggest that a two-layer approximation is a reasonable way to characterize currents at the mooring site with the interface located near 700-800 m. The upper-layer currents are dominated by the Loop Current while generally the upper- and lower-layer currents appear to be decoupled except occasional establishments of coupling between the two layers. Deepwater in the eastern gulf is energetic and barotropic throughout the lower layer, and it appears to be driven by the Loop Current and Loop Current rings. Deepwater at the mooring site appears to be relatively energetic characterized by 40-50 day variability with 10-30 cm s^{-1} currents. Short-duration energetic events lasting a few days could result in strong deepwater currents exceeding 1 knot all the way to the bottom. These energetic events in deepwater appear to take place when the Loop Current makes notable northward extension preceding the formation of Loop Current rings. Deepwater currents at mooring site appear to be manifestations of a modon pair which forms underneath a Loop Current ring in the eastern Gulf of Mexico. Shorter time scales associated with deepwater flow at the mooring site is a reflection of smaller deepwater eddies resulting from deepwater eddies interacting with the bottom topographic constriction located between the eastern and the central gulf. So far every one of the three deployments turns out to be unique, confirming the previous observation that every Loop Current ring formation is unique and a long-term measurement is required in order to establish basic statistics of ocean dynamics in the eastern Gulf of Mexico.

TABLE OF CONTENTS

PAGE

CHAPTER

LIST OF FIGURES

LIST OF FIGURES
(continued)

LIST OF FIGURES
(continued)

LIST OF FIGURES
(continued)

LIST OF FIGURES
(continued)

LIST OF TABLES

ACKNOWLEDGMENTS

We would like to thank the Coastal Marine Institute at LSU that is funded by the Minerals Management Services and the Office of Research and Economic Development at LSU for providing the necessary funding for this project. We would like to acknowledge the essential role of the CSI Field Support Group in carrying out the field program for this project and the CSI faculty and staff in providing the necessary support for this project. We would like to thank the crew of Pelican and Longhorn in helping us service the mooring. Additional assistance in analyzing the data was provided by Dr. Dongho Park.

CHAPTER 1

INTRODUCTION

As the first attempt to observe deep water manifestation of the Loop Current (LC) and the Loop Current rings (or Loop Current Eddies, LCEs) in the Eastern Gulf of Mexico (GOM), a deepwater mooring was deployed at 25.5°N and 87°W at a water depth of 3356 m in a flat bottom area away from the slope water region in the eastern GOM (Figure 1-1). This particular location in the eastern GOM was selected because this is where the center of the LC tends to be found and all the LC rings appear to pass on their generally westward journey toward the western GOM (Figure 1-2) (Vukovich, 2007). It has been shown that the formation of a LC ring is preceded by significant northward extension of the LC in the eastern GOM (Leben, 2005). It is worth noting that because of the topographic steering exerted by the Campeche Bank on the LC high-speed jet located along the western wall of the LC (Oey et al., 2005), whenever any notable northward extension of the LC which would result in the formation of a LC ring takes place in the eastern GOM, the high-speed jet is expected to pass over the vicinity of the mooring site (Figure 1-3).

The mooring was equipped with two ADCPs, one upward-looking set at 140 m and the other downward-looking set at 3200 m, and six Aanderra current meters at 155, 750, 1500, 2500, 3000, and 3200 m in order to sample the entire water column. A two-year deployment (June 2000 – June 2002) of a deep-water mooring was successfully completed. The third-year deployment took place from April 2003 to June 2004.

1.1 Background

The surface waters of the GOM have been studied in great detail through many recent field programs funded by the Minerals Management Services (MMS) and others. The upper-layer circulation in the eastern GOM is dominated by the LC and the separation of anticyclonic eddies or LC rings. The LC rings migrate westward and dominate the circulation in the central and western GOM. The contribution of anticyclonic vorticity from rings is a major factor in the maintenance of a western boundary current as well as the existence of an eastward current that runs along the shelf break from the northwestern corner to the Mississippi River. Secondary circulation associated with rings, such as parasitic eddies and eddy pairs, can produce strong velocity shear and offshore transport of coastal water.

The GOM is a semi-enclosed basin with maximum depths of approximately 3400 m in the eastern basin and 3700 m in the western basin (Figure 1-1). The deep eastern basin is connected to the deeper western basin by a constriction located near 88°W. This bottom topographic constriction appears to limit exchange of deep water between the eastern and western basins (Welsh and Inoue, 2002; Weatherly et al., 2005). Flow enters the GOM from the Caribbean Sea through the Yucatan Channel with sill depths of approximately 1900 m and exits through the southern Strait of Florida with sill depths of about 800 m (Figure 1-3). Despite the isolation of deep water below the sill depths, deep water in the GOM appears to be well

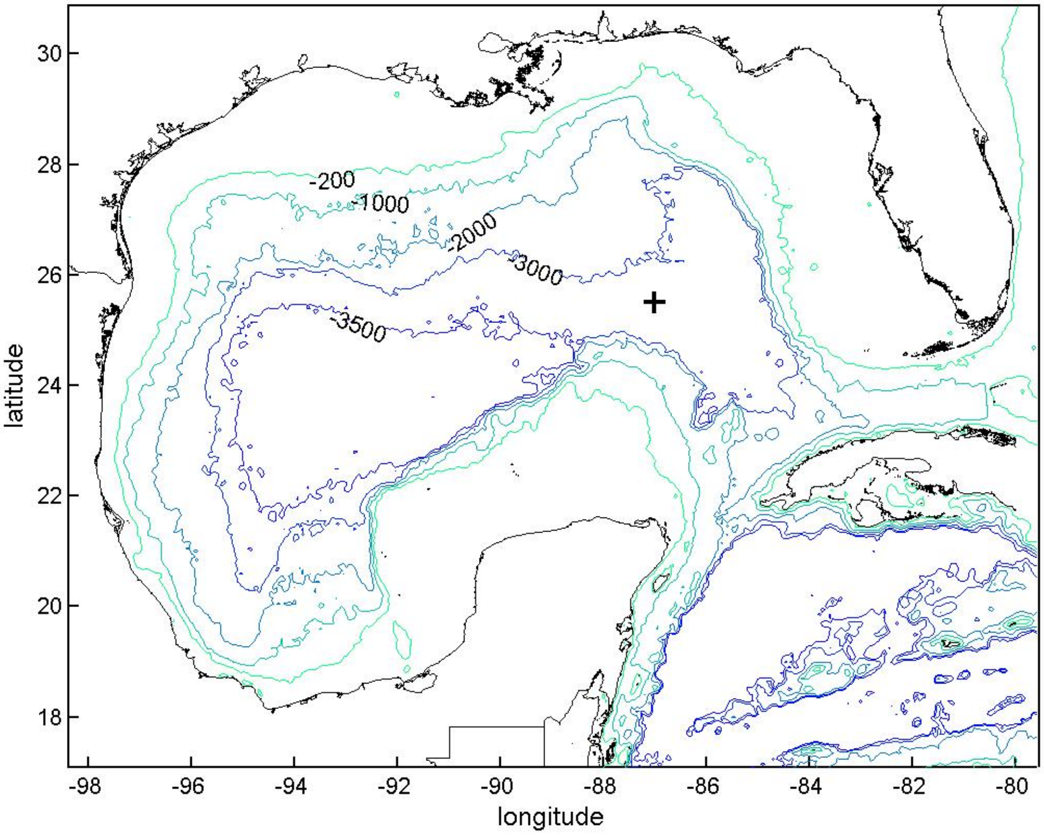

Figure 1-1. Bottom bathymetric contours (in meters) in the Gulf of Mexico. Our mooring site at 25.5°N and 87°W is indicated (+).

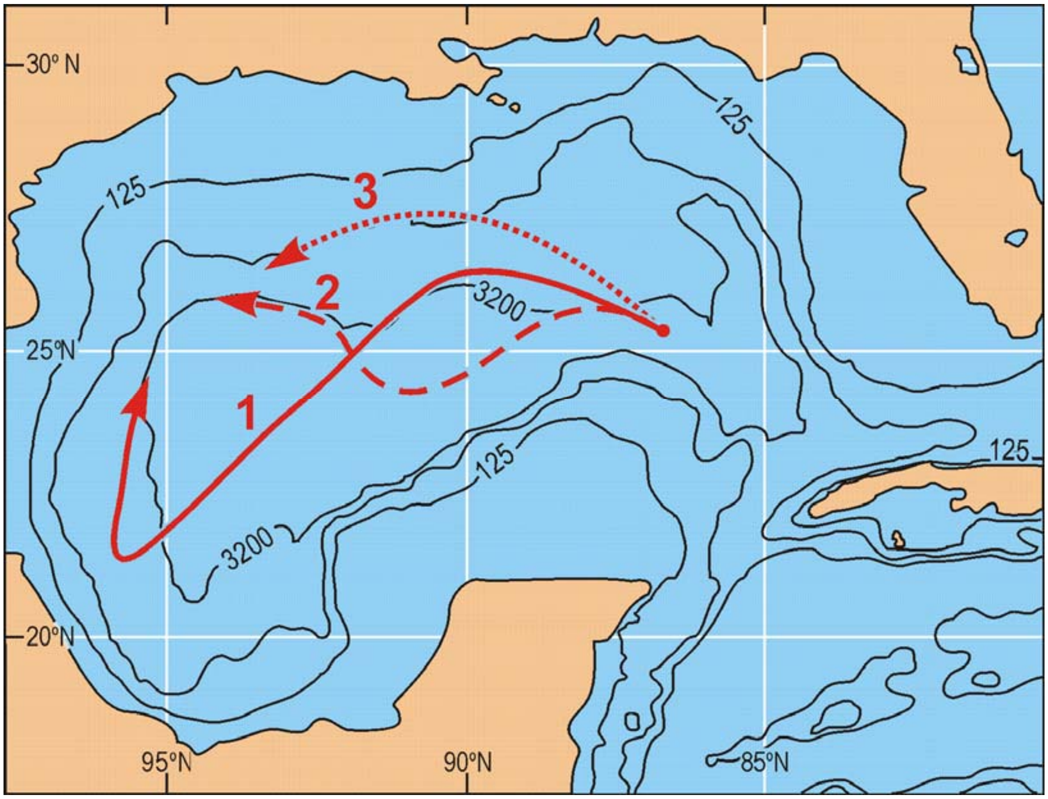

Figure 1-2. Three types of trajectories taken by the Loop Current Rings on their westward migration from the eastern GOM to western GOM identified in Vukovich and Crissman (1986) (Replotted from their Figure 7).

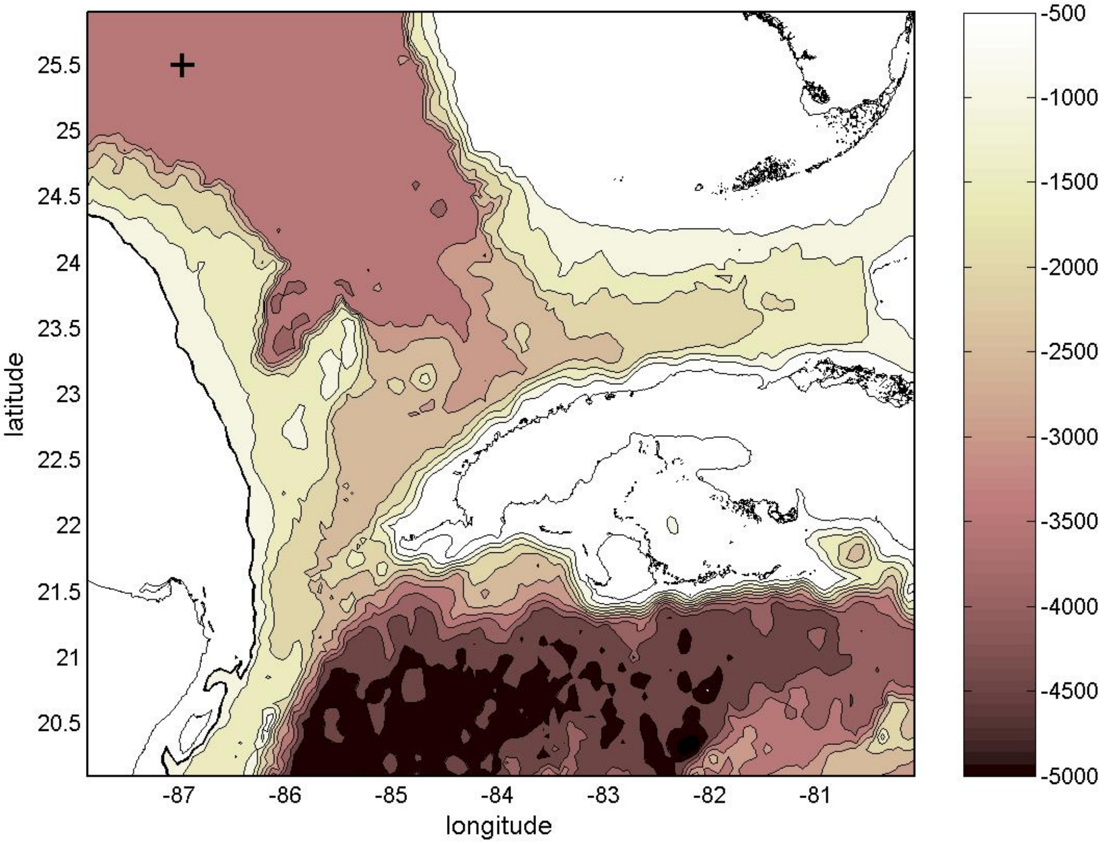

Figure 1-3. Detailed bottom bathymetric contours (in meters) in the eastern GOM. The mooring site is indicated (+).

ventilated and oxygenated. The residence time in the deep GOM is estimated to be only 100 years from both simple volume flux calculations and analysis of barium concentrations in the deep sea (Buerkert, 1997). This suggests some energy propagation from the upper layer to deep water inside the GOM contributing toward vertical mixing of deep water . Dominant energetic cyclones in deep water (e. g., Hurlburt and Thompson, 1982) and their interaction with bottom topography appear to play an important role in the ventilation of deep water. The deep GOM is also ecologically interesting. Along the continental slope there may be distinct habitats that are zoned according to depth and it is not understood what controls the diversity in the deep sea (Carney, 1996). Well-ventilated deep water in the GOM dictates that detailed knowledge about transport, mixing and ventilation processes in deep water is needed in order to assess what the environmental impacts of significant activities in deepwater exploration and production of oil and gas are going to be on the deep sea communities. Observations of energetic events with strong currents in the northern slope water region have been reported (Hamilton and Lugo-Fernandez, 2001; Hamilton, 2007). Their possible relationship to the LC and LC rings via topographic Rossby Waves (TRWs) have been suggested (Hamilton, 1990; Hamilton and Lugo-Fernandez, 2001; Oey and Lee, 2002; Hamilton, 2007).

Among the limited previous direct observations published on the deep currents in the GOM, the first extensive study was done by Hamilton (1990) using moored current meter data. Most of the current meters used by Hamilton were located over the continental slope at depths ranging from 1000 m to 3174 m in the far eastern, north central and western portions of the GOM. The deep currents were highly coherent in the vertical below 1000 m and appear to be excited by the ring separation process in the eastern GOM. The wave-like motions were observed to become progressively decoupled from the surface expression of the ring and were interpreted as TRWs (Hamilton, 1990; Hamilton and Lugo-Fernandez, 2001; Hamilton, 2007). However, all the current meter moorings used by Hamilton were located either over the continental slope or over the continental rise, where TRWs are to be expected (Oey and Lee, 2002).

The effects of the formation and migration of LC rings on the deep circulation in the GOM have been described by previous model studies (Hurlburt and Thompson, 1982; Sturges et al., 1993; Welsh, 1996; Welsh and Inoue, 2000). These models suggest: 1) an anticyclone-cyclone pair, which Hurlburt and Thompson (1982) refer to as a 'modon,' is generated in the lower layer during the formation of a LC ring in the upper-layer; 2) during westward migration, the axis of the modon is oriented close to the direction of propagation of the ring with the anticyclone leading; and 3) the westward propagation speed of the modon is slightly faster than the ring. The formation of an anticyclone-cyclone pair (modon) below the upper-layer anticyclone can be understood by the simple explanation presented by Cushman-Roisen et al. (1990) (Welsh and Inoue, 2000). When an anticyclone forms in the upper layer, there is a deepening of the interface between the upper and lower layers. The lower layer on the leading edge is compressed (higher potential vorticity) while the lower layer on the trailing edge is stretched (lower potential vorticity). A deep anticyclone forms under the ring, and a deep cyclone forms in the lower layer behind the eddy. Hurlburt and Thompson (1982) report that in the case with idealized bathymetry, the modon is confined to the abyssal plain and is steered by the bathymetry. Topographic steering of the deep eddy pair is also apparent in the models of

Sturges et al. (1993) and Welsh (1996). Therefore, the westward migration path of the ring in the upper layer is also affected by the bottom topography.

Sturges et al. (1993) and Welsh (1996) note that the deep motions are highly coherent in the vertical from between 1000 m and 1300 m to the bottom as reported by Hamilton (1990). The deep eddy pairs in the model do not decouple from the LC rings, but migrate westward in tandem. In both Sturges et al. (1993) and Welsh (1996), once the deep anticyclone-cycclone pair enters the central GOM, the trailing cyclone strengthens relative to the leading anticyclone and dominates the circulation in the deep western basin.

Since the previous observation of LC rings are usually confined to the upper-layer, there are no direct observations of the formation and migration of deep eddies in conjunction with LC rings. The only observation of a deep cyclone beneath a LC ring in the western GOM was made by Hoffman and Worley (1986) using indirect methods. They used an inverse technique to compute geostrophic currents from quasi-synoptic hydrographic data collected by the Hidalgo over the entire GOM. It is interesting to note the similarity of Hoffman and Worley's calculation of the geostrophic velocity of a ring and a cold-core eddy in the western GOM to the model results of Welsh (1996).

In addition to the dominance of the LC and LC rings in the upper-layer in the eastern GOM, another important feature is the inflow of colder and saltier deepwater from the Caribbean Sea through Yucatan Channel (McLellan and Nowlin, 1963; DeHaan and Sturges, 2005). Near the Yucatan Channel, the Caribbean is approximately 0.1^{o}C cooler and slightly saltier near the sill depth than the Gulf of Mexico. The inflowing colder and saltier water from the Caribbean tends to hug the right-hand slope in the eastern gulf, and gives rise to a counterclockwise circulation near the bottom of the slope water in the Gulf of Mexico (DeHaan and Sturges, 2005). This counterclockwise deepwater circulation has been delineated in the historical hydrographic data (DeHaan and Sturges, 2005) as well as in numerical models of GOM (e. g., Welsh and Inoue, 2002). Due to the inflowing colder and saltier Caribbean Deep Water, some mixing with ambient deep water in the eastern GOM is expected.

Topographic Rossby waves over the northern continental slope water region have been noted in various numerical model studies as well as in observations (e. g., Hamilton, 1990; Hamilton and Lugo-Fernandez, 2001; Oey and Lee, 2002, Hamilton, 2007). These studies have suggested that interaction of the LC and the LC rings with bottom topography in the northern slope water region excites TRWs. However, no previous measurements of deepwater currents away from the slope water region in the eastern GOM had been collected. In order to fully understand deep-water dynamics and circulation in the central and western GOM, knowledge of the upstream condition, i. e., the LC and deepwater beneath the LC in the eastern GOM away from the northern slope water region, is required.

The objective of this proposed study is to observe the upstream condition near 87^{o}W and 25.5^{o}N at a water depth of 3356 m in the eastern GOM, i. e., currents and water mass properties in the eastern GOM below the LC in a flat bottom area away from the slope water region. The selected site corresponds to the origination point where all of the three major trajectories preferred by the LC rings on their westward journey from the eastern GOM to western GOM converge (Vukovich and Crissman, 1986; Vukovich, 2007). According to Figure 2 of Vukovich (2007), the water mass directly associated with the LC is expected to be found approximately 65% of the time at this mooring site. Furthermore, the western frontal boundary of the LC is expected to be in the vicinity of the mooring site when the LC makes its characteristic northward intrusion prior to the formation of a LC ring. Based on the 28-year monthly frontal analyses for the period 1976-2003, Vukovich (2007) estimated that about 80% of the time, the LC orientation angle is between north-south and north-northwest-south-southeast, resulting in the western frontal boundary of the LC being in the vicinity of the mooring site.

CHAPTER 2

MOORING DEPLOYMENT

2.1 Deployment

Under the initial funding, a total of three deployments were completed. Although the detailed configuration of the mooring did differ from deployment to deployment, the basic configuration remained intact throughout the first three deployments. The mooring was equipped with two ADCPs, one upward-looking set at 140 m and the other downward-looking set at 3200 m, and six Aanderaa current meters set at 155, 750, 1500, 2500, 3000, and 3175 m in order to sample the entire water column. In Deployment 3, an additional Aanderaa current meter was used at 500 m. A total of five Microcats were used to sample temperature, conductivity and pressure. They were set at 157 m, 285 m, 752 m, 1502 m and 2502 m. The two ADCPs measured current velocity profiles at intervals of 8 m. The top ADCP was designed to measure near-surface currents while the bottom ADCP was intended to sample near-bottom currents. The mooring was designed for a bottom depth of 3340 m, and all the deployments were successful in locating the target site close to the design depth. Due to the relatively flat bottom in the vicinity of the target site, it was without much difficulty to set each deployment close to the target depth.

Deployment 1 extended from May 31, 2000 to August 1, 2001. Deployment 2 extended from August 3, 2001 to June 3, 2002. Deployment 3 extended from April 19, 2003 to June 1, 2004. Tables 2-1 through 2-3 show detailed information on the mooring configuration and deployment. Overall, nearly continuous two-year coverage encompassing Deployments 1 & 2, and nearly 14 month Deployment 3 have been accomplished. Overall data return was very good. However, a Microcat at the shallowest depth (either 155 m or 157 m) failed. In addition, a Microcat at 285 m in Deployment 2, and a Microcat at 302 m and an Aanderaa at 1500 m in Deployment 3 failed.

All raw data records were downloaded, and underwent quality control to flag bad and suspicious data values. Current meter records were corrected for declination, Earth's changing magnetic field, by correcting for a declination value at mid-way point during each deployment. For a typical one-year deployment, declination varied slowly and a constant declination correction is considered to be justifiable. Estimated value of magnetic declination was obtained from National Geophysical Data Center (http://www.ngdc.noaa.gov/seg/geomag/jsp/Declination.jsp). The estimated declination values for the three deployments were

Deployment 1:	-0.389 degree
Deployment 2:	-0.501 degree
Deployment 3:	-0.703 degree

The original current meter data were recorded at 60-minute intervals while Microcats recorded data at 30-minute intervals. The current velocity records were aligned along east-west (U-component) and north-south (V-component). Other than the instruments that failed, there were no data gaps for other instruments; therefore, no interpolation was necessary.

Table 2-1

Mooring Information during Deployment 1 Deployed at 25°30.456 N and 86°58.063 W

Instrument	Meter type & identification number	Design Depth (m)	Start	End	Duration (Days)	Data recovery rate
ADCP	300kHzADCP	150	5/31/00 18:00	8/1/01 23:00	427.2	100%
Aanderaa	RCM 7, 10191	155	5/31/00 18:00	8/1/01 21:49	427.2	100%
Microcat	SBE 37, 1113	157	No data	No data	0.0	0%
Microcat	SBE 37, 1333	285	5/31/00 17:00	7/14/01 21:00	234.9	55%
Aanderaa	RCM 7, 10193	750	5/31/00 18:00	8/1/01 22:01	427.2	100%
Microcat	SBE37, 1335	752	5/31/00 17:00	8/1/01 22:30	427.2	100%
Aanderaa	RCM 7, 11639	1500	5/31/00 18:00	8/1/01 21:49	427.2	100%
Microcat	SBE 37, 1336	1502	5/31/00 17:00	8/1/01 22:30	427.2	100%
Aanderaa	RCM 8, 12699	2500	5/31/00 18:00	8/1/01 22:00	427.2	100%
MicroCat	SBE 37, 1338	2502	5/31/00 17:00	8/1/01 23:00	427.3	100%
Aanderaa	RCM 8, 12700	3000	5/31/00 18:00	8/1/01 22:00	427.2	100%
Aanderaa	RCM 8, 12701	3175	5/31/00 18:00	8/1/01 22:01	427.2	100%
ADCP	300kHzADCP	3190	5/31/00 18:00	8/1/01 20:00	427.1	100%
Bottom		3340				

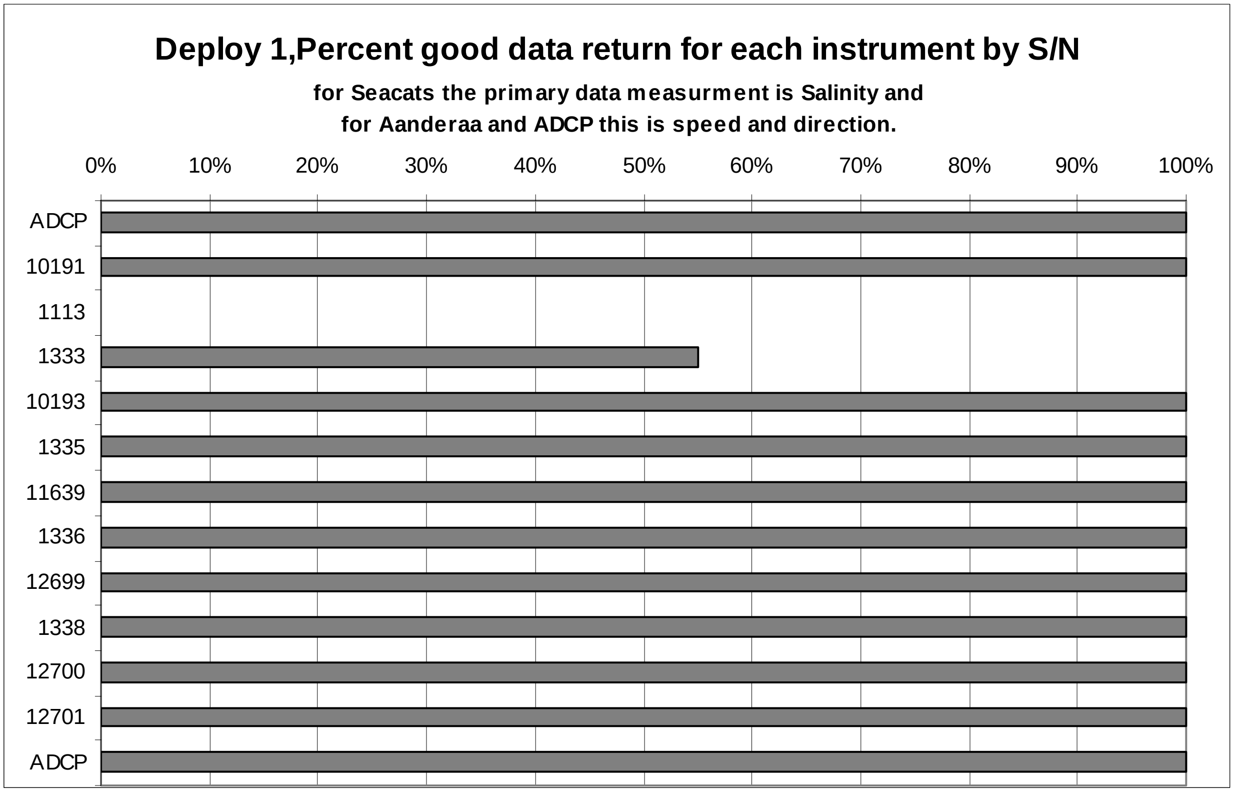

Table 2-2

Mooring Information during Deployment 2 Deployed at 25°30.626 N and 86°57.825 W

Instrument	Meter type &identification number	Design depth (m)	Start	End	Duration (Days)	Data recovery Rate
ADCP	300 kHzADCP	150	8/3/01 0:00	6/3/02 19:00	304.8	100%
Aanderaa	RCM 7, 10169	155	8/3/01 0:00	6/3/02 21:52	304.9	100%
Microcat	SBE 37, 1112	157	No data	No data	0.0	0%
Microcat	SBE 37, 1333	285	No data	No data	0.0	0%
Aanderaa	RCM 7, 11639	750	8/3/01 1:00	6/3/02 17:52	304.7	100%
Microcat	SBE 37, 1335	752	8/3/01 0:00	6/3/02 19:00	304.8	100%
Aanderaa	RCM 7, 10191	1500	8/3/01 1:00	6/3/02 17:52	304.7	100%
Microcat	SBE 37, 1336	1502	8/3/01 0:00	6/3/02 19:00	304.8	15%
Aanderaa	RCM 8, 12699	2500	8/3/01 1:00	6/3/02 18:00	304.7	100%
MicroCat	SBE 37, 1338	2502	8/3/01 0:00	6/3/02 19:00	304.8	100%
Aanderaa	RCM 8, 12700	3000	8/3/01 0:00	6/3/02 18:00	304.8	100%
Aanderaa	RCM 8, 12701	3175	8/3/01 1:00	6/3/02 18:01	304.7	100%
ADCP	300kHzADCP	3190	8/3/01 0:00	6/3/02 23:00	305.0	100%
Bottom		3340				

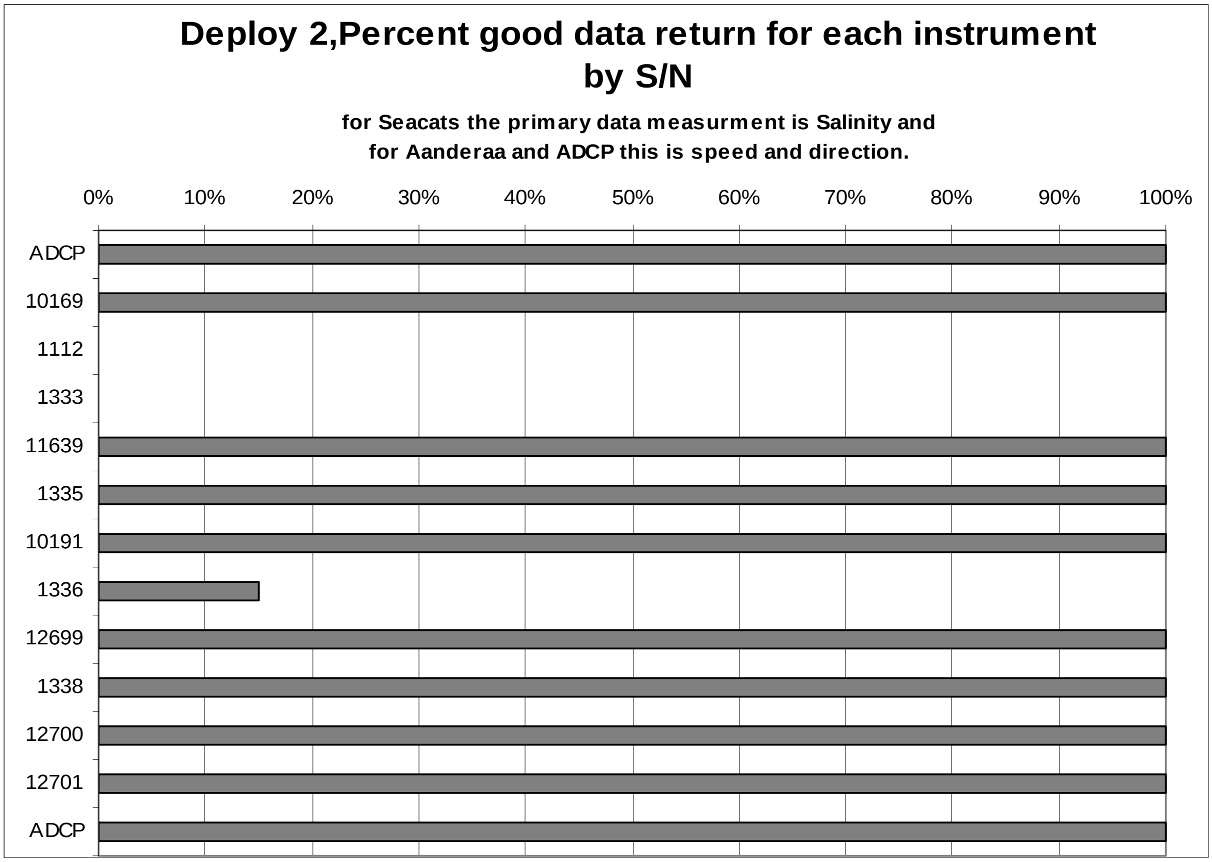

Table 2-3

Mooring Information during Deployment 3 Deployed at 25°31.017 N and 86°58.32 W

Instrument	Meter type & identification number	Design depth (m)	Start	End	Duration (Days)	Data recovery rate
ADCP	300kHzADCP	150	4/19/03 16:59	6/11/04 7:00	418.6	100%
Microcat	SBE 37, 1112	155	No data	No data	0.0	0%
Aanderaa	RCM7, 10196	300	4/19/03 16:00	6/11/04 13:59	418.9	100%
Microcat	SBE 37, 2452	302	no data	no data	0.0	0%
Aanderaa	RCM7, 11639	500	4/19/03 15:59	6/11/04 13:49	418.9	100%
Aanderaa	RCM7, 10191	750	4/19/03 15:59	6/11/04 13:49	418.9	100%
Microcat	SBE 37, 1335	752	4/19/03 16:00	6/11/04 15:00	419.0	100%
Aanderaa	RCM7, 10259	1500	no data	no data	0.0	0%
Microcat	SBE 37, 1336	1502	4/19/03 16:00	6/11/04 14:00	418.9	100%
Aanderaa	RCM8, 12699	2500	4/19/03 16:00	6/11/04 14:00	418.9	100%
MicroCat	SBE 37, 1338	2502	4/19/03 16:00	6/11/04 14:00	418.9	100%
Aanderaa	RCM8, 12700	3000	4/19/03 16:00	6/11/04 13:00	418.9	100%
Aanderaa	RCM8, 12701	3187	4/19/03 16:00	6/11/04 14:00	418.9	100%
ADCP	300kHzADCP	3190	4/19/03 16:00	6/11/04 14:00	418.9	100%
Bottom		3340				

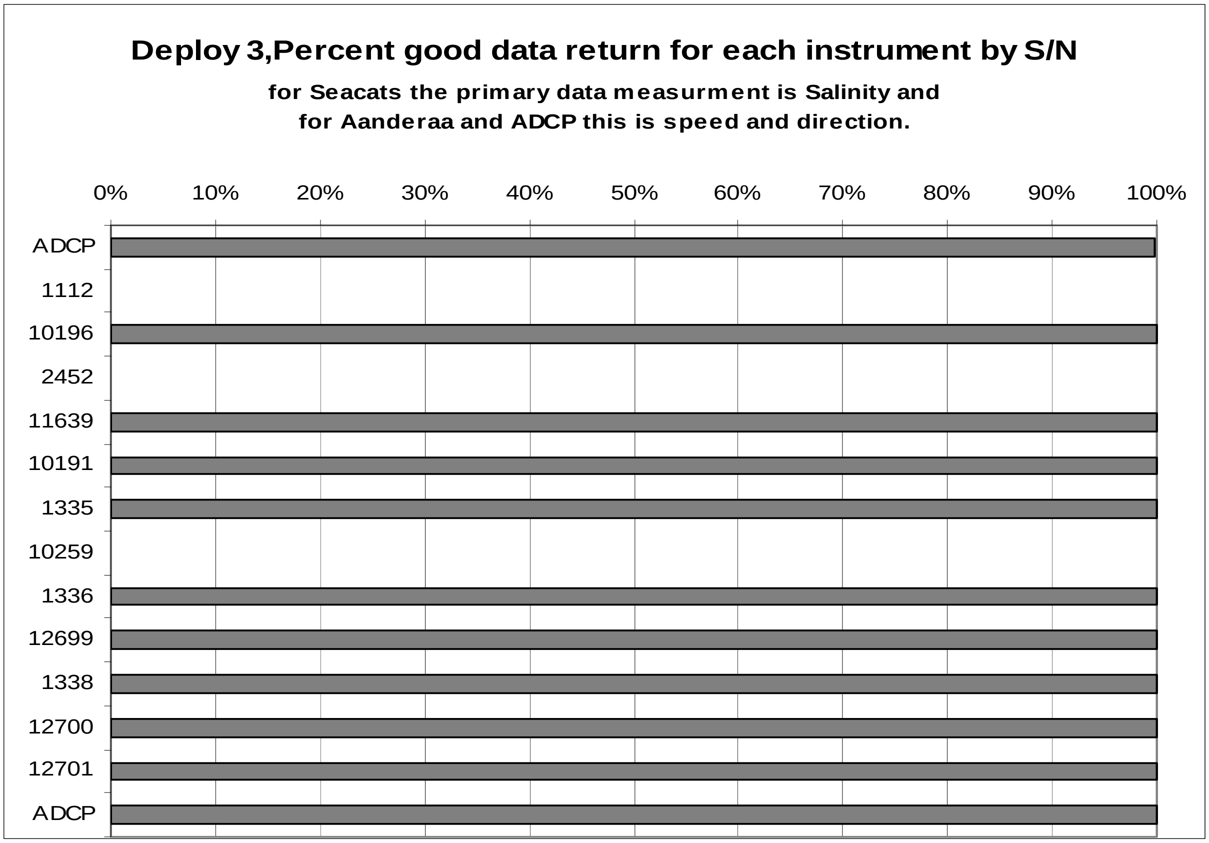

2.2 Basic Statistics

In order to examine low-frequency current variability that excludes dominant semi and diurnal tides and inertial oscillations, the original hourly sampled current meter data were low pass filtered with a 40-hour low-pass (40-HRLP) filter (specifically 6-th degree Butterworth filter). Statistics of currents during the three deployments for both raw hourly-sampled data and 40-HRLP are presented in Table 2-4.

Current vector plots of 40-HRLP current meter data are presented in Figures 2-1 through 2-3 for the three deployments. It is evident that currents in GOM can be approximated by a two-layer system with its interface located near 700~800 m. The upper-layer flow above the interface, which has a characteristic of surface-intensified flow pattern, is dominated by the LC and LC rings at the mooring site. The lower-layer flow, in general, does not appear to be related to the upper-layer flow. However, occasionally, coupling between the upper-layer flow and the lower-layer flow is established. A notable characteristic of the lower-layer currents is that unlike the surface-intensified upper-layer currents, they are nearly depth independent throughout the lower-layer, i. e., current magnitude and direction do not change with depth. Near the bottom (corresponding to the bottom half of the ADCP range), there appear to be frequent occurrences of high-frequency energetic currents. However, they appear to be instrumental noise perhaps due to the occurrences of lack of scattering layer near the bottom. Therefore, in the following discussion, these high-frequency variability near the bottom was not included. Additionally, the first couple of bins for the bottom ADCP consistently showed somewhat weaker currents, probably due to the expected low reliability of ADCP current measurements for the first few bins closest to the instrument.

Inspection of Figures 2-1 through 2-3 reveals that the upper-layer currents, represented by current measurements down to 700~750 m, and presumably driven by the LC and LC rings, behave differently than the lower-layer, represented by currents below 1500 m. Similar decoupling of intermediate depth circulation near 900 m from the surface circulation suggested by satellite altimeter data has been identified by Weatherly et al. (2005) at least in the central and western GOM using PALACE float data. This decoupling is confirmed in the eastern GOM at least at the mooring site. Currents at 700~750 m appears to be near the interface between the upper and lower layers. The interface near 700~750 m is presumably dictated by the shallower sill depths (800 m) in Florida Strait compared to the deeper sill depths of ~1900 m in Yucatan Channel, thus limiting the depth penetration of the LC that is continuous from the entrance (Yucatan Channel) to the exit (Florida strait) (e.g., Bunge et al., 2002).

Record-length statistics of current speed including mean, maximum and one standard deviation around the mean are graphically presented in Figures 2-4 through 2-6 for the three deployments. In all three deployments, the observed currents generally display vertical profile that can be approximated by a combination of the barotropic mode and the first baroclinic mode. It is interesting that the depth of the interface between the upper- and lower-layer appears to be close to the zero crossing of the first baroclinic mode estimated at the mooring site (Figure 2-7). The very strong near-surface currents were difficult to measure due to blow-over experienced by the top ADCP. The strongest currents measured by the top ADCP ranged from 119 cm s^{-1} in

Table 2-4

Basic statistics of observed currents for Deployments 1, 2, and 3. Depth refers to nominal design depth.

Deploy 1	Mean Raw			Maximum Raw			Standard Deviation Raw			Standard Deviation 40HLP			Ratio KE40: KEraw	Principal Axis Direction
Depth(m)	U	V	Speed	U	V	Speed	U	V	Speed	U	V	Speed	(%)	(True)
60	32.7	26.9	61.3	145.0	146.0	173.5	35.7	45.7	37.3	35.0	45.1	37.1	98	31
100	28.2	22.7	55.2	124.0	109.0	128.7	30.4	41.1	29.6	29.7	40.7	29.2	98	25
140	22.7	19.1	48.1	91.0	103.0	119.0	24.7	36.9	23.3	23.9	36.5	22.9	98	20
226	19.0	22.3	49.6	94.6	110.1	112.1	26.6	37.8	23.2	25.8	37.3	22.8	97	14
702	3.6	6.7	13.6	38.1	49.8	52.0	8.0	11.5	8.3	7.3	11.0	7.9	91	174
1487	0.6	3.0	10.0	35.6	36.0	38.0	8.9	8.7	8.1	8.8	8.5	7.8	96	132
2514	0.4	3.5	11.2	32.2	39.1	41.8	9.5	9.2	7.8	9.3	9.1	7.7	98	131
3025	0.3	3.9	11.1	31.4	43.2	44.4	9.2	8.9	7.5	9.1	8.8	7.4	97	130
3209	0.4	3.9	11.2	31.6	40.8	42.7	9.2	9.0	7.5	9.0	8.9	7.3	97	132
3238	0.8	3.1	10.8	31.1	37.5	42.5	8.8	8.9	7.1	8.6	8.7	7.0	96	140
3246	0.9	3.1	10.9	32.3	39.0	44.2	8.9	9.0	7.2	8.7	8.8	7.1	96	139
3254	0.9	3.1	11.0	32.0	38.5	44.2	8.9	9.0	7.2	8.8	8.8	7.1	95	139
3262	0.9	3.1	11.1	32.3	38.5	43.5	9.0	9.2	7.2	8.8	8.8	7.1	94	140
3270	0.8	3.2	11.3	34.0	39.9	44.6	9.1	9.3	7.2	8.8	8.8	7.1	92	140

Deploy 2	Mean Raw			Maximum Raw			Standard Deviation Raw			Standard Deviation 40HLP			Ratio KE40:	Principal Axis
Depth(m)	U	V	Speed	U	V	Speed	U	V	Speed	U	V	Speed	KEraw	
60	6.6	-5.4	38.0	108.8	118.6	119.7	28.5	33.7	24.0	27.6	33.1	24.2	95	163
100	6.3	-5.3	37.3	87.4	107.3	107.7	27.5	32.9	22.8	26.7	32.4	22.9	96	163
140	5.1	-5.5	34.5	75.8	90.8	100.7	25.3	30.7	21.1	24.5	30.1	21.2	96	163
702	0.6	1.1	11.7	35.3	40.5	41.5	9.1	11.0	8.2	8.5	10.6	7.9	90	162
2515	0.1	2.4	12.8	30.1	38.7	40.0	9.2	11.5	7.6	9.0	11.4	7.5	98	160
3026	-0.3	2.9	12.4	28.3	42.9	43.5	8.9	11.0	7.4	8.8	10.9	7.3	98	157
3209	-0.4	2.8	12.3	26.5	40.9	41.8	8.7	11.3	7.6	8.6	11.1	7.5	98	157
3232	-0.4	2.4	12.3	25.2	41.0	43.6	8.8	11.0	7.3	8.7	10.9	7.2	97	149
3240	-0.4	2.5	12.4	25.4	41.0	44.1	8.9	11.1	7.4	8.7	10.9	7.3	97	155
3248	-0.4	2.5	12.4	26.3	41.6	44.6	8.9	11.1	7.4	8.7	11.0	7.3	97	160
3256	-0.4	2.5	12.6	26.1	40.8	43.4	8.9	11.2	7.4	8.8	11.0	7.3	96	149
3264	-0.4	2.5	12.8	27.9	42.1	44.0	9.1	11.3	7.4	8.8	11.1	7.3	95	155

Deploy 3	Mean Raw			Maximum Raw			Standard Deviation Raw			Standard Deviation 40HLP			Ratio KE40:	Principal Axis
Depth(m)	U	V	Speed	U	V	Speed	U	V	Speed	U	V	Speed	KEraw	
60	12.9	8.1	36.5	127.9	144.5	154.9	31.3	34.9	33.1	29.8	31.7	30.1	88	165
100	13.0	15.4	42.3	101.7	119.6	123.8	28.4	34.4	24.7	27.8	33.9	24.4	97	163
140	11.5	14.4	38.1	79.9	101.5	109.7	25.1	30.6	21.3	24.4	30.1	21.0	96	164
300	7.4	10.8	27.0	58.3	68.1	81.0	17.8	22.4	16.1	17.2	22.0	15.8	96	165
500	4.1	8.0	22.3	68.5	61.0	80.1	15.4	18.4	12.6	14.8	17.9	12.2	95	174
750	2.2	6.4	16.7	40.5	49.6	52.8	12.2	14.3	11.0	11.7	13.8	10.4	94	175
2000	-0.7	3.4	17.1	34.6	50.8	50.8	13.5	12.8	8.1	13.3	12.7	7.9	98	63
3000	-0.9	4.5	17.4	36.9	51.6	51.7	13.5	12.8	8.1	13.4	12.7	7.9	98	61
3218	-0.8	4.2	17.1	36.4	48.5	48.5	13.3	12.7	7.9	13.1	12.6	7.7	98	59
3247	-0.5	2.5	15.6	40.0	53.7	54.9	12.2	12.1	7.6	12.0	11.9	7.5	97	47
3255	-0.6	2.6	16.4	41.0	54.6	55.8	13.1	12.2	7.7	13.0	12.0	7.6	97	67
3263	-0.6	2.6	16.5	40.4	53.7	55.1	13.3	12.3	7.7	13.1	12.1	7.6	97	68
3271	-0.6	2.6	16.6	42.0	54.1	55.1	13.3	12.3	7.8	13.1	12.1	7.6	97	67
3279	-0.6	2.6	16.8	42.5	54.4	55.3	13.4	12.5	7.8	13.2	12.2	7.6	96	66
3287	-0.6	2.6	17.0	45.5	54.4	56.4	13.5	12.7	7.9	13.2	12.3	7.6	95	64

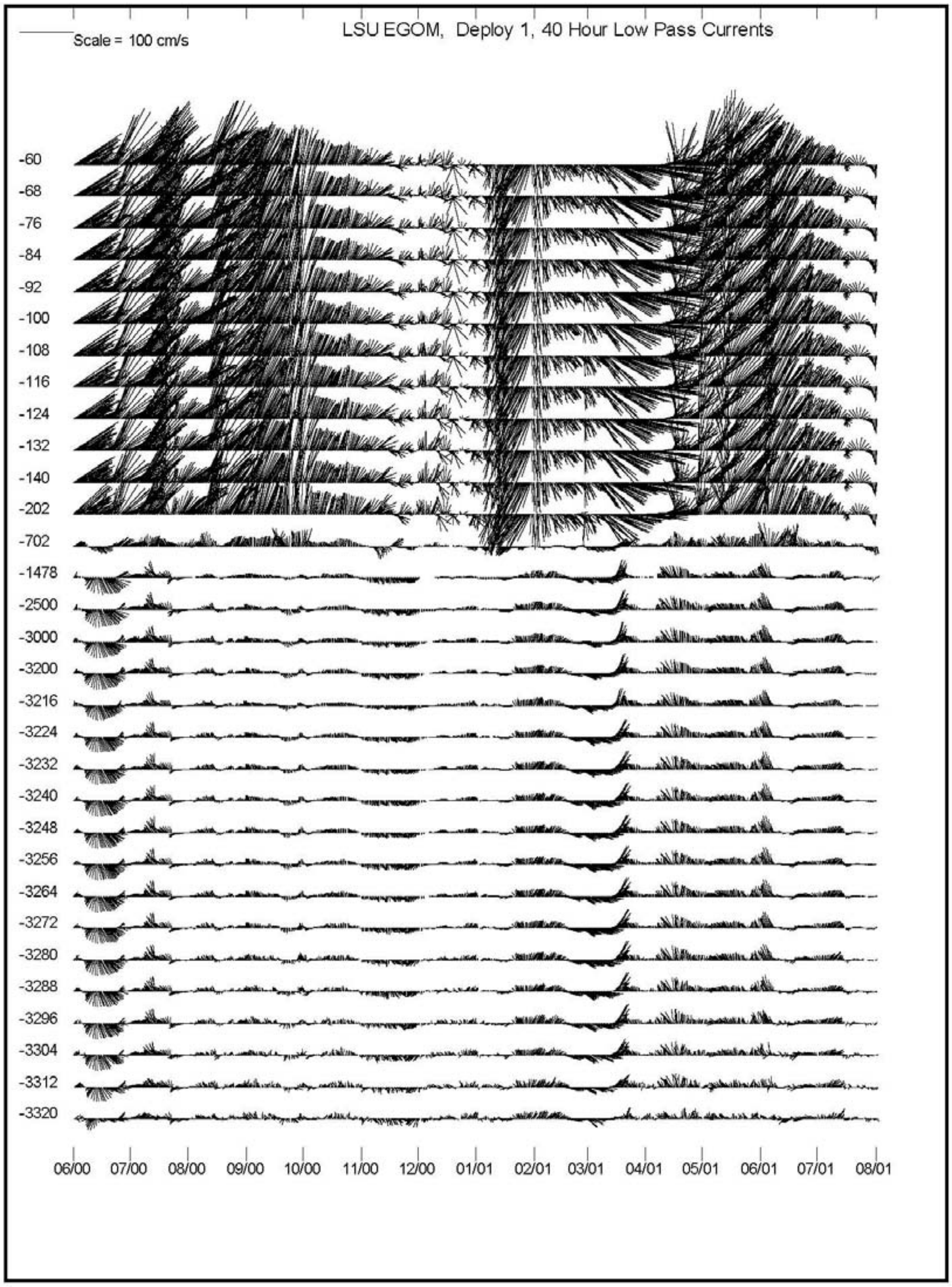

Figure 2-1. 40-HRLP current vectors during Deployment 1 for the indicated depths.

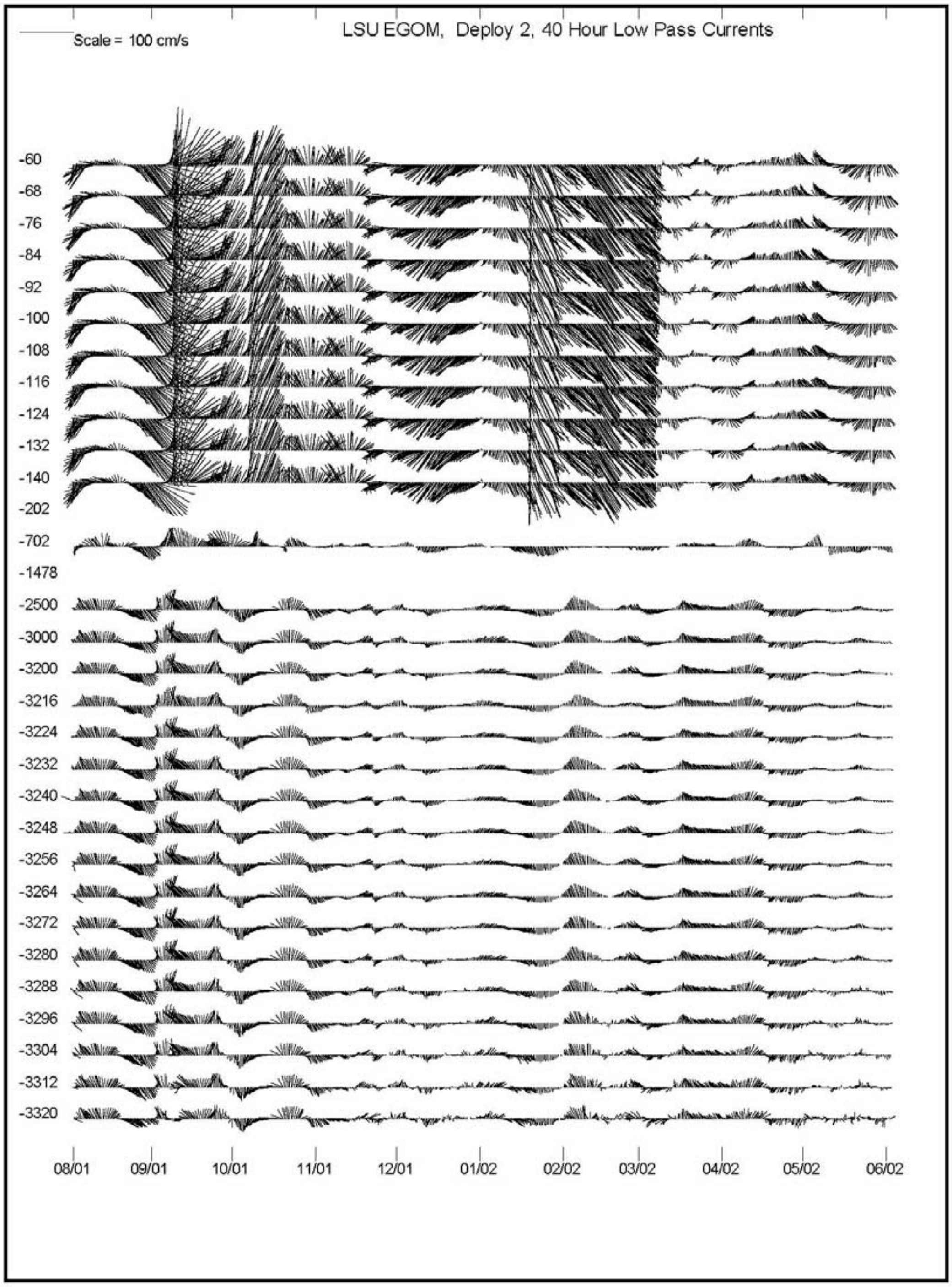

Figure 2-2. 40-HRLP current vectors during Deployment 2 for the indicated depths.

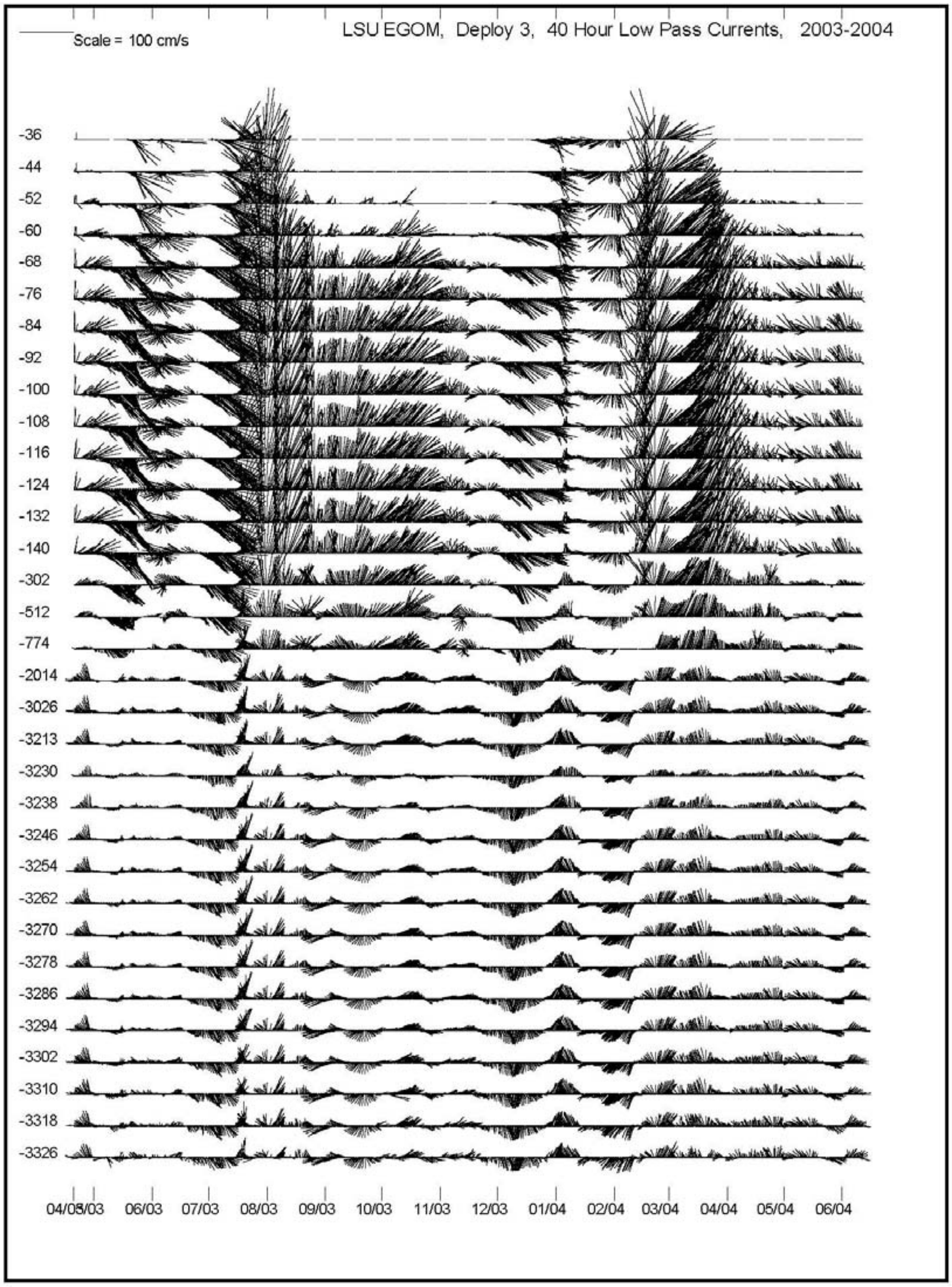

Figure 2-3. 40-HRLP current vectors during Deployment 3 for the indicated depths.

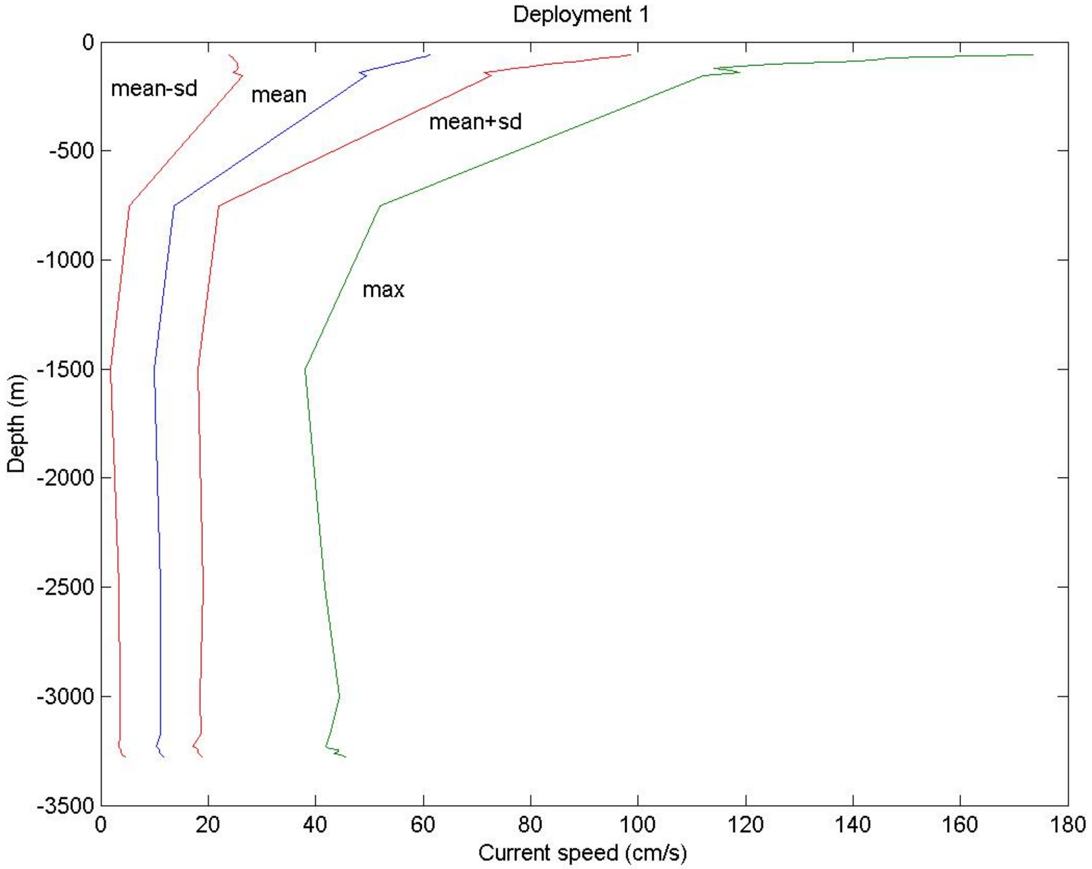

Figure 2-4. Record-length statistics (mean, maximum, 1 standard deviation around mean) of current speed during Deployment 1.

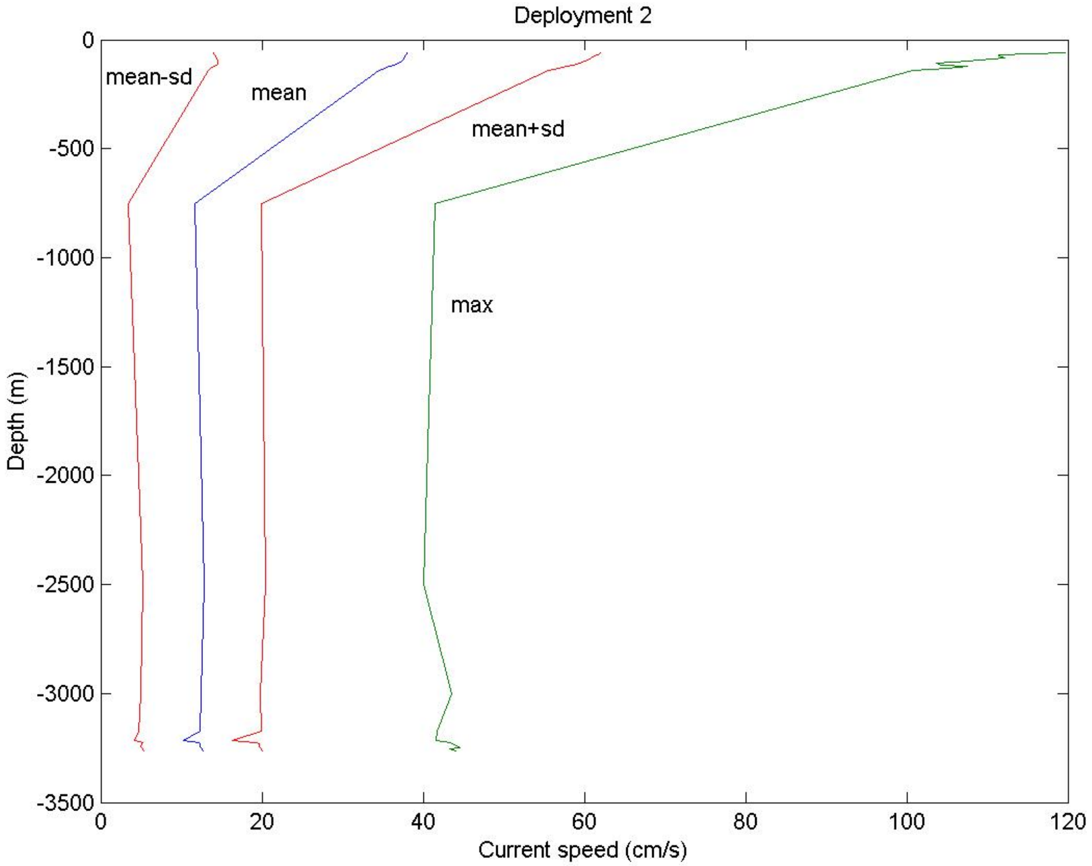

Figure 2-5. Record-length statistics (mean, maximum, 1 standard deviation around mean) of current speed during Deployment 2.

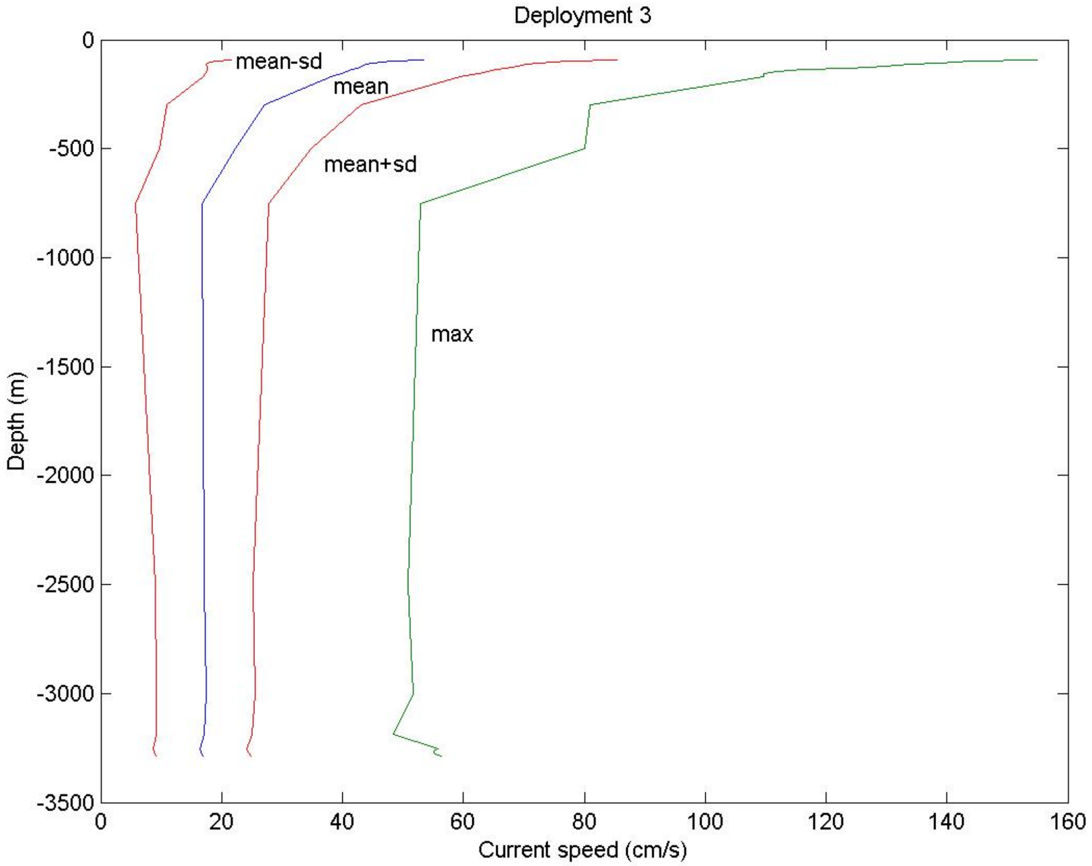

Figure 2-6. Record-length statistics (mean, maximum, 1 standard deviation around mean) of current speed during Deployment 3.

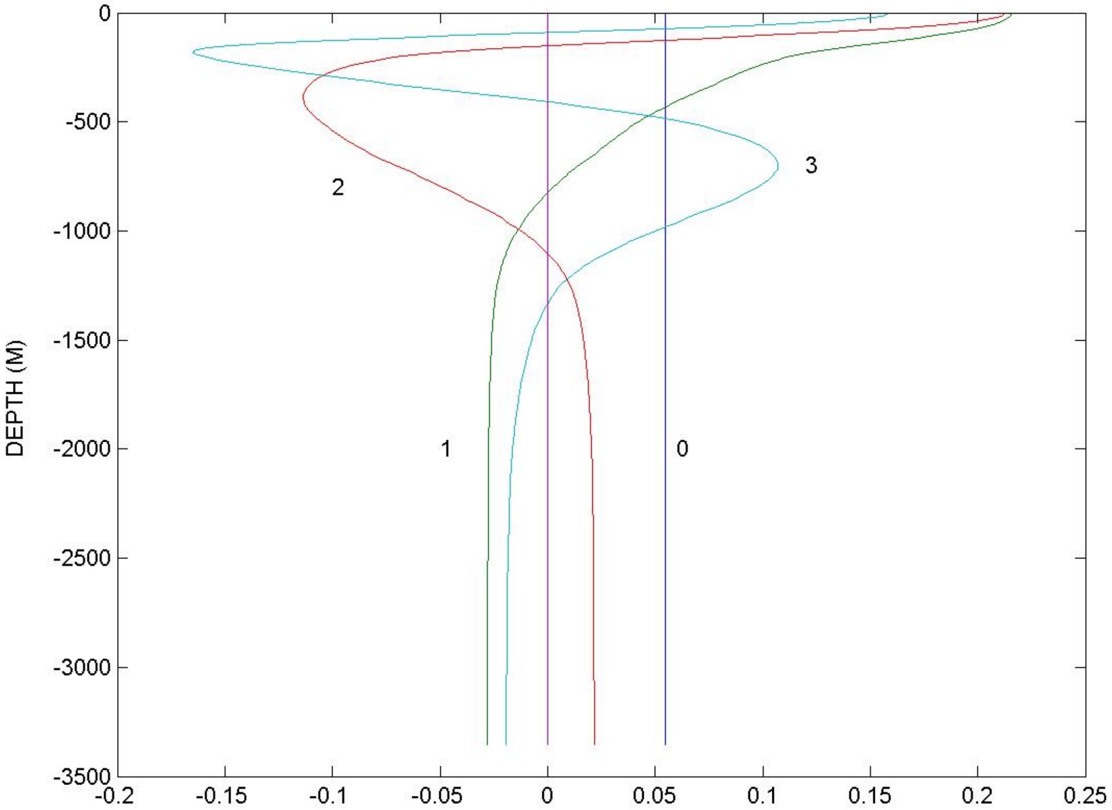

Figure 2-7. Vertical profiles of dynamic normal modes computed for the mooring site using mean temperature and salinity profiles sampled by CTD stations taken during deployments. Mode 0 is barotropic mode, Mode 1 refers to the first baroclinic mode, etc.

Deployment 2 to 173 cm s^{-1} in Deployment 1 at 60 m depth (Table 2-4). In contrast, in lower-layer maximum currents varied from 43~44 cm s^{-1} in Deployments 1 & 2 to 55 cm s^{-1} in Deployment 3. A notable characteristic of deepwater currents is that they are nearly depth independent throughout the lower-layer. Maximum mean near-surface currents ranged from 38 cm s^{-1} near 60 m in Deployment 2 to 61 cm s^{-1} in Deployments 1 (near 60 m). In the lower-layer, mean currents were 11~12 cm s^{-1} in Deployments 1 and 2 to 17 cm s^{-1} in Deployment 3. More energetic Deployment 3 compared to the first two deployments will be discussed in a later chapter. Standard deviation decreases from 37 cm s^{-1} near 60 m to 23 cm s^{-1} at 155 m, 8 cm s^{-1} at 750 m, and 7 cm s^{-1} in deepwater in Deployment 1; from 24 cm s^{-1} at 60 m to 21 cm s^{-1} at 140 m, 8 cm s^{-1} at 700 m and 7 cm s^{-1} in deepwater in Deployment 2; from 29 cm s^{-1} at 97 m, to 21 cm s^{-1} at 169 m, 11 cm s^{-1} at 792 m, and 7 cm s^{-1} in deepwater in Deployment 3.

The resulting mean velocity vectors and standard deviation ellipses from raw hourly sampled data and from 40-HRLP current data are presented in Figures 2-8 through 2-10 for each of the three deployments. Corresponding table is found in Table 2-4. In Figures 2-8 through 2-10, near-bottom currents are not shown because of unrealistically large variances recorded probably due to occasional lack of scattering layers near the bottom.

The upper-layer currents display strong directionality with its mean currents presumably pointing to the direction of the LC, northeasterly direction in Deployments 1 and 3, and southeasterly direction in deployment 2. The orientation of the major axis of ellipse generally aligns with the dominant direction of the currents. However, during Deployment 3, the major axis runs northwest-southeast direction while the mean currents point northeasterly direction. The upper-layer currents weaken rapidly below 200 m reflecting the surface-intensified character of the LC. In comparison to generally strong upper-layer currents, currents in the lower-layer are generally much weaker with weak mean currents pointing northward while current variability represented by standard deviation ellipses show more isotropic characteristics than the upper-layer counterparts. However, tendency toward more isotropic characteristic varies from deployment to deployment with Deployment 3 displaying the most while Deployment 2 showing the least. With its weaker mean currents and more isotropic current variability in the lower-layer suggest that it may be primarily driven by passage of eddy-like features rather than a steady current. Long-term mean current in the lower-layer is northerly in every deployment, suggesting general northward drift in the deepwater at the mooring site during each of the three deployments. In contrast, the upper-layer is clearly dominated by the LC and the LC rings, though position of the LC relative to the mooring site appears to vary from deployment to deployment. It is evident that during Deployments 1 and 3, high-speed jet which is generally found along the outer wall of the LC (Oey et al., 2005) was in the vicinity of the mooring compared to Deployment 2. It is notable that mean current vectors and size and shape of ellipses are not much different between raw data and 40-HRLP data, suggesting that the observed currents are dominated by low-frequency currents.

2.3 Spectra

Spectra of current components (north-south and east-west components) were calculated for raw hourly-sampled data in the upper-layer (represented at either 124 m or 126 m) and in the lower-layer near the bottom (represented at 3238 m in Deployment 1, 3232 m in Deployment 2,

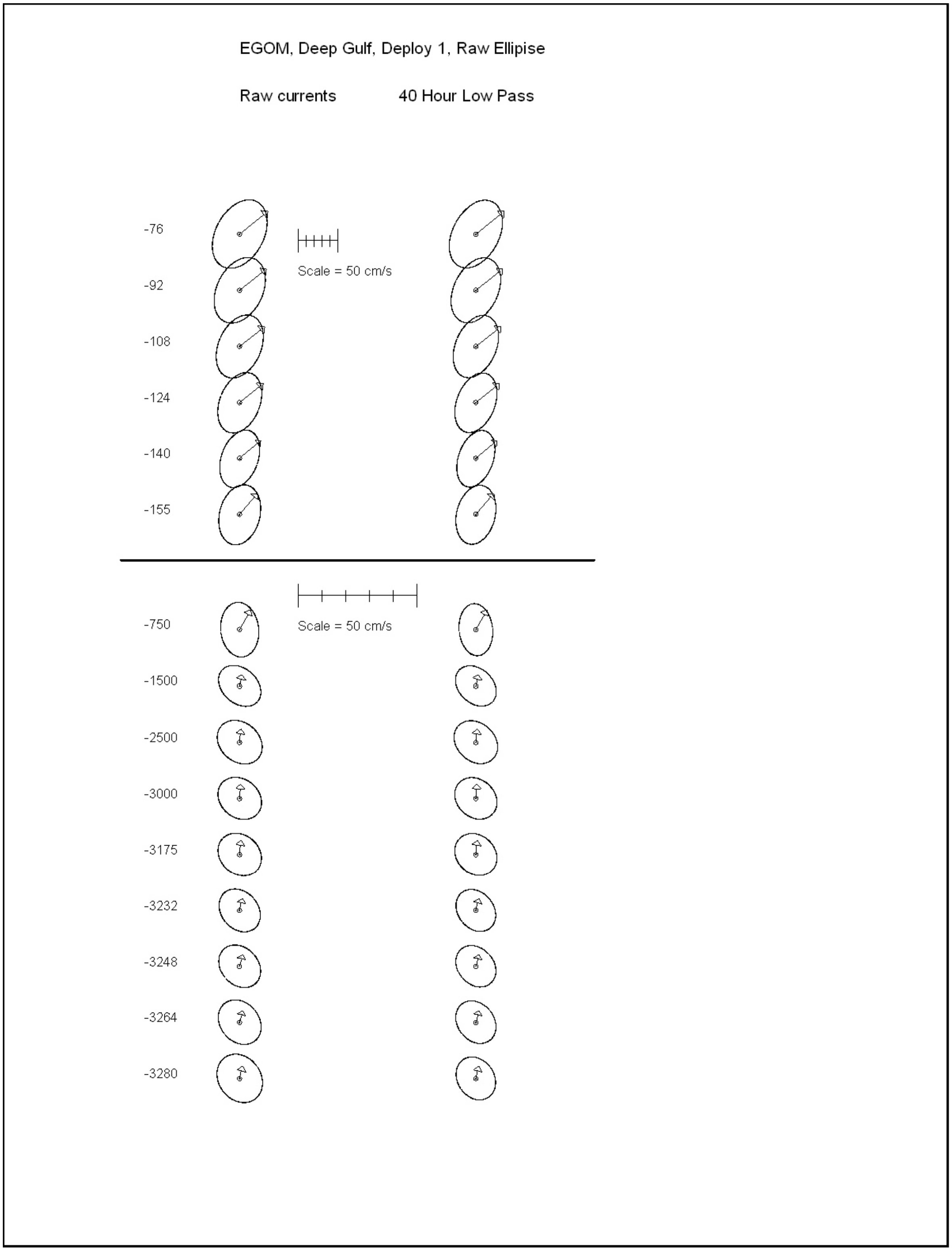

Figure 2-8. Standard deviation ellipses and mean velocity vectors from raw (hourly-sampled) and 40-HRLP current data for various depths during Deployment 1.

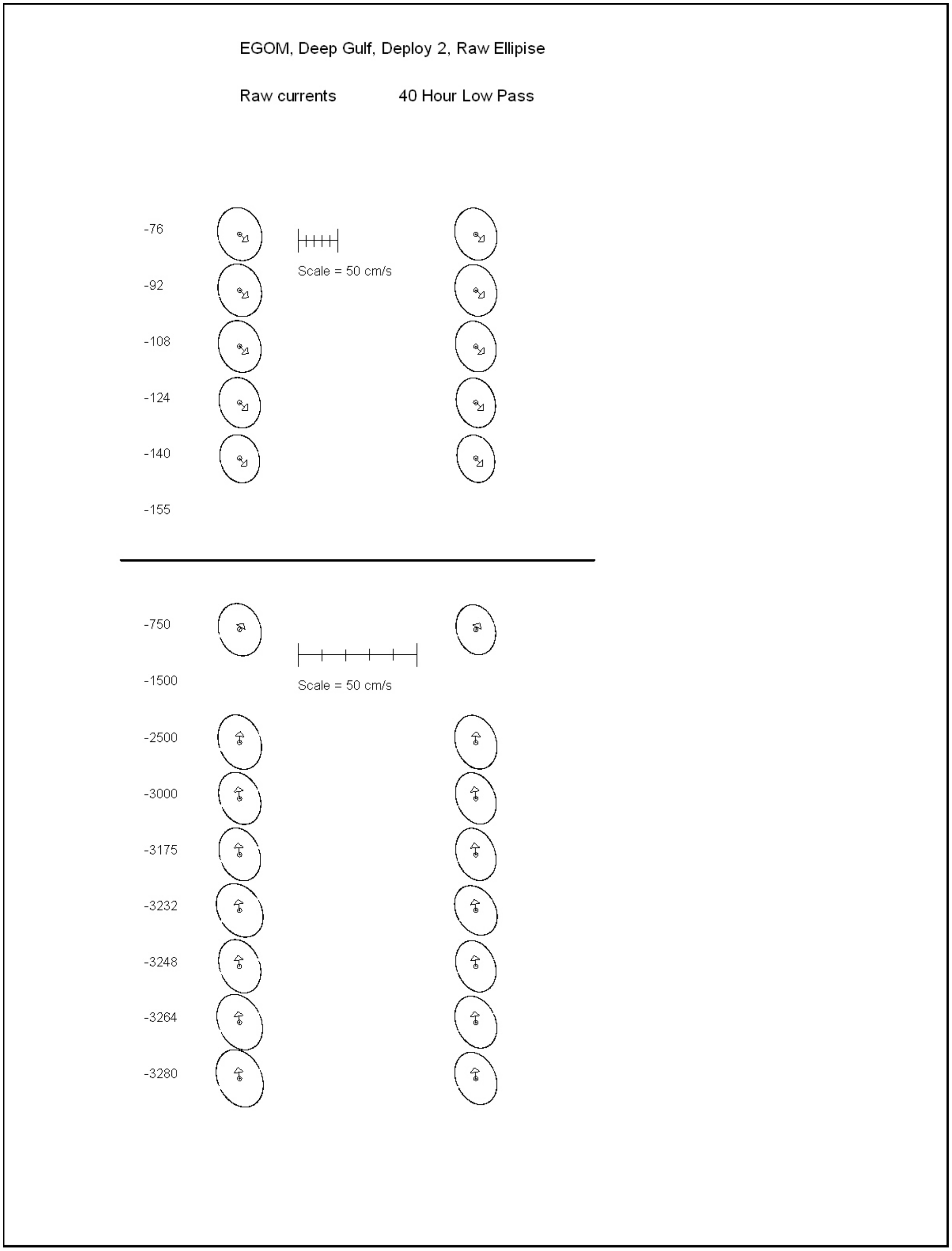

Figure 2-9. Standard deviation ellipses and mean velocity vectors from raw (hourly-sampled) and 40-HRLP current data for various depths during Deployment 2.

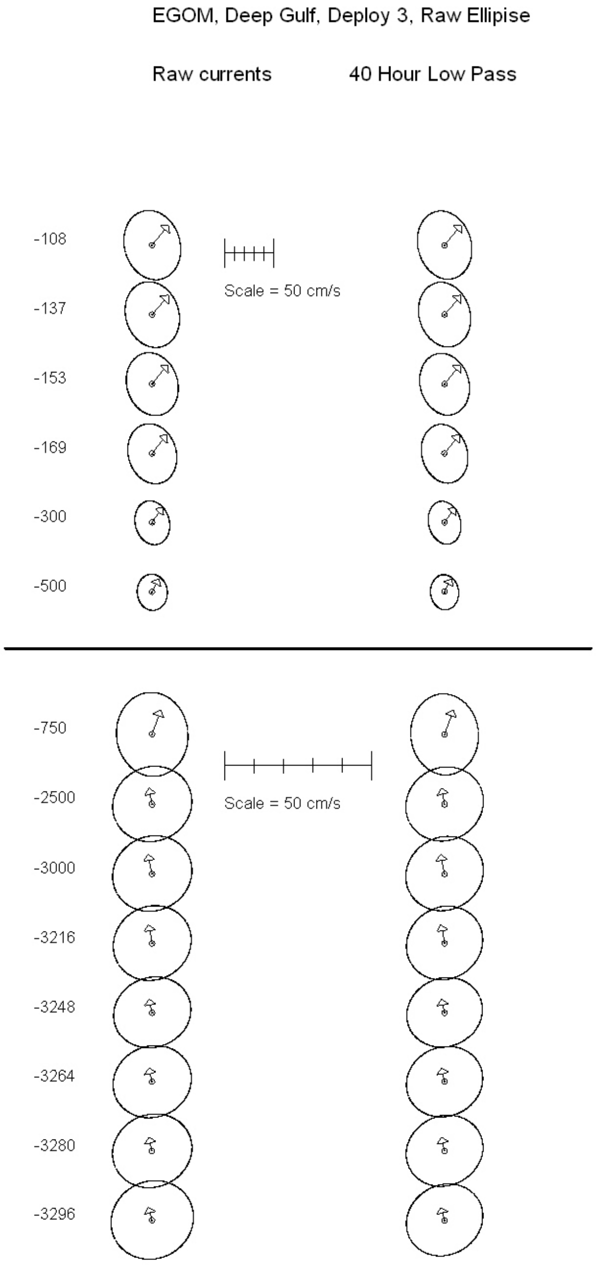

Figure 2-10. Standard deviation ellipses and mean velocity vectors from raw (hourly-sampled) and 40-HRLP current data for various depths during Deployment 3.

and 3248 m in Deployment 3) with additional intermediate depths included. Results are presented in Figures 2-11 through 2-13. Prominent peaks associated with diurnal tides and inertial oscillations (~27.8 hours) are evident throughout the water column. Peaks associated with semi-diurnal tides are more prominent in the lower-layer due to lower overall energy levels in deepwater. In general, periods longer than 50 days, the upper-layer seems to be much more energetic than the lower-layer. In contrast, for periods shorter than 50 days, energy level for the upper-layer and lower-layer gets much closer. For the upper-layer, Deployment 1 shows the most energetic peak near 120 days while it is near 80 days for Deployment 2 and 50 days for Deployment 3. At this most energetic peak, the upper-layer north-south component tends to be more energetic than the east-west component, particularly during Deployment 1. This peak represents high speed currents associated with the passage of the LC frontal jet, thus, representing migrations of LC in the eastern GOM that are often associated with the formations of LC rings (Leben, 2005). How quickly the low frequency spectral peak associated with the LC frontal jet fades with depth can not be addressed due to the paucity of current measurements near the interface between the two layers. However, it is evident that the low-frequency spectral peak diminishes with depth and the transition to lower-layer takes place around 700~750 m where it is least energetic corresponding to the interface between the upper-layer and the lower-layer. This can be seen in Figure 2-13. During Deployment 3, there was an additional current meter set at 500 m depth. The low frequency peak associated with the LC frontal jet is much weaker at 500 m compared to what was measured by the top ADCP. However, it still retains the low-frequency peak characteristics of the upper-layer while currents at 750 m have already transitioned into the lower-layer characteristics. The most energetic peak in the lower-layer corresponds to shorter time scale, ranging from 40 to 50 days. This peak represents eddy-like feature observed in deepwater at the mooring site. There appears to be a peak near 20-14 days in the upper-layer. It is interesting that although overall shape of spectra for the upper- and lower-layer remains more or less similar, details vary from deployment to deployment, suggesting that because of relatively long time scales associated with formation of LC rings in the eastern GOM, any one-year observation is not sufficiently long to capture basic statistics of flow field driven by the LC.

In order to examine relationships between upper-layer and lower-layer current components, coherence squared and phase were computed using the record-length raw current data. For the estimate of squared coherence, the data were averaged over 30 frequencies and two degrees of freedom was used. Records from Deployment 1 and 2 were merged to create a two-year record. Results are presented in Figures 2-14 and 2-15. Deployments 1 and 2 show significant coherence between upper and lower layers for periods ranging from 19 to 50 days for east-west component while north-south component shows coherence between 11 and 32 days. Deployment 3 shows significant coherence between upper-layer and lower-layer currents at periods between 11 and 30 days for north-south component only. Overall, upper-layer and lower-layer currents are said to be decoupled except for periods ranging from 11 to 30 days for north-south component while east-west component displays some coherence in the first two deployments but not during the last one. These observations are consistent with the idea that the upper-layer (probably top 700~750 m) currents are directly driven by the LC and LC rings while lower-layer currents are primarily driven by different mechanisms (Sturges et al., 1993; Welsh, 1996; Oey, 1996; Welsh and Inoue, 2000; Romanou and Chassignet, 2004; Cherubin et al., 2005; Oey et al., 2005).

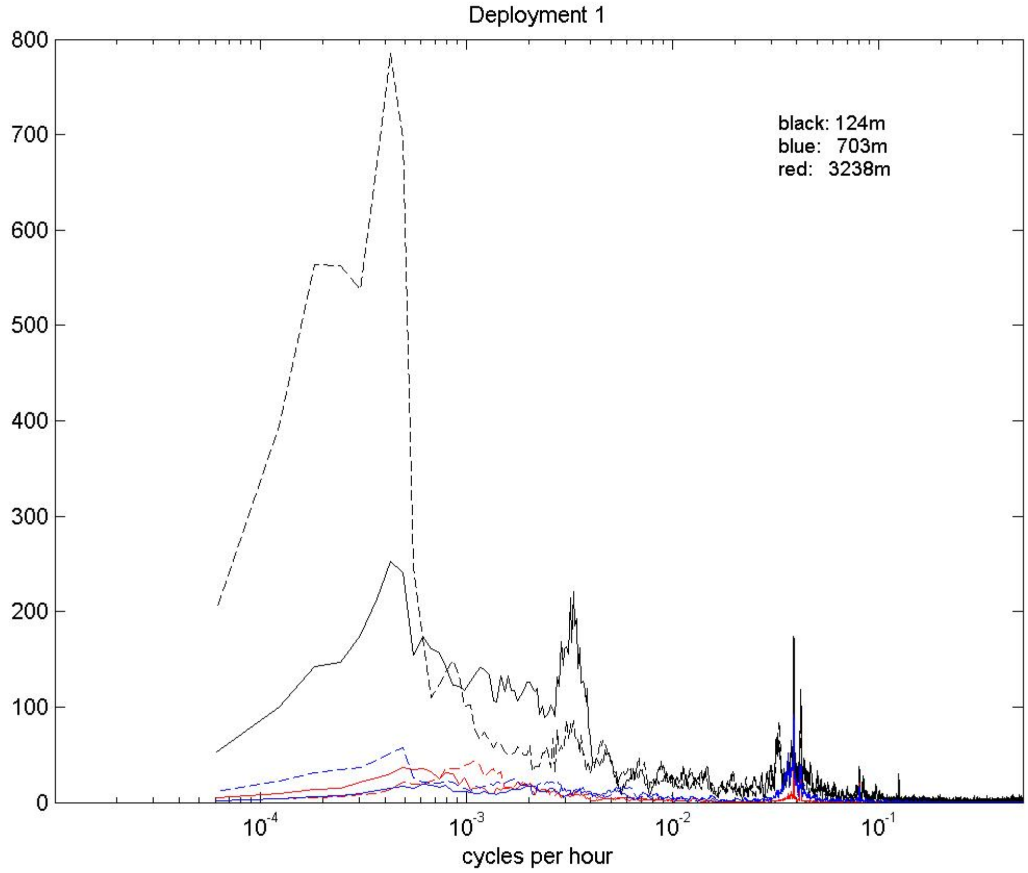

Figure 2-11. Current spectra in variance preserving form, for raw (hourly-sampled) current components (east-west component (solid line), north-south component (dotted line)) at 124 m, 703 m, and 3238 m during Deployment 1.

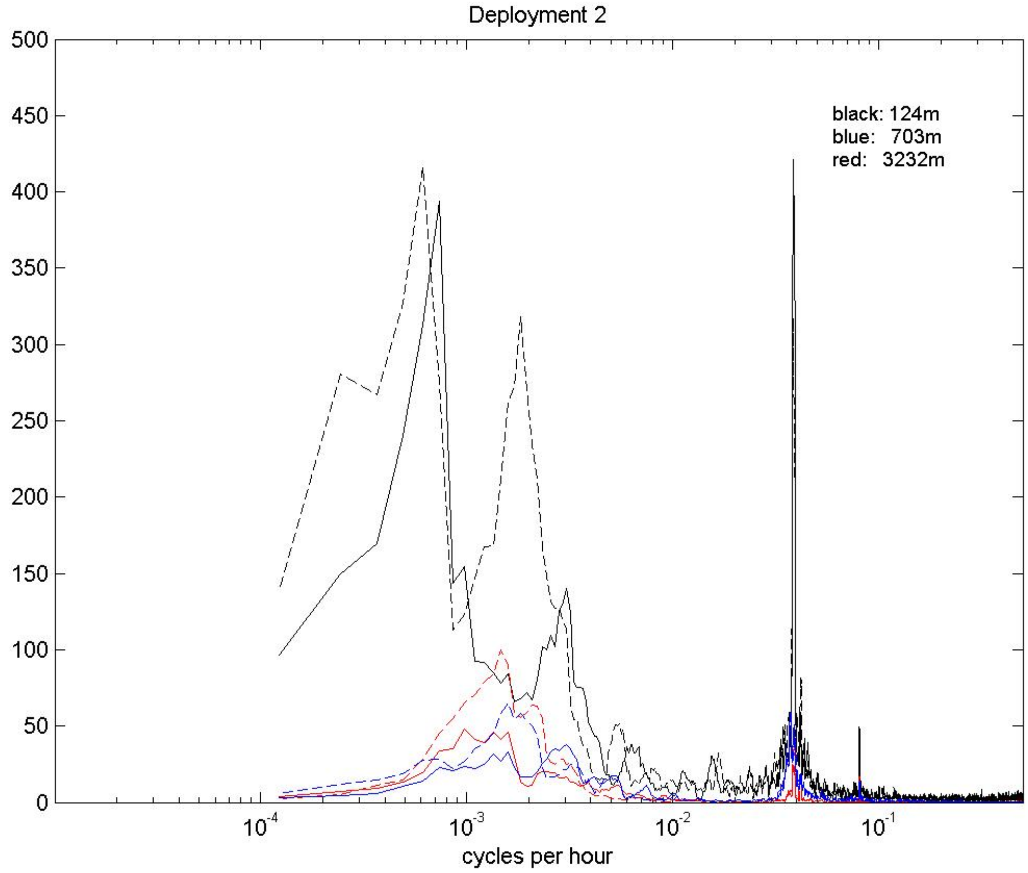

Figure 2-12. Current spectra in variance preserving form, for raw (hourly-sampled) current components (east-west component (solid line), north-south component (dotted line)) at 124 m, 703 m, and 3232 m during Deployment 2.

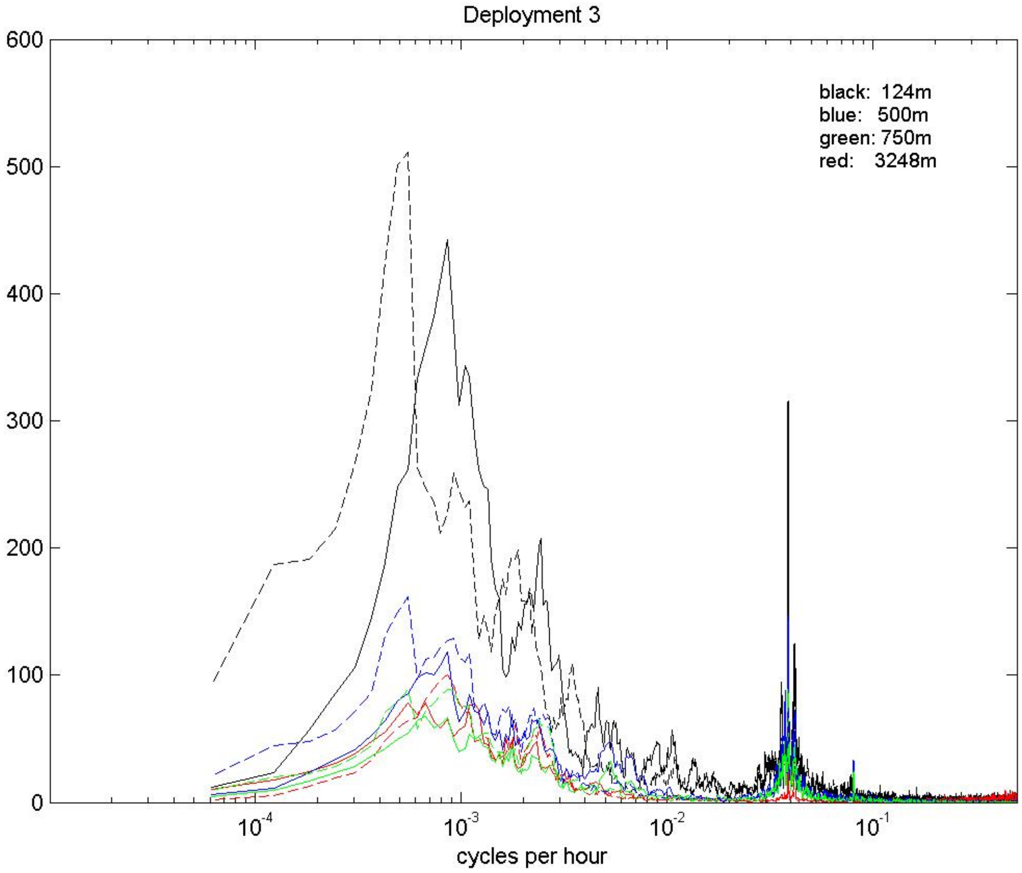

Figure 2-13. Current spectra in variance preserving form, for raw (hourly-sampled) current components (east-west component (solid line), north-south component (dotted line)) at 126 m, 500 m, 750 m, and 3248 m during Deployment 3.

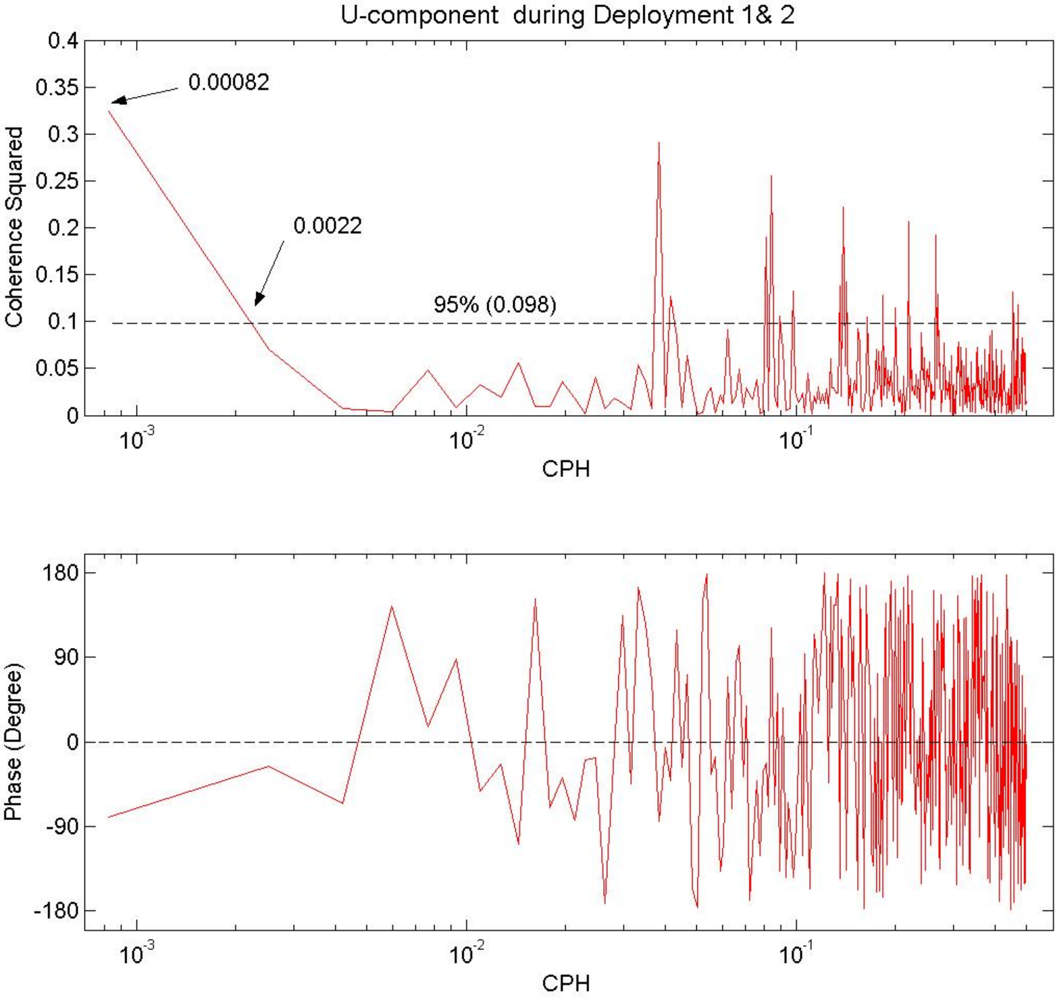

Figure 2-14. Coherence squared (top figure) and phase (bottom figure) between top (124 m) and bottom (3238 m in Deployment 1 and 3232 m in Deployment 2) U-component during Deployment 1 and 2.

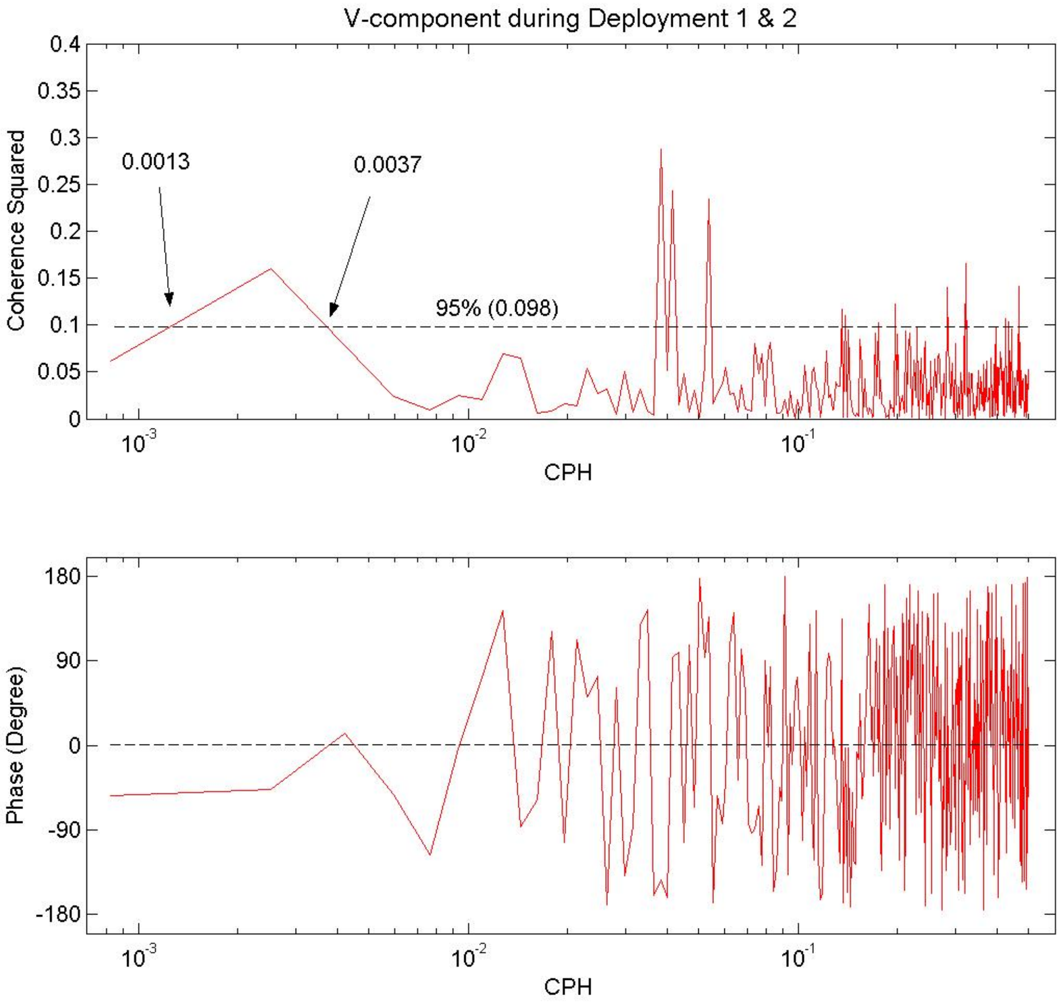

Figure 2-15. Coherence squared (top figure) and phase (bottom figure) between top (124 m) and bottom (3238 m in Deployment 1 and 3232 m in Deployment 2) V-component during Deployment 1 and 2.

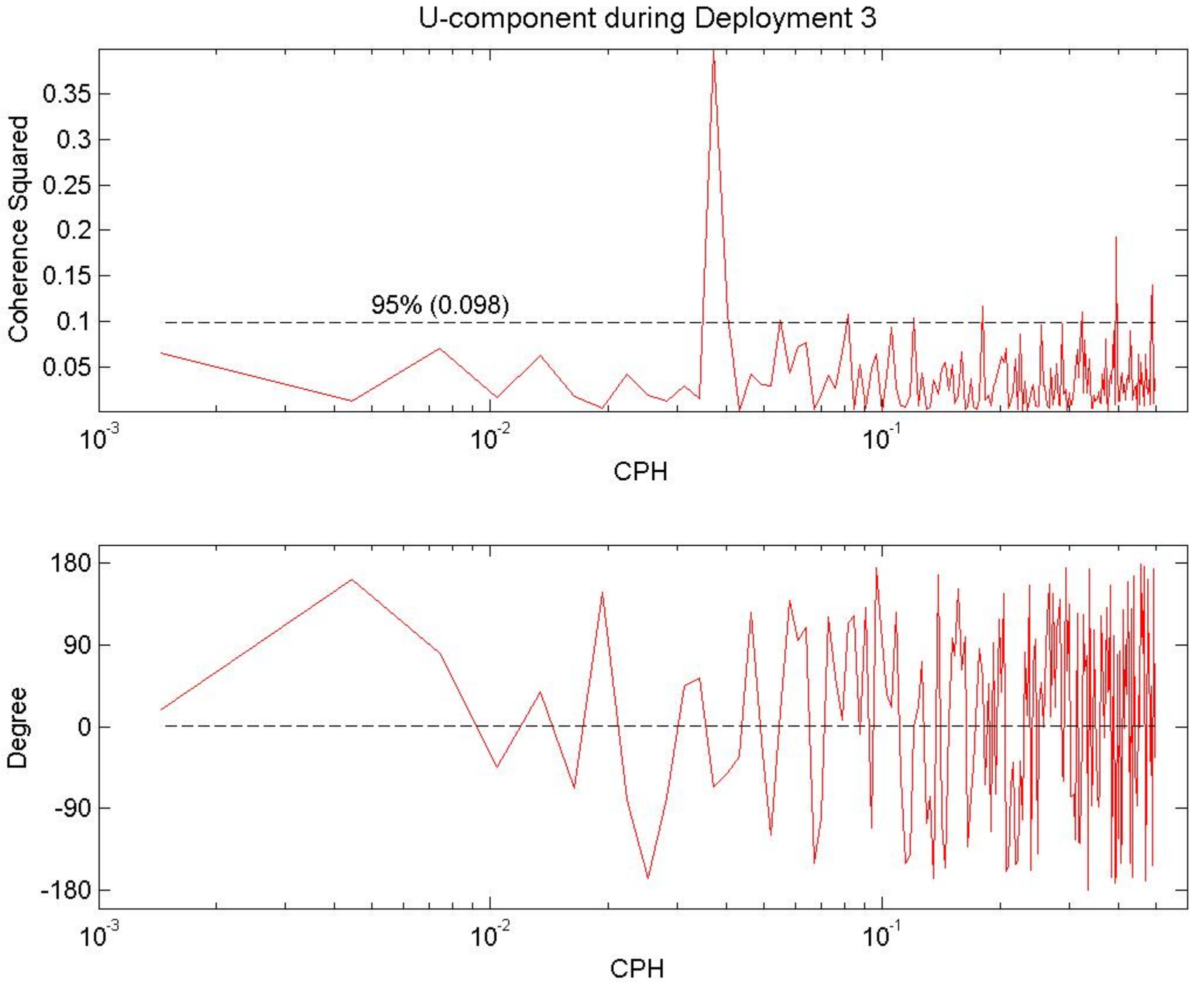

Figure 2-16. Coherence squared (top figure) and phase (bottom figure) between top (126 m) and bottom (3248 m) U-component during Deployment 3.

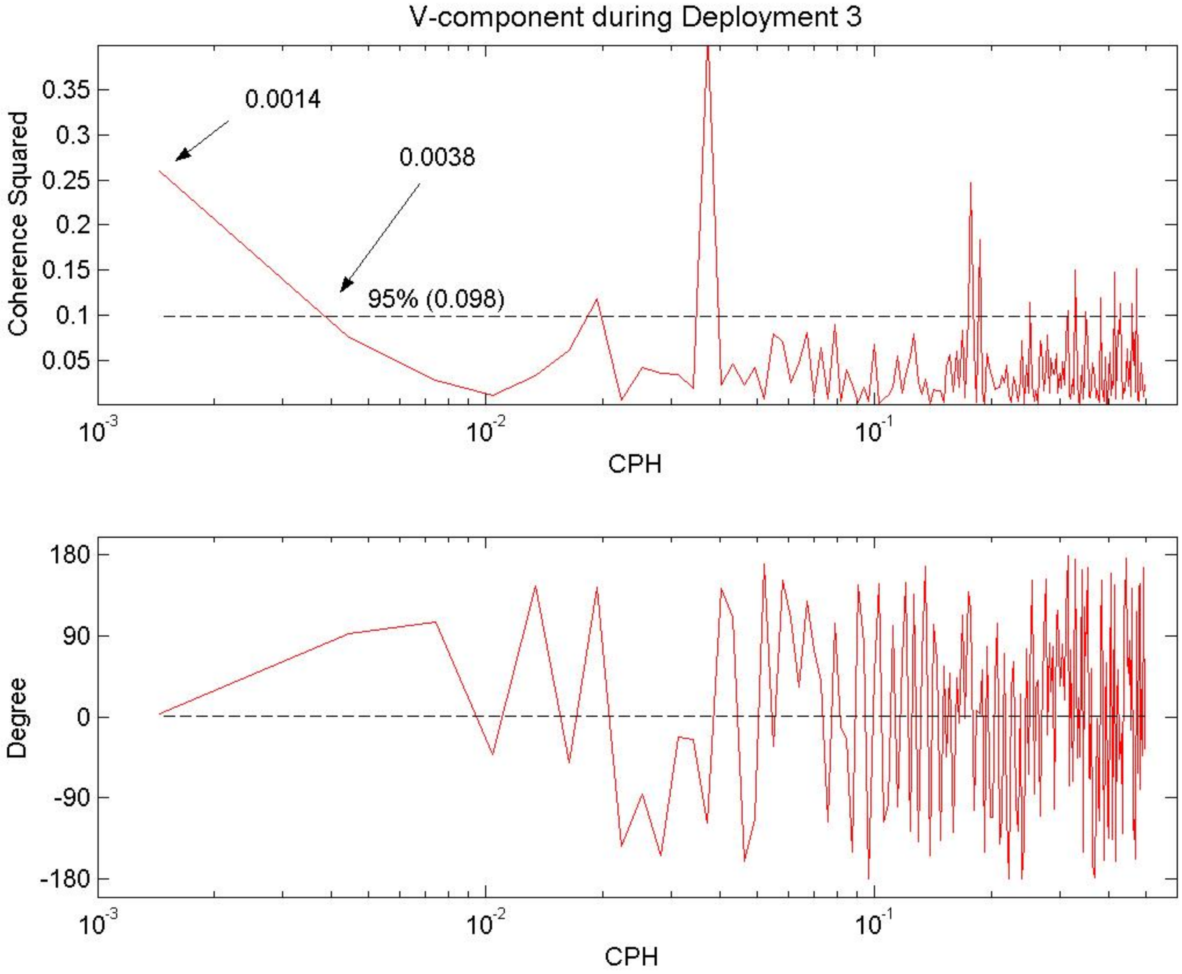

Figure 2-17. Coherence squared (top figure) and phase (bottom figure) between top (126 m) and bottom (3248 m) V-component during Deployment 3.

CHAPTER 3

YEAR-TO-YEAR-VARIABILITY

3.1 Introduction

Examination of the mooring records from the three deployments reveals significant year-to-year variability in the observed currents at the mooring site. Vertical profiles of mean and maximum current speed observed during each deployment are shown in Figures 3-1 and 3-2. In the upper-layer, Deployments 1 and 3 are more energetic than Deployment 2, an indication that the high-speed jet of the LC was in the vicinity of the mooring for a greater portion of the time during these deployments. In contrast, during Deployment 2, there were fewer occasions when the high-speed jet came close to the mooring. A major difference between the first two deployments and the third one is that in terms of both mean and maximum current speeds, the lower layer was much more energetic during Deployment 3. This is also evident in Figure 3-3 which indicates much more energetic deepwater flow regime overall during the third deployment compared to the first two. Energetic events in the upper-layer (above 800 m) always display the surface-intensified characteristic of the frontal jet of the LC and LC rings while energetic events in the lower-layer (below 1500 m) are depth-independent, i. e., magnitude does not change with depth. In the upper-layer during Deployment 3, episodes of energetic events are characterized by deeper depth penetration of these events and not by the magnitude of the near-surface jets, in comparison to Deployments 1 and 2. It is interesting that many of these upper-layer energetic events appear to be associated with high energy expression in the lower-layer (below 1500 m). Furthermore, throughout Deployment 3, there were many more episodes of deep energetic events lasting several days that do not show corresponding upper-layer expression typical of the LC or LC rings. Figures 3-4 and 3-5 present vertical temperature variations during the three deployments. Omnipresence of near-surface warm water indicates that the mooring was generally located inside the LC or LC rings except a three-month period toward the end of Deployment 2 and in February 2004 during Deployment 3.

3.2 Observed Upper-Layer Currents as They are Related to the LC

In order to interpret the observed upper-layer currents during each deployment as they are related to the LC in the eastern GOM, the historical mesoscale altimetry data archived by Dr. Robert Leben at the University of Colorado was examined. Figures 3-6 through 3-8 show a sequence of maps of sea surface height in the eastern GOM measured by satellite altimeter. The contours on each map range from -30 cm to 30 cm by 10 cm intervals. According to Leben (2005), the outer edge of the high speed core of the LC corresponds to the 17-cm contour of the total SSH (anomaly + mean) in the eastern GOM. The 17-cm SSH anomaly contour has also been used to track LC eddies in the western GOM, where there is a smaller contribution from the mean (Leben, 2005). The 17-cm contour is easily located in this sequence of figures because it lies within the boundary between the yellow and red filled color contours. The red-filled contours symbolize the core of both LC and LC rings and the highest velocities are expected to occur just inside the red-shaded areas.

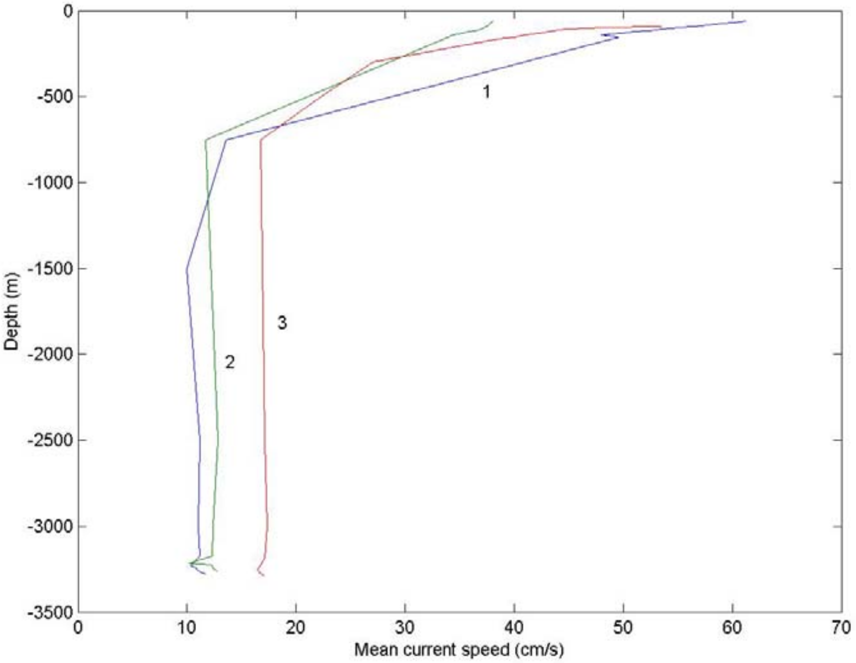

Figure 3-1. Mean current speed observed during each of the three deployments.

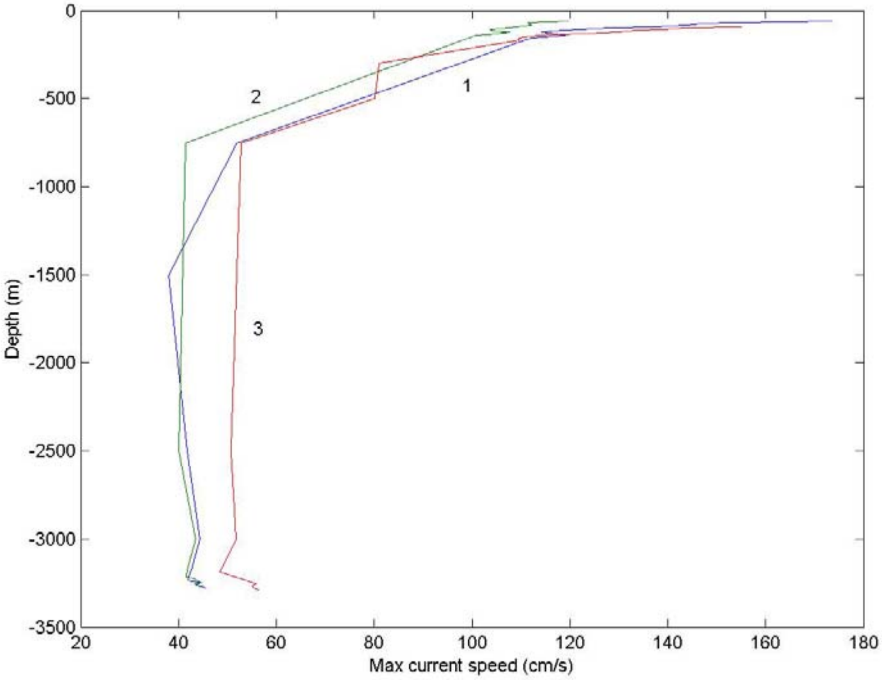

Figure 3-2. Maximum current speed observed during each of the three deployments.

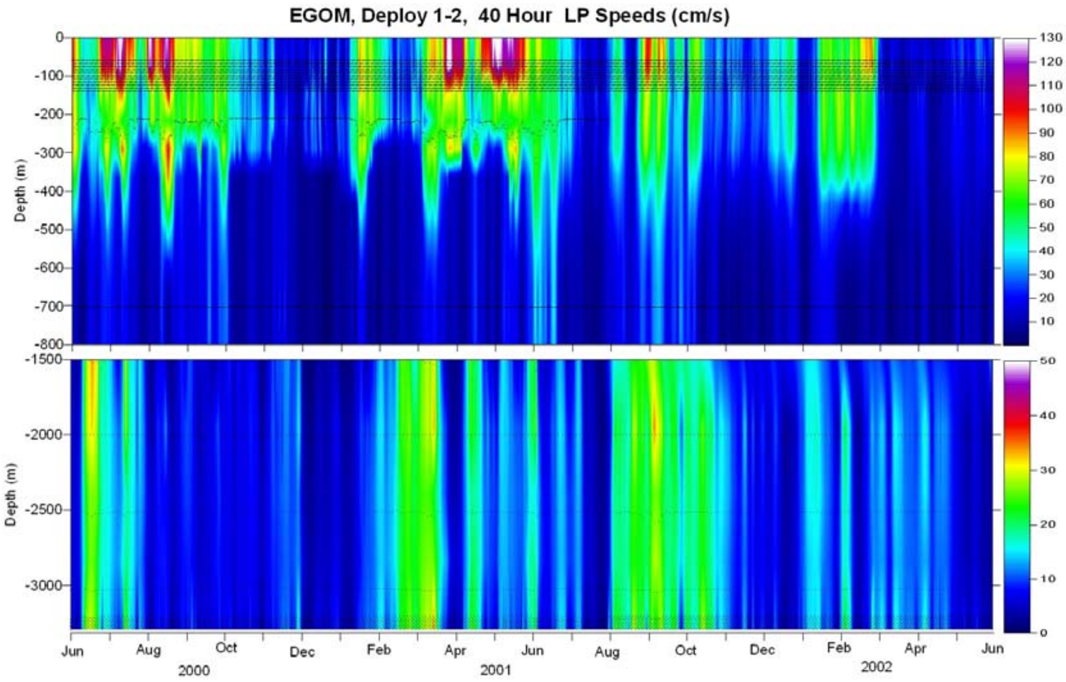

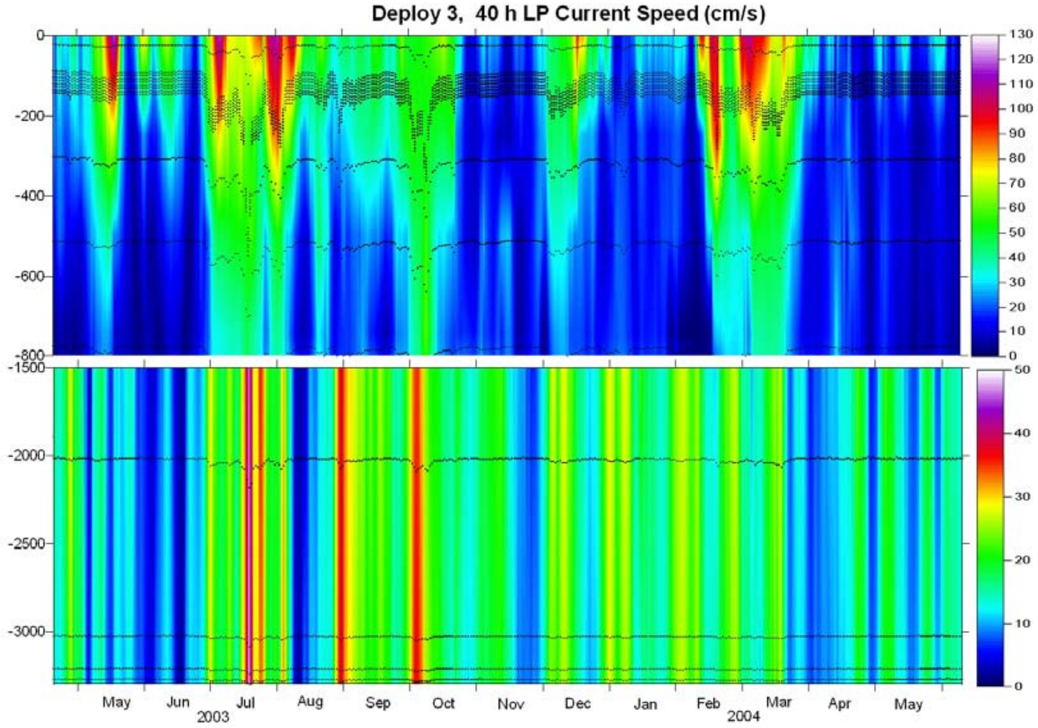

Figure 3-3. Vertical section of 40-HRLP current speed during Deployments 1 and 2 (top) and Deployment 3 (bottom). Black dots indicate depth variations of current measurements. Depth of top ADCP was not corrected for blow-over due to the lack of nearby pressure measurement.

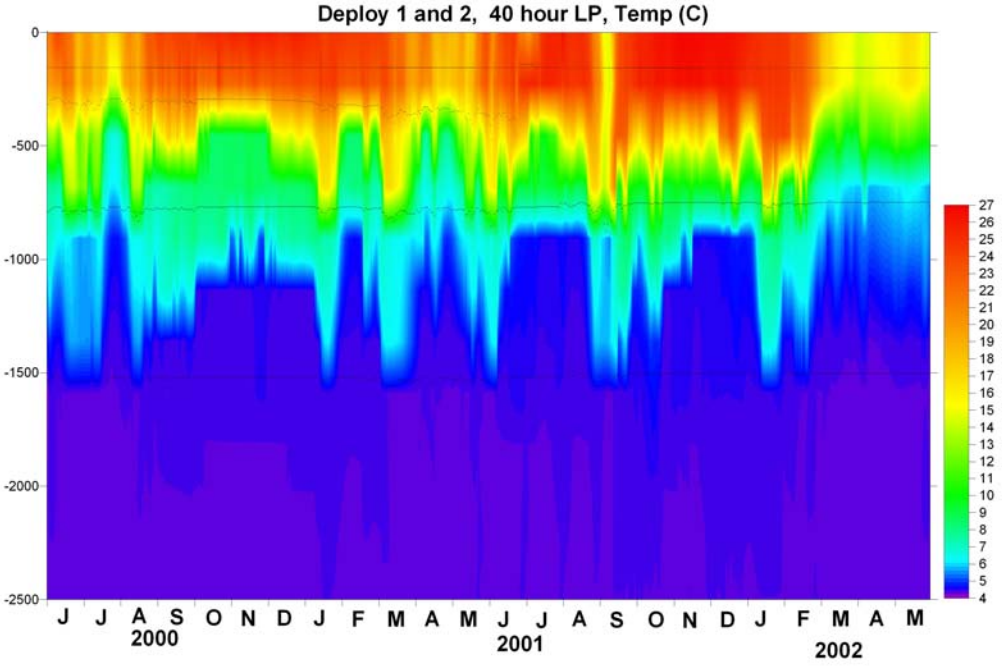

Figure 3-4. Vertical temperature section during Deployments 1 and 2. Black dots indicate depth variations of temperature measurements.

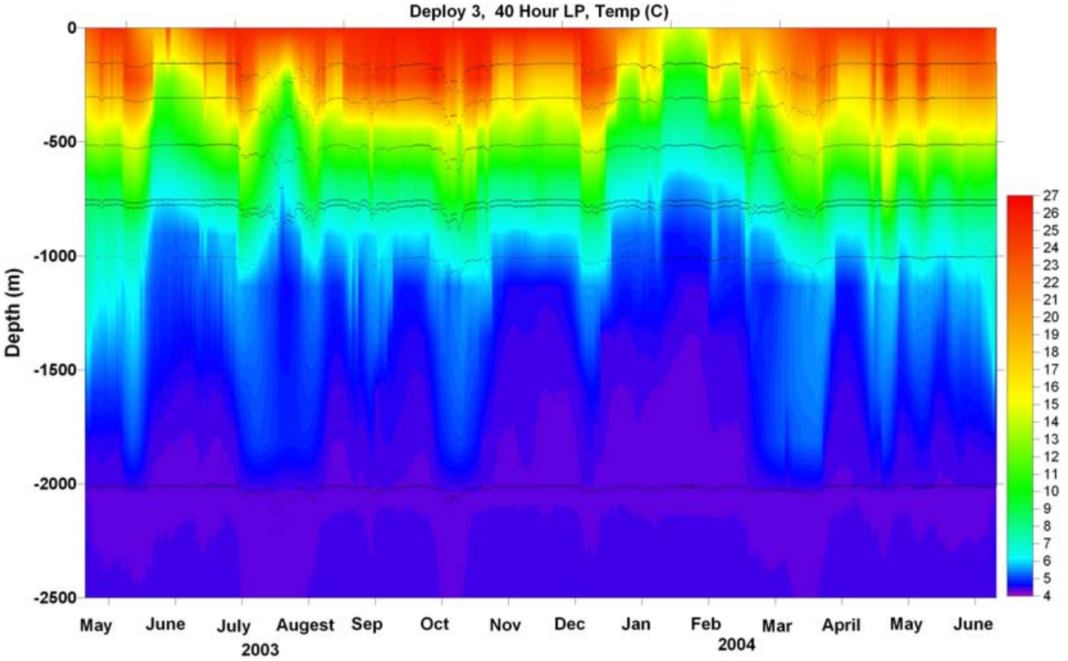

Figure 3-5. Vertical temperature section during Deployment 3. Black dots indicate depth variations of temperature measurements.

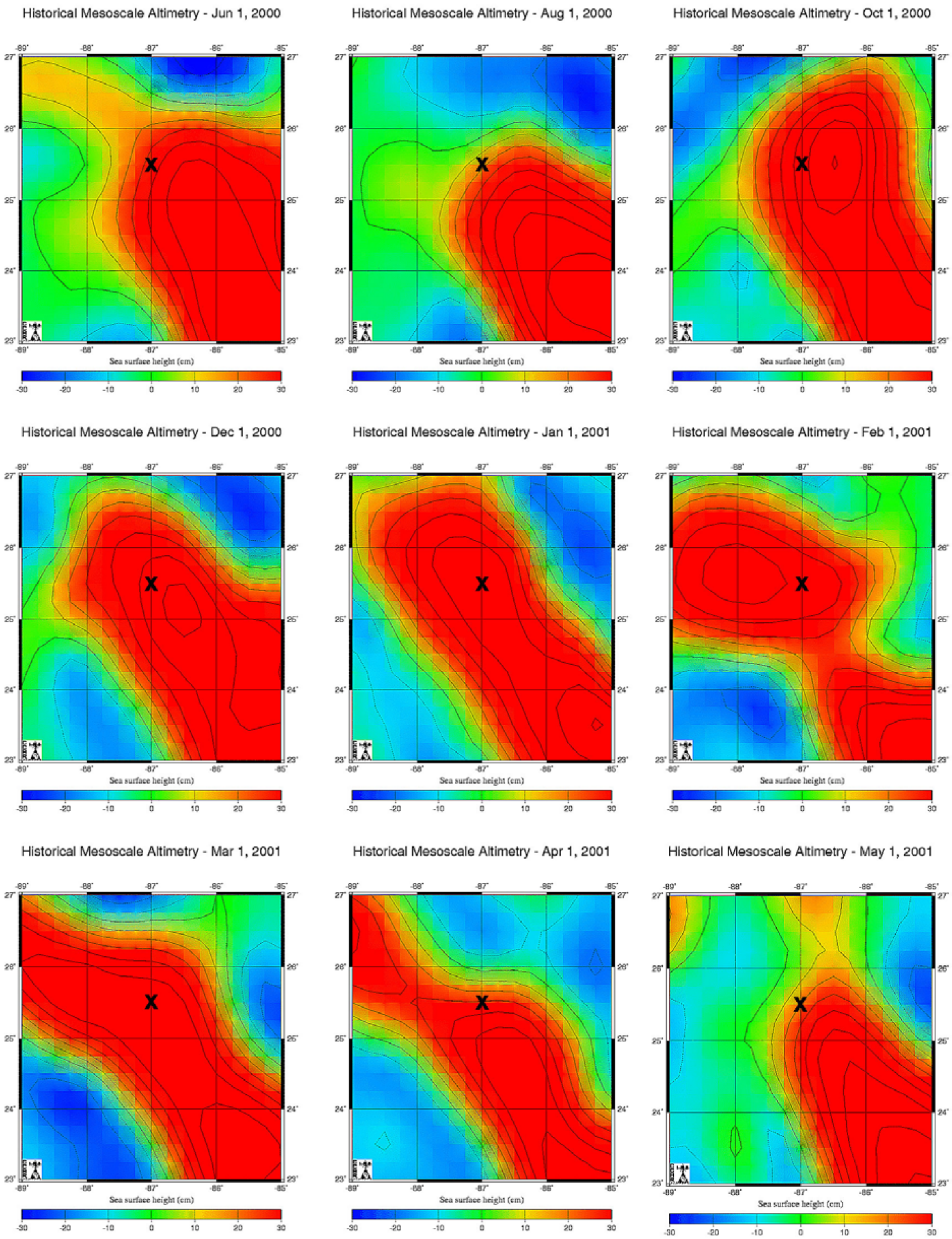
Historical Mesoscale Altimetry - Jun 1, 2000

Historical Mesoscale Altimetry - Aug 1, 2000

Historical Mesoscale Altimetry - Oct 1, 2000

Historical Mesoscale Altimetry - Dec 1, 2000

Historical Mesoscale Altimetry - Jan 1, 2001

Historical Mesoscale Altimetry - Feb 1, 2001

Historical Mesoscale Altimetry - Mar 1, 2001

Historical Mesoscale Altimetry - Apr 1, 2001

Historical Mesoscale Altimetry - May 1, 2001

Figure 3-6. Sea surface height map during Deployment 1 replotted from historical mesoscale altimetry data archived by Dr. Robert Leben at the University of Colorado.

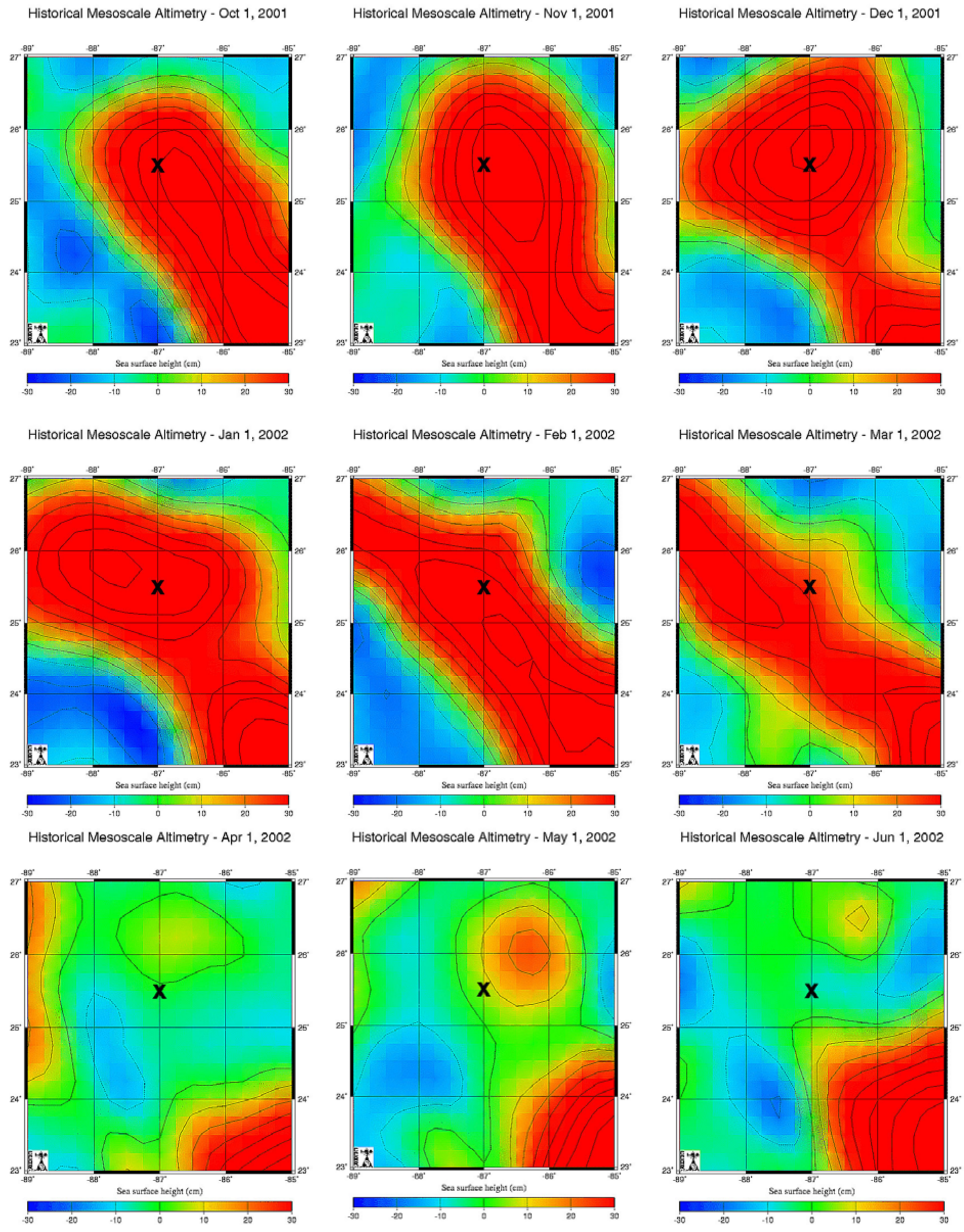

Figure 3-7. Sea surface height map during Deployment 2 replotted from historical mesoscale altimetry data archived by Dr. Robert Leben at the University of Colorado.

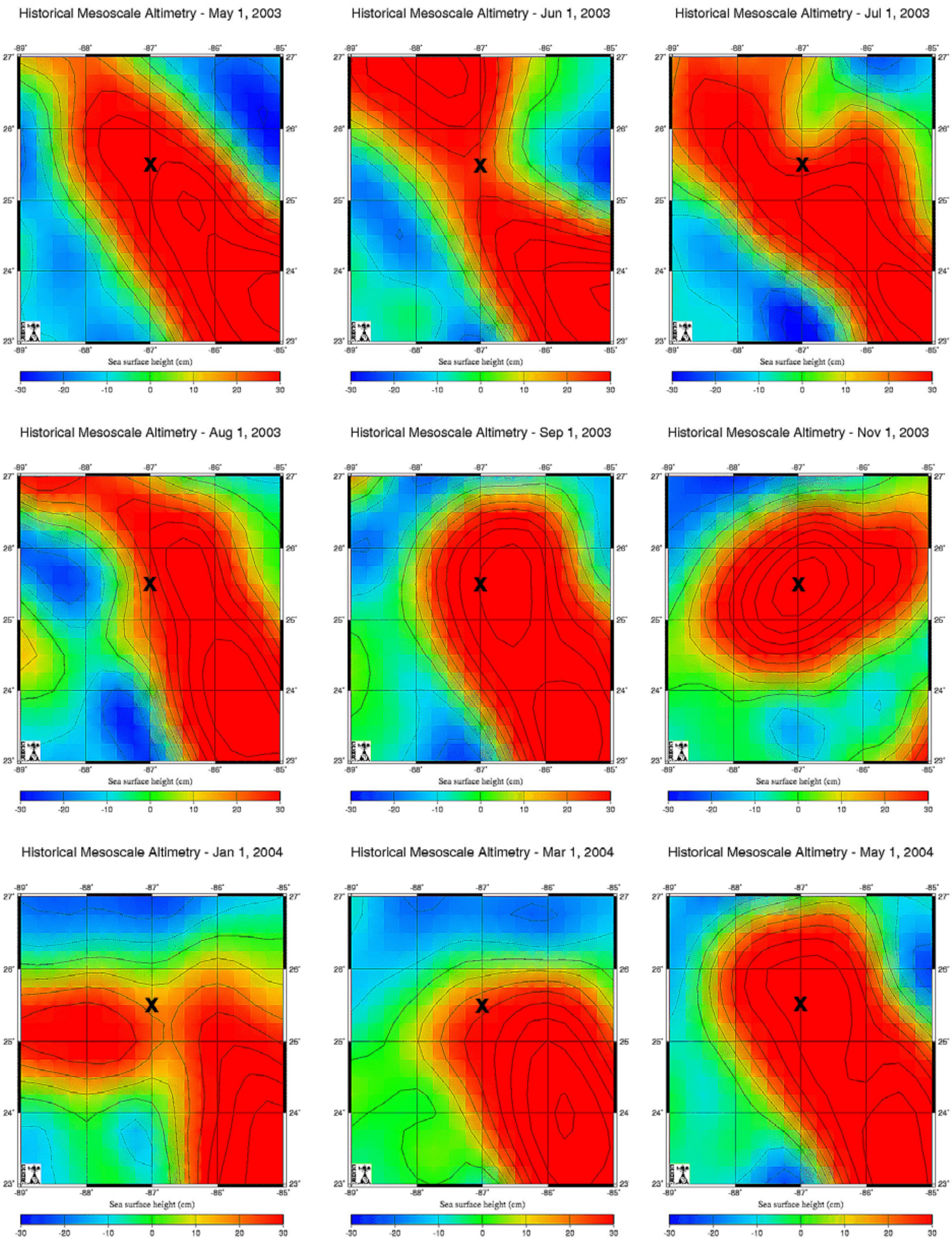

Historical Mesoscale Altimetry - May 1, 2003

Historical Mesoscale Altimetry - Jun 1, 2003

Historical Mesoscale Altimetry - Jul 1, 2003

Historical Mesoscale Altimetry - Aug 1, 2003

Historical Mesoscale Altimetry - Sep 1, 2003

Historical Mesoscale Altimetry - Nov 1, 2003

Historical Mesoscale Altimetry - Jan 1, 2004

Historical Mesoscale Altimetry - Mar 1, 2004

Historical Mesoscale Altimetry - May 1, 2004

Figure 3-8. Sea surface height map during Deployment 3 replotted from historical mesoscale altimetry data archived by Dr. Robert Leben at the University of Colorado.

Early in Deployment 1 (June through September 2000), the mooring was located near the northwest corner of the LC (Figure 3-6). Consequently, strong northeasterly and northerly upper-layer currents associated with the high-speed core of the LC were recorded (Figure 2-1). Subsequently from October 2000 to January 2001, the LC extended northwestward, and the mooring moved closer to the center of the LC where upper-layer currents were weaker. On January 26, 2001, a ring detached, but it reattached on January 30. In February 2001, the LC became very elongated toward the northwest and the mooring experienced southerly and southeasterly upper-layer flow associated with the eastern branch of the LC circulation. A ring separated (Eddy Millennium) on April 10, 2001 (Leben, 2005). During the separation of the ring, mid-March through mid-April, the flow over the mooring was easterly, but became northerly as the LC extended northward again and the mooring was positioned in the western branch of the LC (Figure 3-6). From June 2001 to the beginning of Deployment 2 in August 2001, the mooring remained well inside the LC, and upper-layer currents remained relatively weak. From September 10 to13, 2001, a small ring appeared to separate and reattach, and on September 22, Eddies Odessa and Nansen were formed (Leben, 2005). These eddies were extremely small and were re-captured by the LC in early December. From mid-September through mid-November, the mooring recorded primarily northward currents in the upper 140m, which were associated with the western branch of the LC.

From mid-November 2001 to January 2002, the mooring remained well inside the LC, and weak upper-layer currents were recorded (Figures 2-2 and 3-7). In February and March 2002, the LC extended far into the northwestern GOM and the eastern branch of the LC was flowing over the mooring, which was reflected in southeasterly upper-layer currents recorded. Eddy Pelagic separated in the western GOM on February 28, 2002 and Eddy Quick separated on March 13, 2002, in the central GOM at approximately 89°W (Leben, 2005). The LC reformed south of 25°N, which left the mooring well outside of the LC in April 2002 and weak upper-layer flow was observed for the rest of Deployment 2.

At the beginning of Deployment 3 in April 2003 the LC was well-developed and extended northwesterly, leaving the mooring well within the LC circulation (Figures 2-3 and 3-8). During the third week of May, the LC began to constrict very close to the mooring in preparation for a ring separation. The mooring experienced strong southeasterly surface currents for about a week. On June 1, that ring was very close to separating and the constriction was almost directly over the mooring (Figure 3-8), but the ring was re-absorbed and flow over the mooring became weak and variable. During the first week of July the mooring experienced strong easterly currents again as another ring began to form. On July 13, this ring detached, but reattached on July 20 and the mooring was now positioned to the west of the LC. At the end of July, the western branch of the LC moved westward over the mooring and remained there through mid-October. Eddy Sargassum separated on August 5, 2003 (Leben, 2005). Another ring separated on September 25, 2003, and moved directly over the mooring, which resulted in very weak and variable currents from the third week of October through the end of November, when the ring reattached. The next separation resulted in Eddy Titanic on December 31, 2003 (Leben, 2005), which was quite small and separated to the west of the mooring (Figure 3-8). Eddy Titanic drifted slowly westward and for several weeks the mooring experienced weak southwesterly flow associated with the eastern side of the ring. During the second week of February, the LC extended northward again and the mooring experienced strong northward currents that continued until the latter part of March, 2004. From the end of March until the end of the record, the mooring was within the interior of the LC and the upper layer currents were weak and variable.

3.3 Inter-Deployment Energy Shift

Figures 3-9 and 3-10 show raw current speed in deepwater during Deployments 1 & 2 and Deployment 3, respectively. There appears to have been a shift in baseline energy level between the first two deployments and Deployment 3, especially after June 2003 (Figure 3-10). During Deployments 1 and 2, minimum currents were nearly zero throughout, while during Deployment 3, the baseline was shifted upward by 5~6 cm s^{-1} (this can also be seen in Figure 3-1). These observations suggest that the inter-deployment variability at the mooring site includes a shift in energy level in deepwater, i.e., deepwater during Deployment 3 was much more energetic than during Deployments 1 and 2.

3.4 Short-Duration Energetic Events

Examination of Figures 3-9 and 3-10 reveals that there were short-duration energetic events recorded during each deployment. These energetic events lasted only a few days. However, they represent the strongest currents ever recorded during the three deployments. The strongest event for each deployment was identified in Figures 3-9 and 3-10, and current vectors during each of the three events (Events 1 through 3) are plotted in Figures 3-11 through 3-13 for corresponding one-month duration. The most notable feature is that deepwater currents during each event were characterized by vertically coherent northward currents, while upper-layer flow varied from event to event. Upper-layer currents during Event 1 were toward the southeast, while the lower-layer currents flowed northward. Some phase-locking between upper-layer and lower-layer, whereby the entire water column was flowing approximately in the same direction, was observed during the peak periods of Events 2 and 3 (Figures 3-12 and 3-13).

Events 1 and 2 display current speeds of approximately 40 cm s^{-1}, but Event 3 is associated with deepwater currents exceeding 50 cm s^{-1} (1 knot), by far the strongest deepwater currents observed at the mooring site. It is interesting that during these strong deepwater events, near-surface currents did not appear to show proportional strengthening. However, it should be noted that these strong events resulted in severe blow-over of the entire mooring, thus the top ADCP was measuring currents significantly deeper than the design depth. Consequently, during these events the strongest near-surface currents were not captured. For example, during Event 3, all the instruments were submerged 180~200 m deeper than their design depths with most of the blow-over taking place in deepwater due to the strong deepwater currents observed. The mooring design adopted turned out to be less rigid than expected.

In order to interpret the observed current during each energetic event, historical mesoscale altimetry data archived at the University of Colorado were examined. Figure 3-14 through Figure 3-16 show maps of sea surface height measured by satellite altimeter at 4- or 7-day intervals during each event. According to Figure 3-14, the mooring was located on the

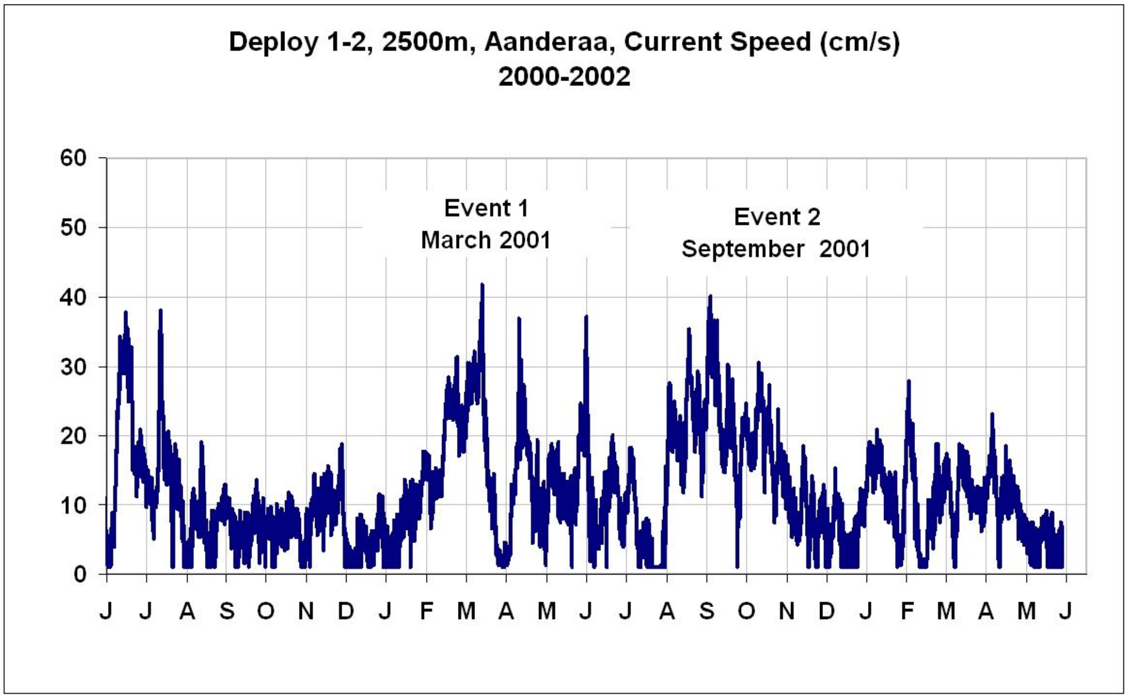

Figure 3-9. Raw current speed (cm/s) at 2500 m during Deployments 1 and 2.

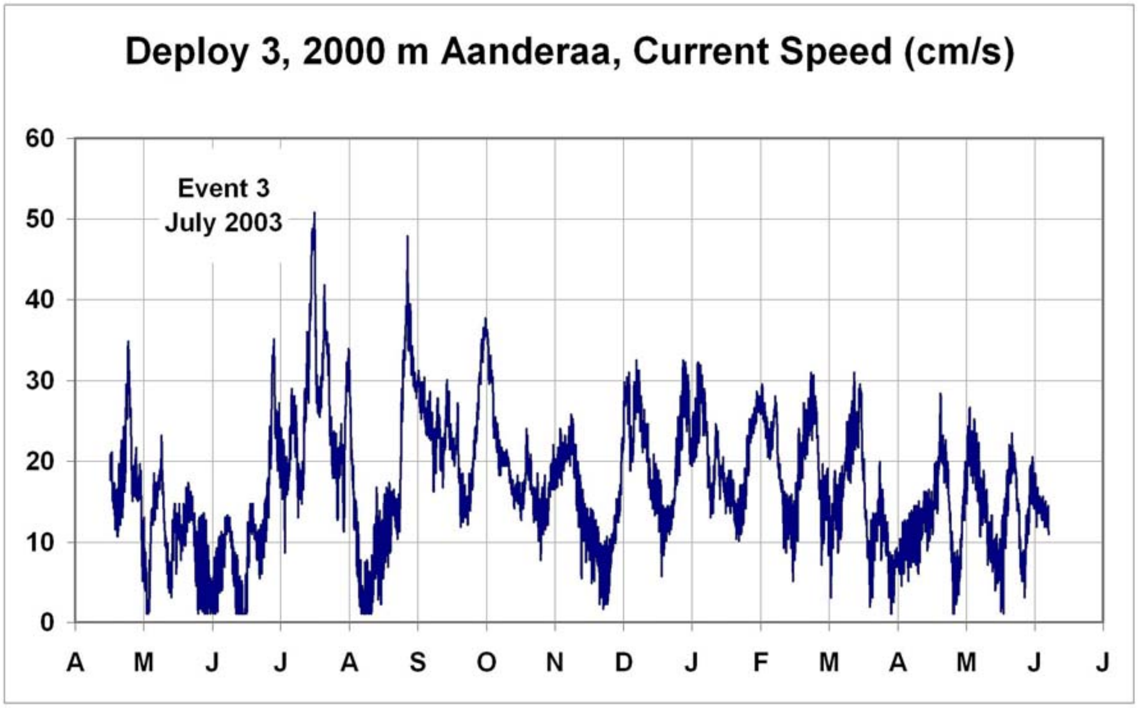

Figure 3-10. Raw current speed (cm/s) at 2000 m during Deployment 3.

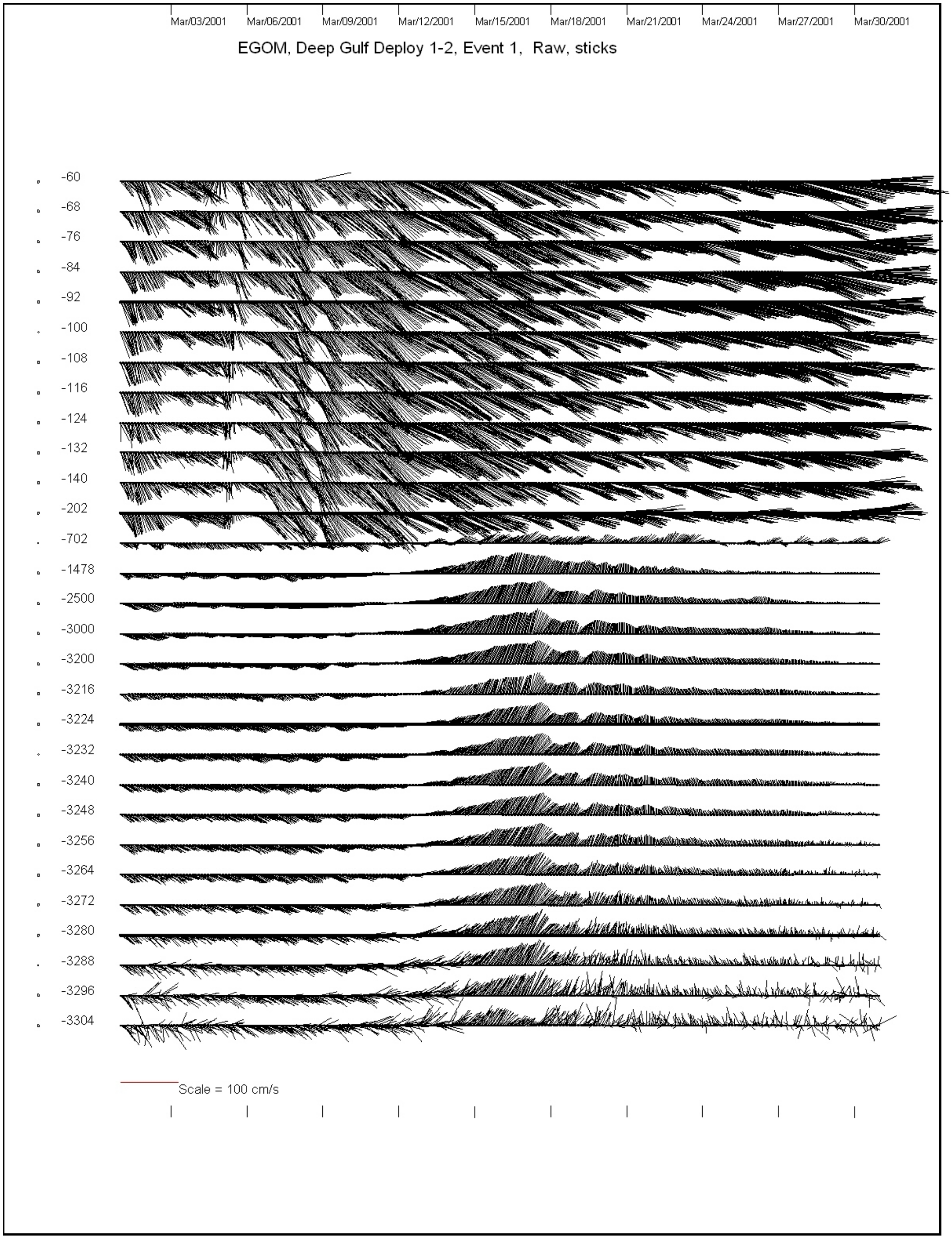

Figure 3-11. Raw current vectors observed during Event 1.

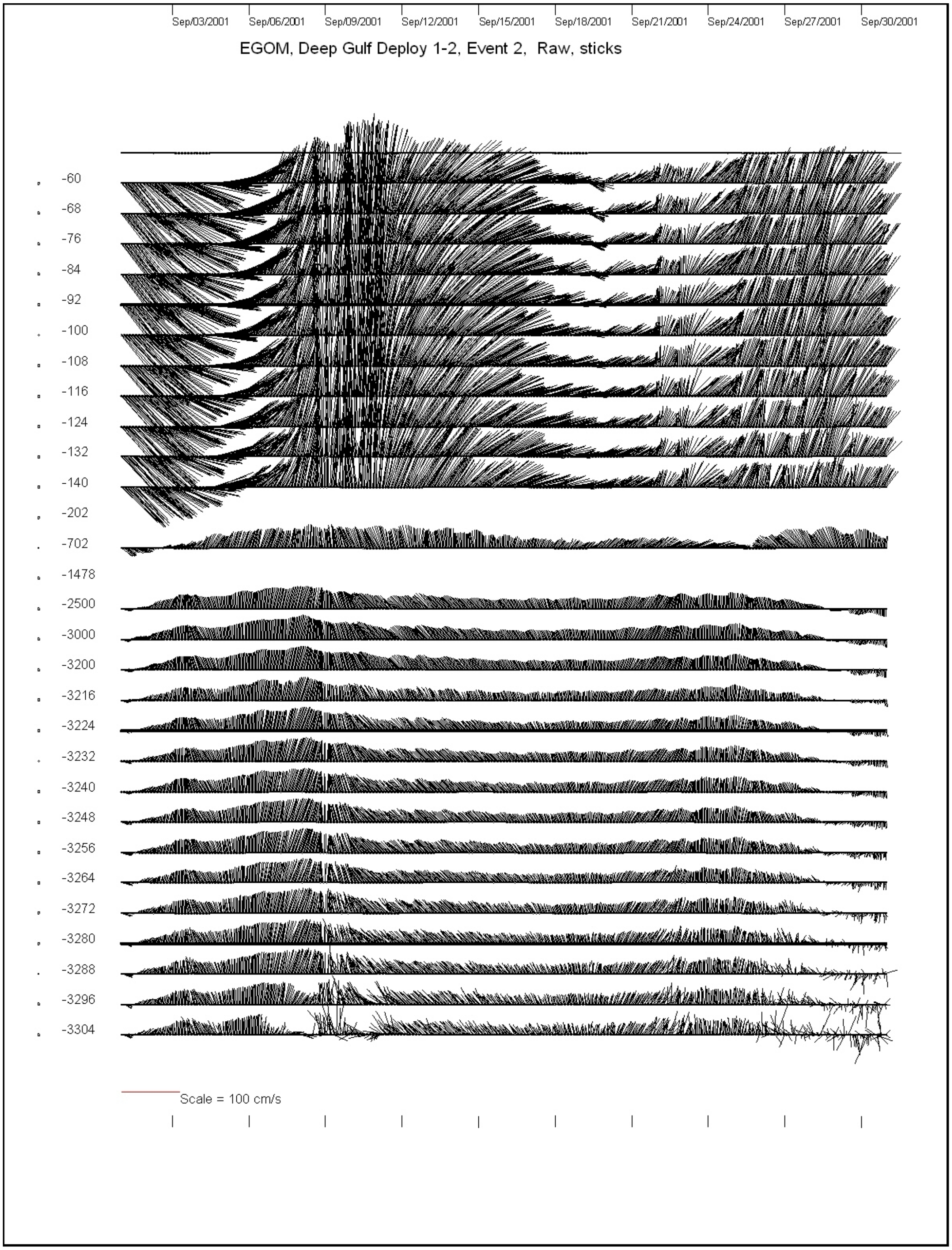

Figure 3-12. Raw current vectors observed during Event 2.

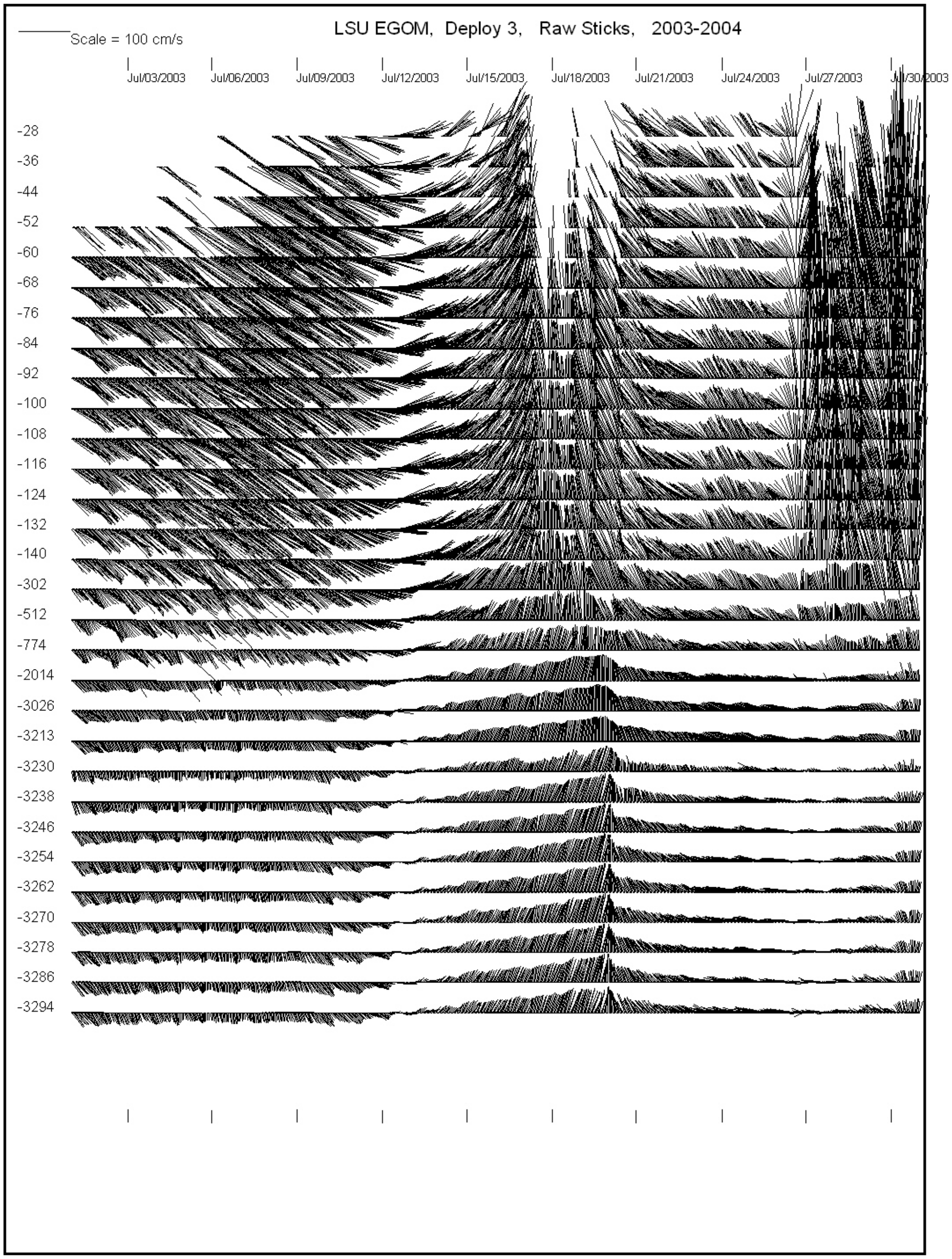

Figure 3-13. Raw current vectors observed during Event 3.

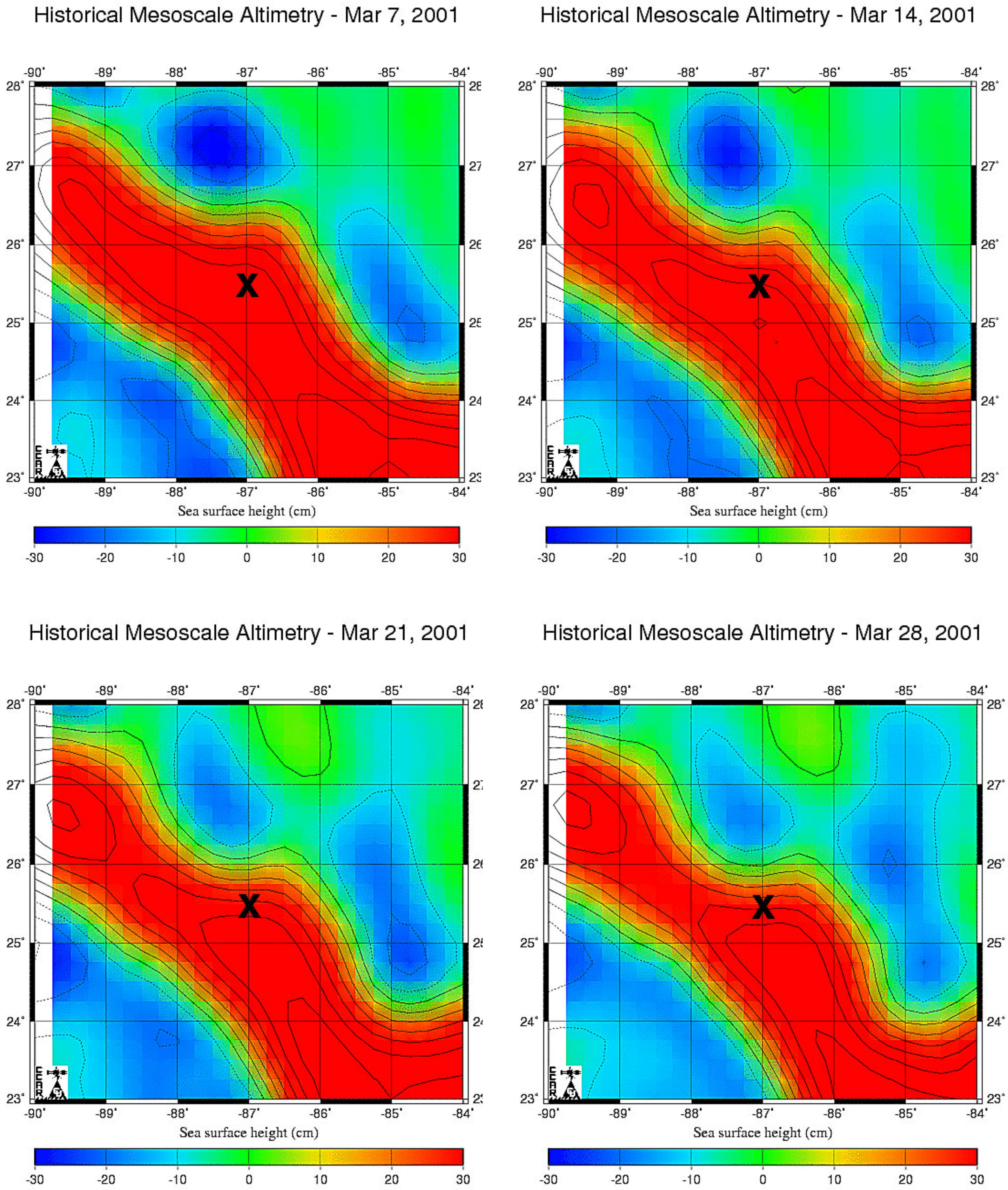

Historical Mesoscale Altimetry - Mar 7, 2001

Historical Mesoscale Altimetry - Mar 14, 2001

Historical Mesoscale Altimetry - Mar 21, 2001

Historical Mesoscale Altimetry - Mar 28, 2001

Figure 3-14. Sea surface height map at 7-day intervals during Event 1 replotted from historical mesoscale altimetry data archived by Dr. Robert Leben at the University of Colorado.

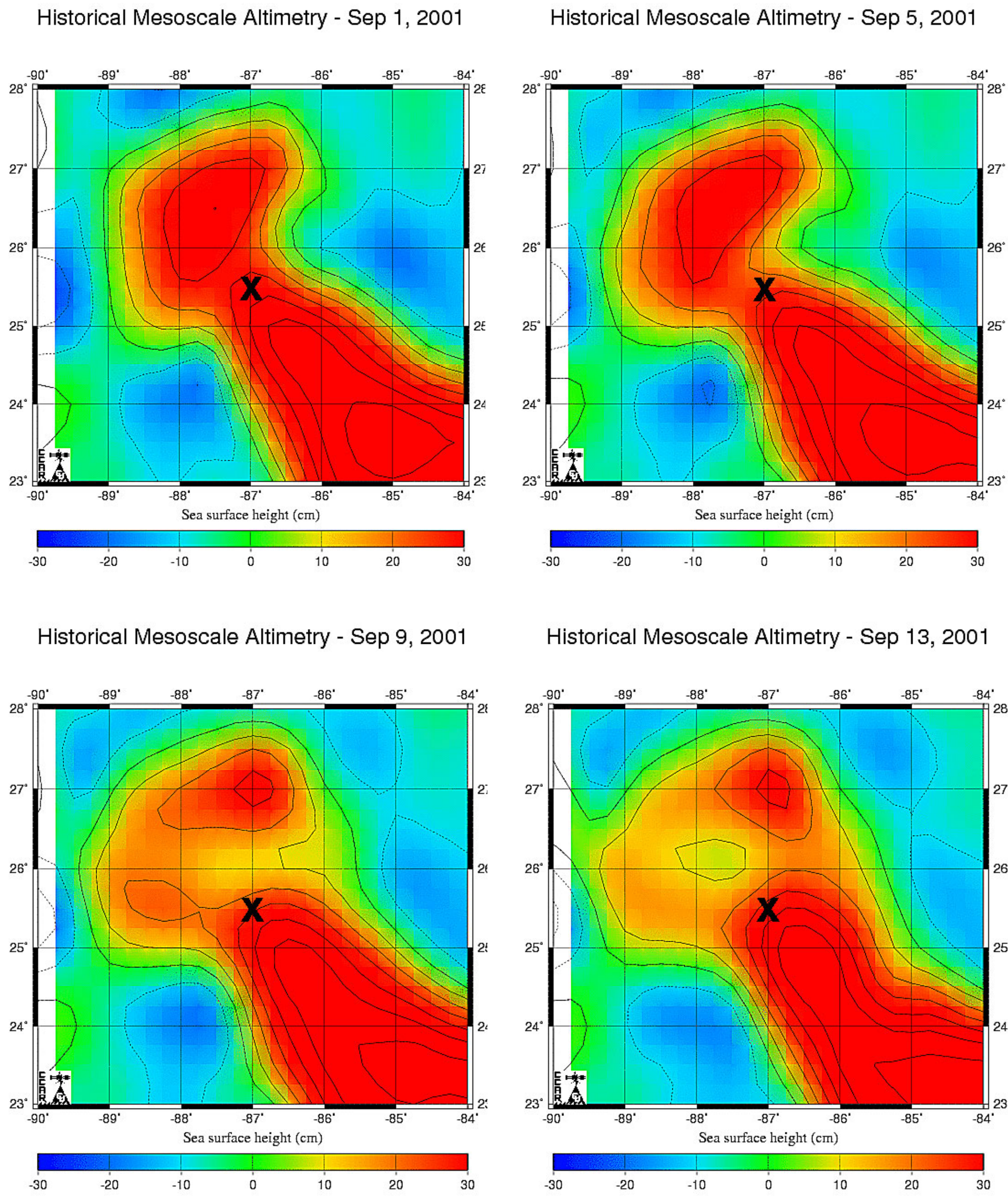

Historical Mesoscale Altimetry - Sep 1, 2001

Historical Mesoscale Altimetry - Sep 5, 2001

Historical Mesoscale Altimetry - Sep 9, 2001

Historical Mesoscale Altimetry - Sep 13, 2001

Figure 3-15. Sea surface height map at 4-day intervals during Event 2 replotted from historical mesoscale altimetry data archived by Dr. Robert Leben at the University of Colorado.

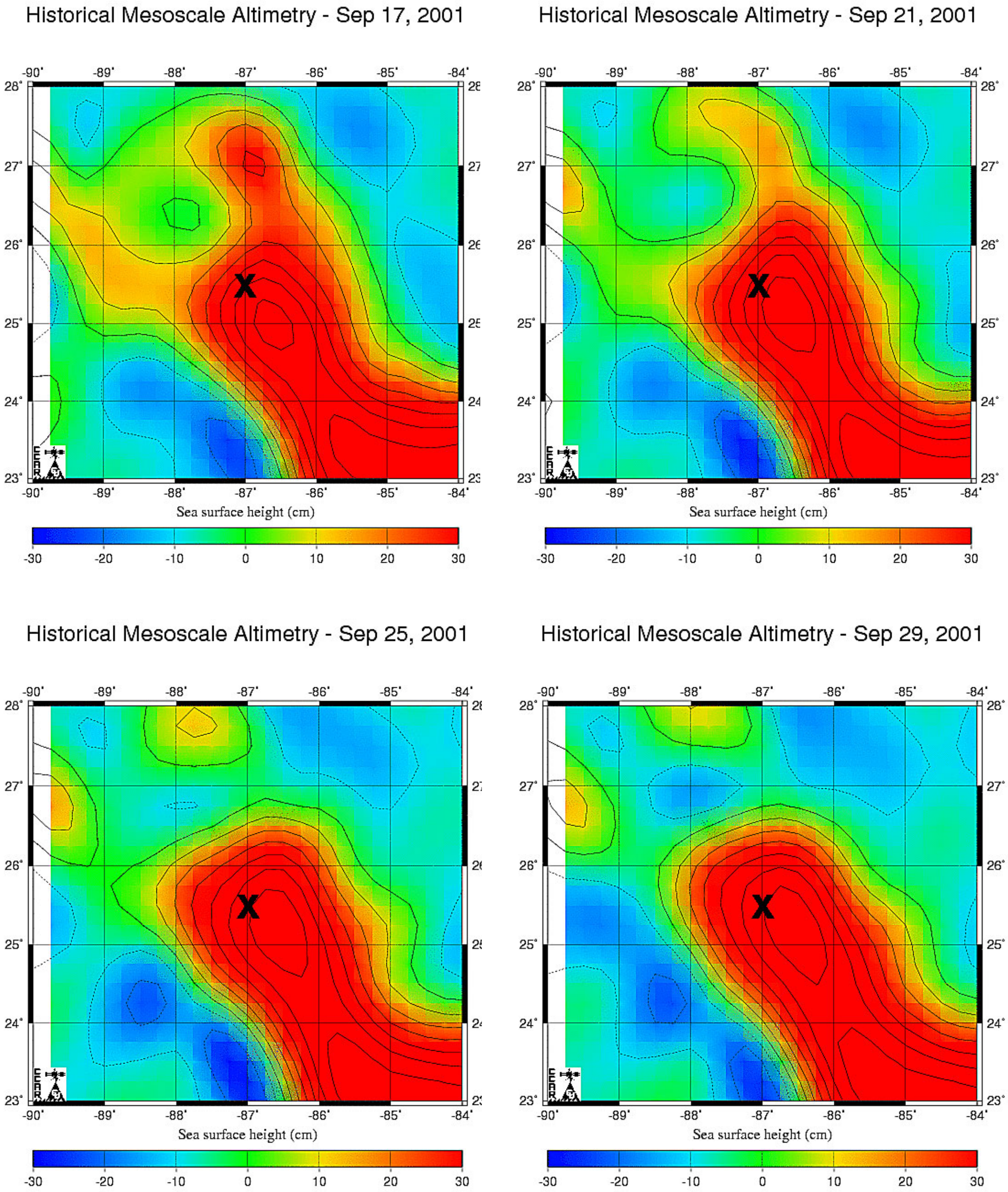

Historical Mesoscale Altimetry - Sep 17, 2001

Historical Mesoscale Altimetry - Sep 21, 2001

Historical Mesoscale Altimetry - Sep 25, 2001

Historical Mesoscale Altimetry - Sep 29, 2001

Figure 3-16. Sea surface height map at 4-day intervals during Event 2 replotted from historical mesoscale altimetry data archived by Dr. Robert Leben at the University of Colorado.

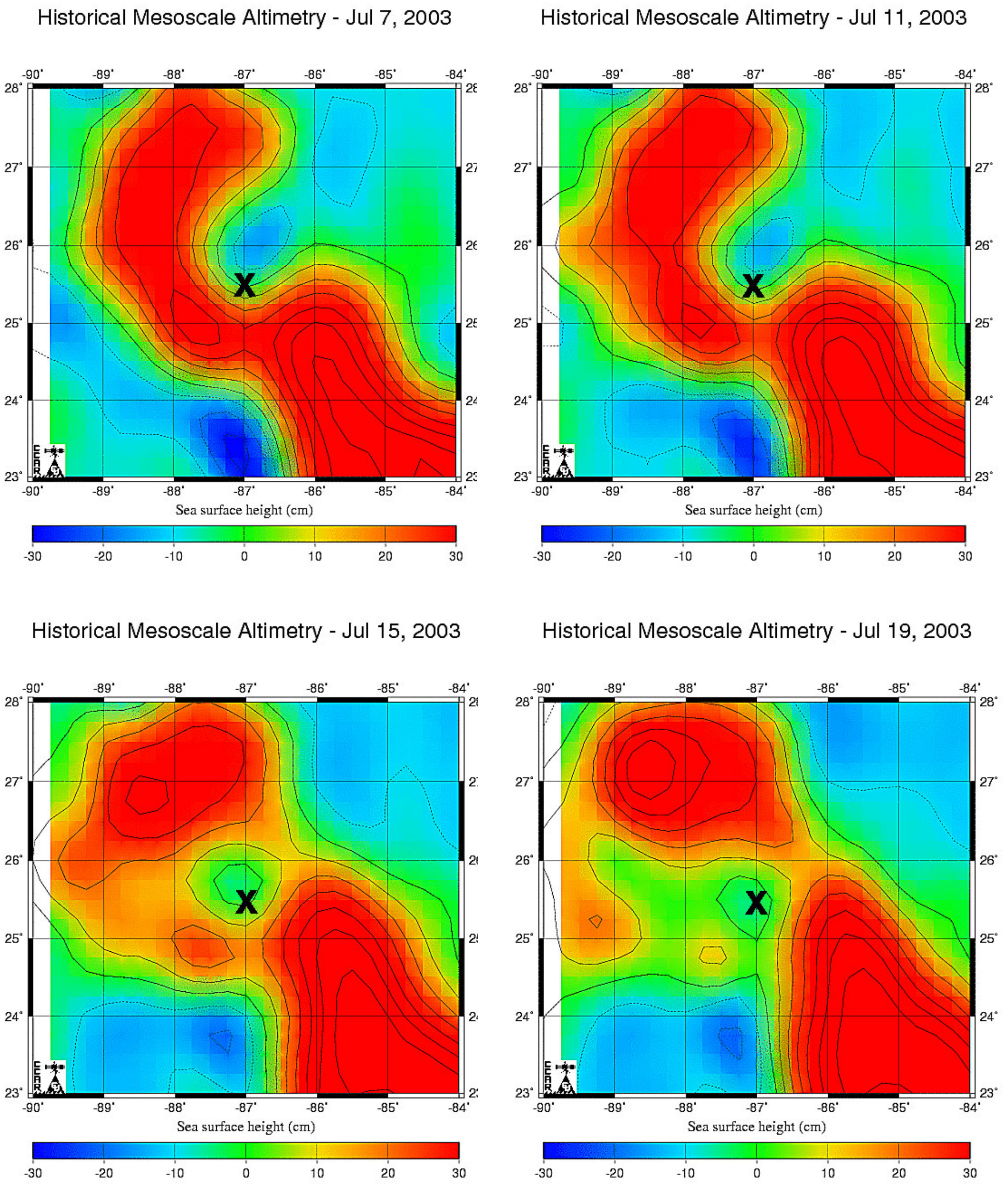

Historical Mesoscale Altimetry - Jul 7, 2003

Historical Mesoscale Altimetry - Jul 11, 2003

Historical Mesoscale Altimetry - Jul 15, 2003

Historical Mesoscale Altimetry - Jul 19, 2003

Figure 3-17. Sea surface height map at 4-day intervals during Event 3 replotted from historical mesoscale altimetry data archived by Dr. Robert Leben at the University of Colorado.

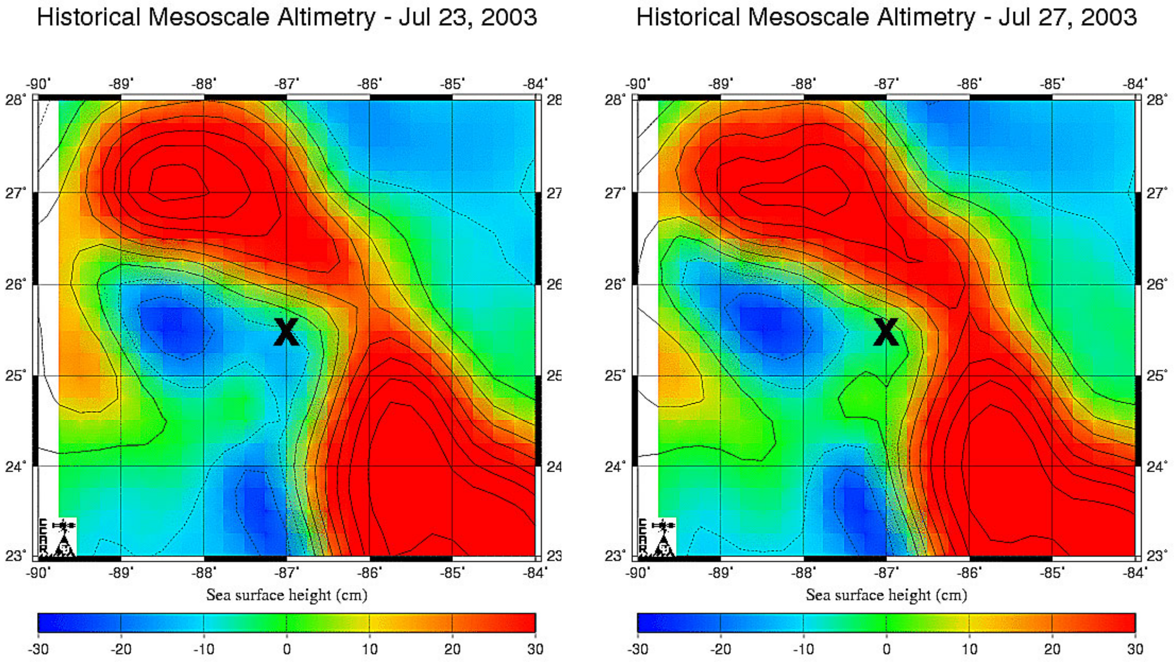
Historical Mesoscale Altimetry - Jul 23, 2003

Historical Mesoscale Altimetry - Jul 27, 2003

Figure 3-18. Sea surface height map at 4-day intervals during Event 3 replotted from historical mesoscale altimetry data archived by Dr. Robert Leben at the University of Colorado.

eastern side of the LC during Event 1. Consequently, the mooring was recording southeasterly flow in the upper layer. In contrast, deepwater currents remain weak until around March 13, 2001 when sudden strengthening of northeasterly flow was observed (Figure 3-11). This northeasterly flow peaked around March 18, 2001 and gradually weakened thereafter while its direction shifted more northerly. By March 21, 2001, the flow returned to the strength of pre-Event 1 flow. Using historical altimetry maps, the LC was observed to elongate toward the northwest in late February, 2001, and actually extended north of 27 N and west of 90 W. In mid-March, a closed circulation feature began to form at the tip of the LC, which led to the separation of Eddy Millennium on April 10 (Leben 2005). Interestingly, the observed strengthening of deepwater flow at the mooring site (Figure 3-11) appears to coincide with the formation of the circulation feature that became Eddy Millennium (Figure 3-14).

During Event 2, the mooring remains in the vicinity of the northwestern corner of the LC while its distance to the high-speed jet varied (Figure 3-15). It is noted that Event 2 coincided with the formation of Eddies Odessa and Nansen described by Leben (2005). By closer examination of the altimeter data, it appears that Eddy Nansen was formed on May 12, 2001, and Eddy Odessa was formed in early September, 2001. Northward deepwater flow appeared in early September 2001, and it strengthened until it peaked around September 8 (Figure 3-12). Then, it gradually weakened. Upper-layer flow down to 702 m, displays southeasterly flow in early September. However, it shifted to northeast direction around September 6, when the upper-layer appears to become phase-locked with the lower-layer flow. This phase locking continued until toward the end of September, 2001. The timing of the phase-locking between the upper- and lower-layers is coincident with the separation of the tip of the LC that resulted in the formation of Eddy Odessa and Eddy Nansen (Figure 3-15).

Event 3 resulted in the strongest deepwater currents observed throughout the three deployments with currents exceeding 50 cm s^{-1} (1 knot) in deepwater. Again Event 3 appears to precede the formation of an eddy, Eddy Sargassum which separated on August 5, 2003 (Leben 2005). Around July 7, 2003, the mooring was located of the eastern side of the LC extension (Figure 3-16) which resulted in the southwesterly upper-layer flow at the site (Figure 3-13). As the LC shifted eastward between July 13 and July 15, the upper layer currents over the mooring shifted to northeasterly and northerly. Relatively weak deepwater flow was found in early July, and phase-locking between upper- and lower-layers already existed at this time. As the flow in the upper-layer shifted to the northeasterly direction, deepwater flow followed closely. Then, deepwater flow gained strength around July 15, and it reached peak strength around July 18-19. At this time, the upper-layer was moving quite fast, perhaps signaling the presence of a high-speed jet nearby. This was followed by weakening of flow in both upper and lower layers, as the high speed jet moved away from the mooring.

It should be noted that all three energetic events captured by the mooring appeared to have preceded the formation of LC rings and regardless of the upper-layer flow, deepwater flow at the mooring site was northward. These strong northward deepwater currents lasted only a few days and extend from below the interface all the way to the bottom. Two more eddies separated from the LC during Deployment 3 that were not accompanied by strong deep northward currents at the mooring. The first of these, which can be observed in the historical altimetry maps, detached on September 23, 2003, and reattached on November 28. Only one month later on

December 31, 2003, a much smaller eddy separated, which was named Eddy Titanic (Leben 2005).

A question arises as to the impact of these strong deepwater currents in the eastern GOM on stirring up deepwater. Figures 3-17 and 3-18 show temperature and salinity together with current speed observed in deepwater for Deployments 1 & 2, and Deployment 3. Figures 3-19 through 3-21 are similar figures for each of the three energetic events. At these deep depths, 2500 m in Deployments 1 & 2, and 2000 m in Deployment 3, the range of variability for temperature and salinity is relatively small. However, the sensitivity of Microcats used allows the detection of signal associated with changes in water mass properties at the mooring site even at these depths. Range of salinity variability was 0.003 at 2500 m during Deployments 1 & 2, and it remained similar at 2000 m during Deployment 3. Range of temperature variability was 0.02 C^o at 2500 m during Deployments 1 & 2, while it was 0.05 C^o at 2000 m during Deployment 3. It is apparent in Figures 3-17 and 3-18 that some of the short bursts of low salinity episodes were accompanied by warmer temperatures.

Event 1 was characterized by concomitant changes toward increasing temperature and decreasing salinity. This event was followed by appearance of slightly cooler and saltier water. Event 2 was associated with appearance of cooler and saltier water. Deployment 3 appears to be notably different in that temperature changed more widely with significantly more energy at time scales of one week to a month. Unfortunately, the conductivity sensor on Microcat at 2000 m during Deployment 3 stopped functioning after November 2003. However, there is a clear indication of comparable energy peaks at similar time scales in salinity signal as well. Furthermore, strong current events during Deployment 3 appear to be associated with notable signal in temperature and salinity. Event 3, for example, was followed by significant cooling and increase in salinity at the mooring site, indicating that notable disturbance in water mass properties in deep water took place following this event. These observations suggest that Event 3 was so energetic that local water mass was disturbed. These energetic events might play an important role in local mixing of water masses in the eastern GOM. Since a single Microcat was deployed in deepwater below 1500 m in each of the three deployments, it is not clear that the observed larger variability of temperature at 2000 m during Deployment 3 was anomalous compared to the first two deployments. However it is interesting to note that the observed salinity exhibits comparable energy peaks at similar time scales (one week to a month).

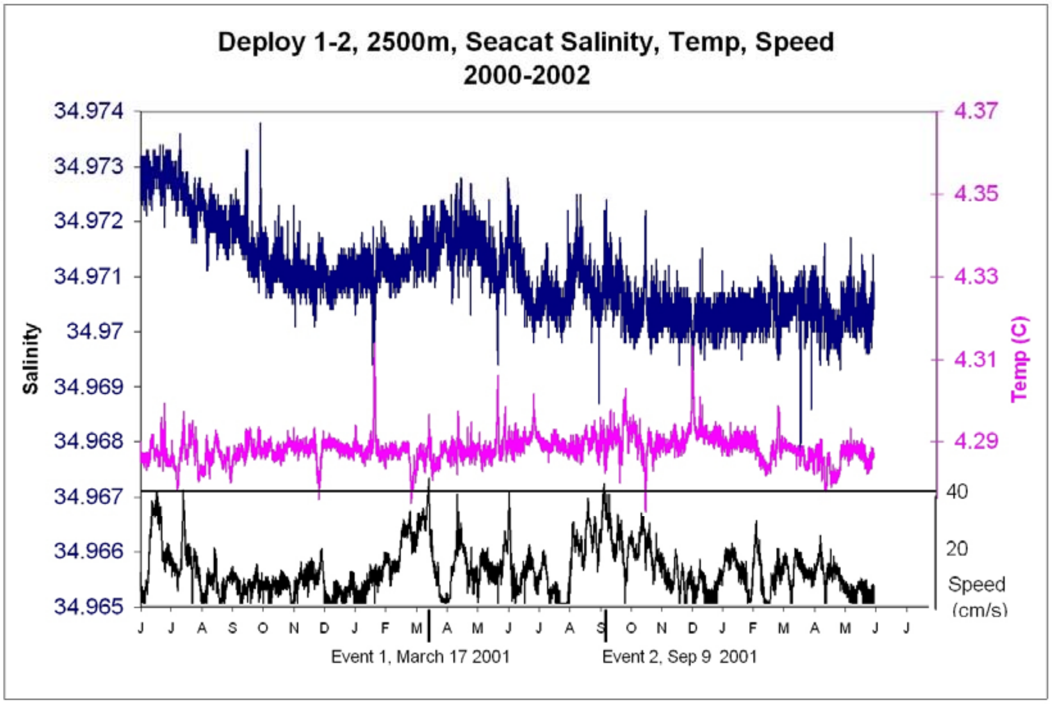

Figure 3-19. Salinity, temperature and current speed observed at 2500 m during Deployments 1 and 2.

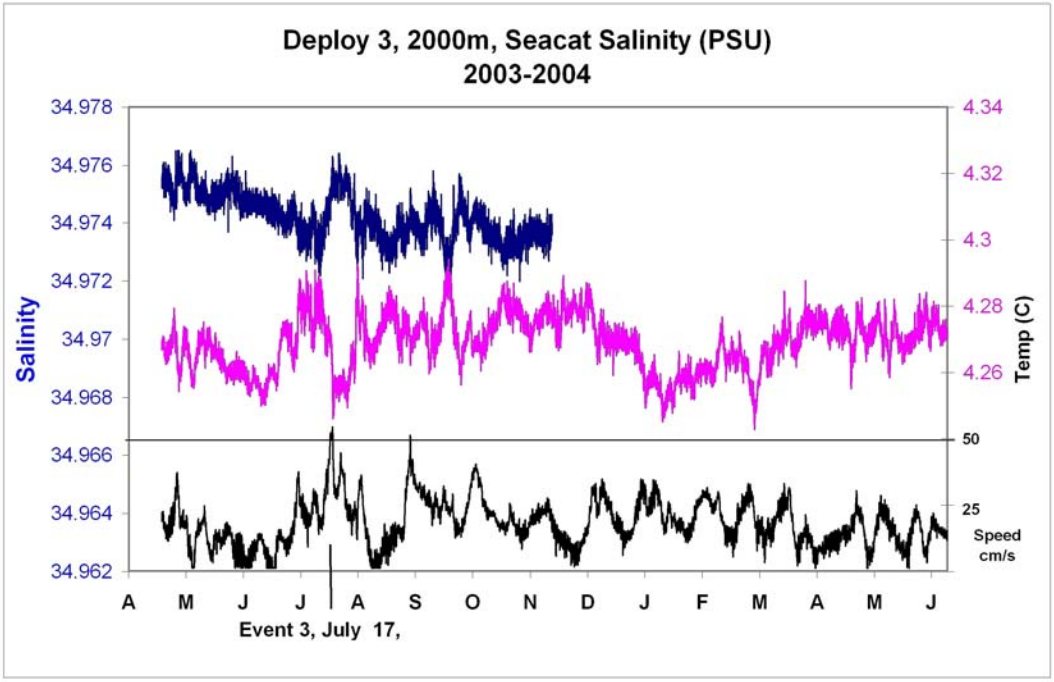

Figure 3-20. Salinity, temperature and current speed observed at 2000 m during Deployment 3.

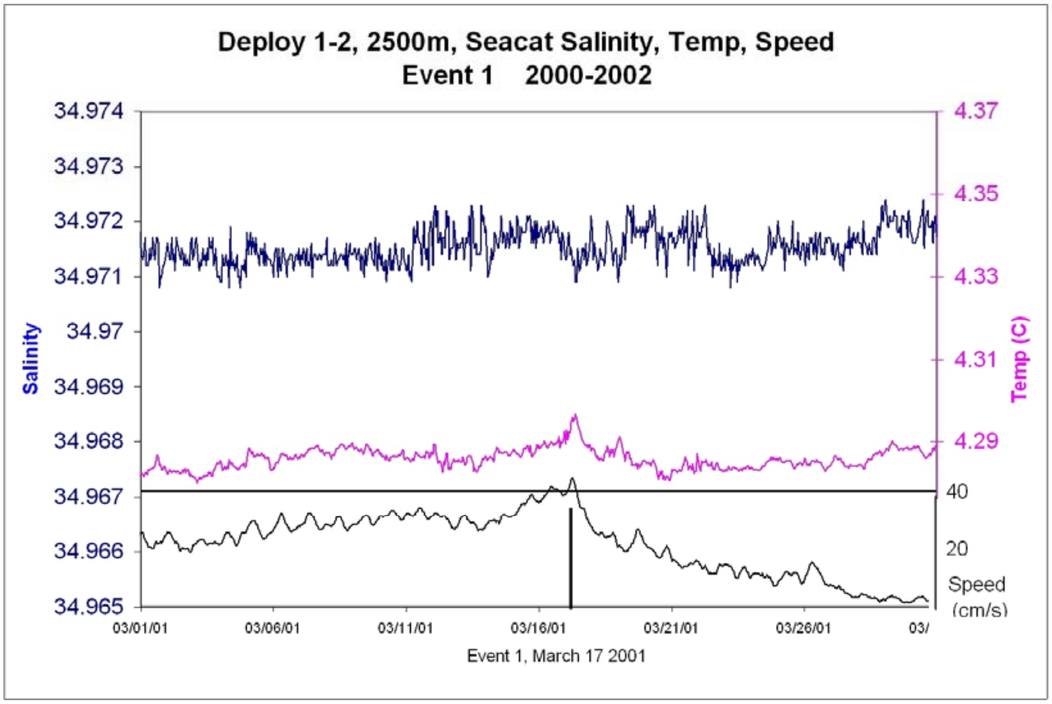

Figure 3-21. Salinity, temperature and current speed observed during Event 1.

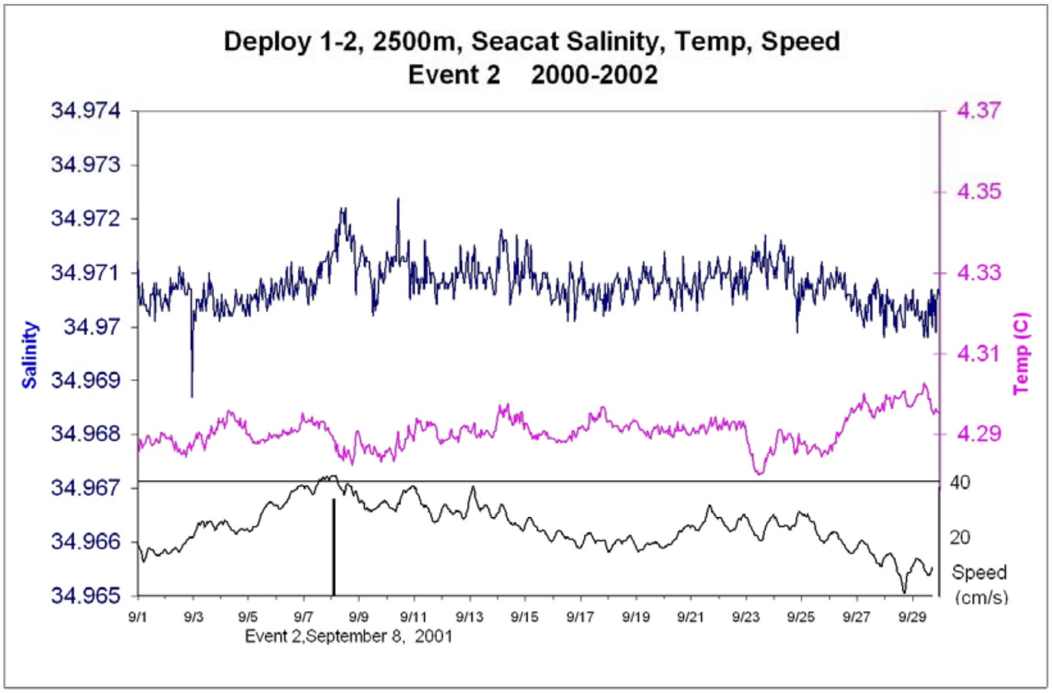

Figure 3-22. Salinity, temperature and current speed observed during Event 2.

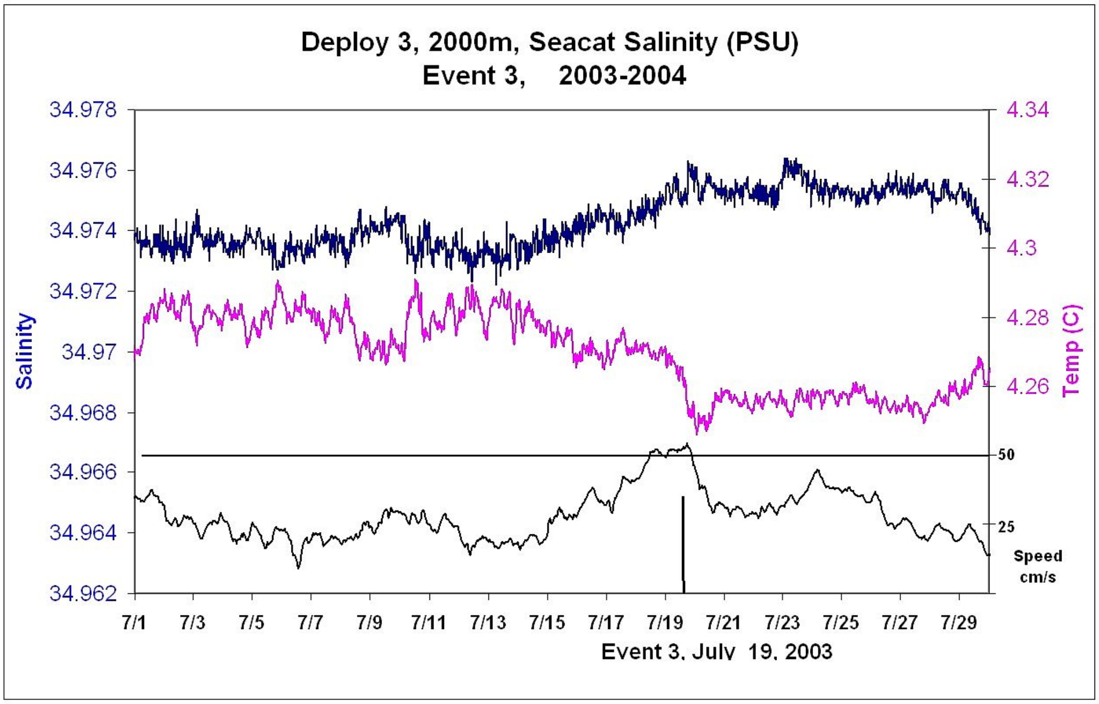

Figure 3-23. Salinity, temperature and current speed observed during Event 3.

CHAPTER 4

DISCUSSION AND SUMMARY

4.1 Summary of Observations

The first observations of the upstream condition in the middle of the eastern GOM using a deepwater mooring have been completed with a total of three deployments, the first two nearly continuous deployments covering a two-year period and the third one separated by slightly less than 11 months. Overall, the mooring site selection was excellent in that it remained within the LC for all of the three deployments, and it is usually in the close proximity of the high-speed jet within the LC. Furthermore, the mooring site appears to be able to capture the strong northward flow in deepwater associated with the formation of LC rings.

During Deployments 1 and 3, the mooring was close to the high-speed jet of the LC while it primarily remained well inside the LC, away from the high-speed jet during Deployment 2. The upper-layer flow above 700-800 m was dominated by the LC and LC rings. In contrast, the lower-layer flow appears to be generally decoupled from the upper-layer flow. In general, dominant time scales for the upper-layer flow are much longer than those for the lower-layer flow. What is interesting is that every deployment turned out to be different for both upper-layer and lower-layer flow dynamics. This is a reflection of the observation that the dominant time scales associated with the LC in the eastern GOM are dictated by time scales associated with the formation of LC rings. The LC ring separation has shown to have significant power near 6, 9, and 11 months (Sturges and Leben, 2000; Leben, 2005). Furthermore, details of the ring formation process vary greatly from eddy to eddy (Leben, 2005; Lugo-Fernandez, 2007). As a result, one-year observation of currents in the eastern GOM is simply not long enough to capture basic statistics for generalization.

In deepwater, Deployment 3 exhibits more energy in terms of background flow as well as peak energy levels than the first two deployments. A few short-duration energy bursts of deepwater events were observed. The strongest event observed had current magnitude exceeding 1 knot in deepwater during Deployment 3. Interestingly, the most energetic events observed appear to coincide with concurrent northward extension of the LC that preceded the formation of LC rings reported by Leben (2005). However, not all the LC rings formed during the duration of deployments were accompanied by significant deepwater currents at the mooring site. The formation of Eddy Titanic in December 2003, did not result in any notable deepwater currents at the mooring site. It should be noted, however, that Eddy Titanic was formed well to the south of all other eddies formed during the three deployments. The three most energetic events recorded showed very strong northward flow in deepwater regardless of the upper-layer flow. Moreover, these strong northward flow events in deepwater lasted only a few days at the mooring site. These energetic events were accompanied by notable temperature and salinity signal in deepwater. In particular, Event 3 resulted in significant cooling and increases in salinity in deepwater. These observations suggest that short-duration energy bursts in deepwater associated with the formation of LC rings could result in stirring of deepwater in the eastern GOM.

A major obstacle in interpreting measurements at a single mooring in the middle of the eastern GOM is how to extrapolate the observations in space. Use of model output is suited for this type of interpretation. In order to interpret the observations from a single mooring, output from the models of GOM will be utilized (For details of the model setup, please refer to Appendix). Similar models of GOM have been used previously (Welsh, 1996; Welsh and Inoue, 2000; Welsh and Inoue, 2002). In order to understand the observations, description of the upper-layer and lower-layer circulation associated with the formation of LC rings in the eastern GOM is presented based on the model output.

4.2 Deepwater Circulation in the Model

The model deepwater circulation is characterized by an energetic eddy field. This behavior has been observed using four different model grid resolutions with different domain boundaries and different methods of forcing the inflow. The first model had 0.25° horizontal resolution and 12 vertical levels (Sturges et al., 1993), the second had 0.125° horizontal resolution with 15 vertical levels (Welsh and Inoue, 2000), the third had 0.10° horizontal resolution with 20 vertical levels (Welsh and Inoue, 2002), and a present version of the model has 0.075 ° horizontal resolution with 100 vertical levels. The deep eddy field in each of these models is highly coherent with depth from between 1000 and 1500 m to the bottom and the maximum model velocities increase slightly as the bottom is approached, perhaps reflecting the prevalence of TRWs (Oey and Lee, 2002). Computer animations of the model temperature and velocity fields reveal that as the LC extends northward into the GOM during the ring-separation process, an anticyclone-cyclone pair develops beneath the newly formed ring (e. g., Welsh and Inoue, 2000).

A sequence of images from the high-resolution model (with 0.075° horizontal resolution and 100 vertical levels) output depicting the separation of an anticyclonic ring from the LC is presented in Figure 4-1. These images show the stream function and velocity vectors in the upper most level of the model, centered at 10 m depth. The corresponding flow in the deep layer is depicted in Figure 4-2, which shows the velocity vectors at 2850 m as well as the stream function. The location of the mooring is indicated on these plots (+), although due to differences in the actual bathymetry and the model grid representation of the ETOPO2 bathymetry, the bathymetric control on the observed flow at the mooring may be slightly different than on the modeled flow at same latitude and longitude.

It is apparent that the stream function is a good indicator of the near-surface flow field (Figure 4-1). On Day 43, the LC is surging northward along the Campeche Bank with the axis of the flow oriented very nearly to the north. Note that the current turns back southward, but there is no discernable center of circulation that would distinguish a nascent LC ring. In the lower level flow (Figure 4-2), there is a continuous current to the northwest direction up against the Campeche Bank, which forms the western side of a newly-forming deep anticyclonic eddy. At this moment the flow observed at the mooring location in the upper and lower layers is nearly in phase.

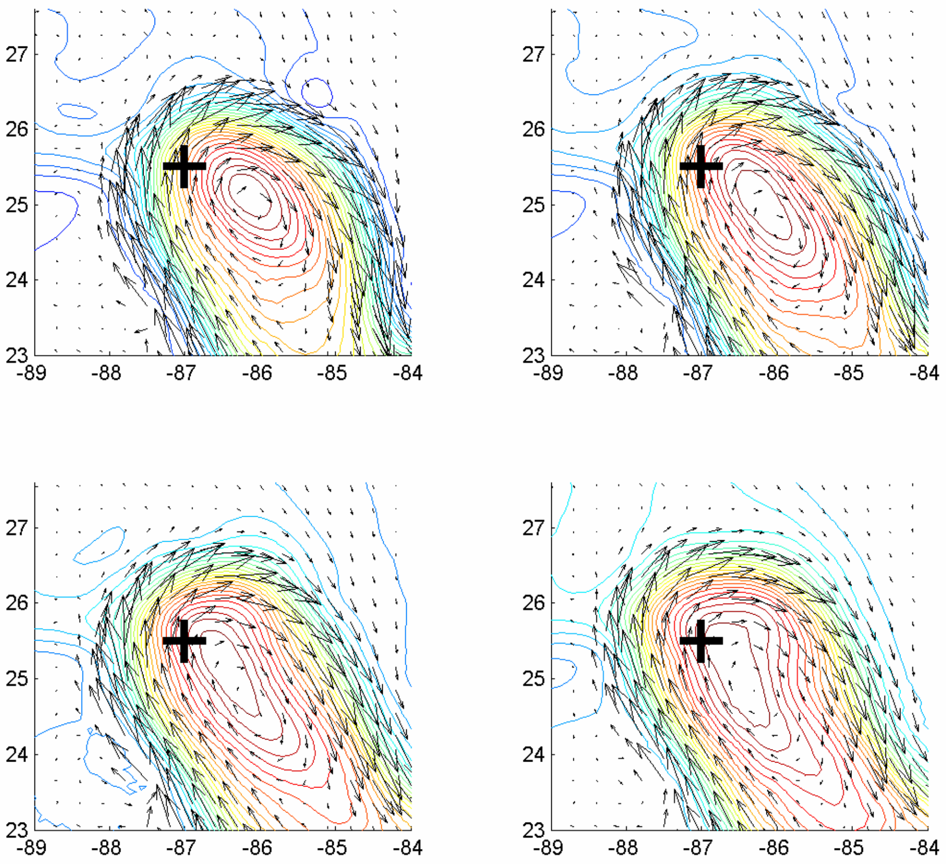

Figure 4-1. Contours of stream function and velocity vectors at level 1 centered at 10 m extending from 0 m to 20 m for model days, 43, 50, 57, and 64. The '+' indicates the location of the mooring.

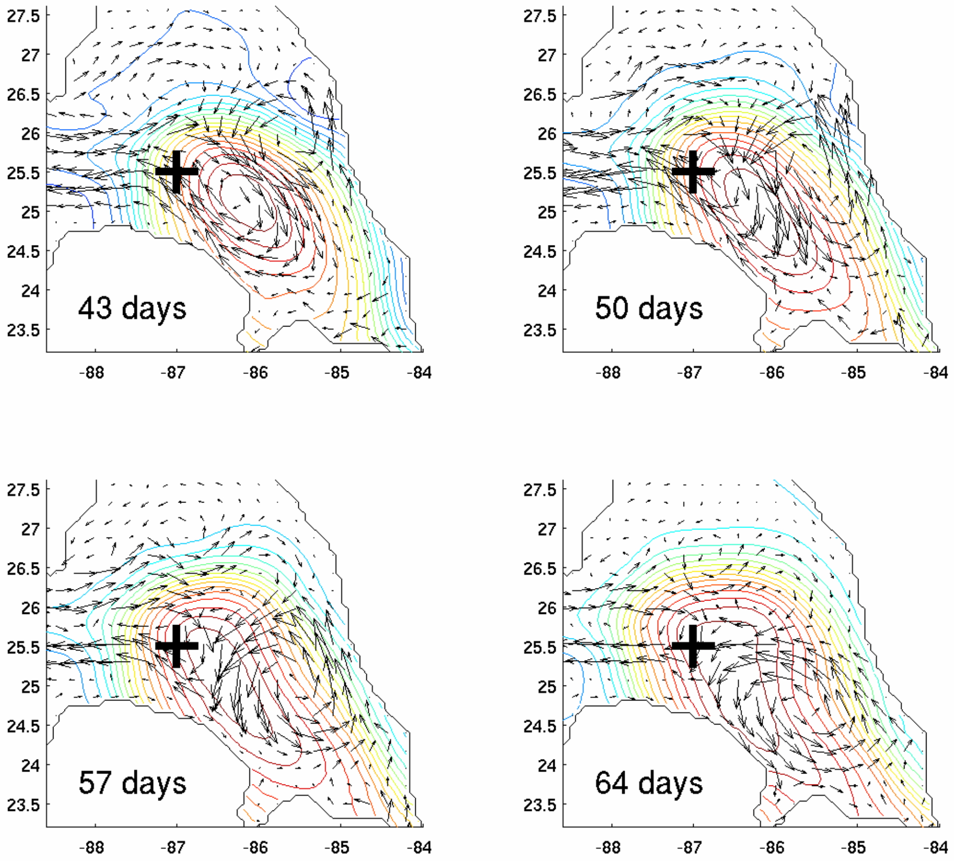

Figure 4-2. Contours of stream function and velocity vectors at level 70 centered at 2850 m extending from 2560 m to 2600 m for model days, 43, 50, 57, and 64. The '+' indicates the location of the mooring.

The northward extension of the LC has increased on Day 50 in Figure 4-1, the greater part of the flow has moved slightly westward, and a definable center of circulation has formed. The lower layer eddy has become much better defined in Figure 4-2 and the upper and lower layer flows are still in phase in the vicinity of the mooring location. As the LC moves over the mooring location on Day 57 in Figure 4-1, the currents weaken in the upper layer. Meanwhile in the lower layer, there has been a transfer of energy from the anticyclone that was just to the south of the mooring location on Day 50 in Figure 4-2 to the weak anticyclone just north of the mooring location. The anticyclone to the south moves north and a cyclone begins to form in the southernmost portion of the eastern basin.

On Day 64, the center of the LC has moved directly over the mooring location in Figure 4-1 and weak surface currents are observed at the mooring site. The anticyclonic eddy in the deep layer has moved north of the mooring location and southward flow is observed at the mooring location (Figure 4-2). On Day 50, the deep cyclonic eddy is beginning to form just east of the mooring location. On Day 64, the LC ring is about to pass over the mooring site (Figure 4-1) while the trailing edge of the deep anticyclone followed by the leading edge of the deep cyclone begins to arrive at the mooring site, giving rise to the appearance of southward current in deep water.

The sequence of the events described above fits nicely into the conservation of potential vorticity mechanism of Cushman-Roisin et al. (1990) noted by Welsh and Inoue (2000) to explain the prevalence of a modon-pair underneath the LC ring in the eastern GOM. The conservation of potential vorticity requires that the lower-layer response to vortex squeezing/stretching of the lower-layer due to the changes in the upper-layer thickness would result in the acquisition of respective relative vorticity (negative/positive) for the lower-layer. As the upper-layer anticyclone propagates, it changes the thickness of the lower-layer. The lower-layer shrinks ahead of the upper-layer anticyclone, and it stretches behind the upper-layer anticyclone. Consequently, a lower-layer anticyclone forms ahead of the upper-layer anticyclone, and a lower-layer cyclone forms behind it. Utility of a two-layer system is clearly indicated by the observations at the mooring site. Furthermore, current in the lower layer below the interface behaves nearly barotropic, i. e., magnitude and direction of currents do not change throughout the lower layer below the interface all the way to the bottom. It should be noted that this is what would be expected based on the conservation of potential vorticity mechanism.

Figure 4-3 shows simulated current vectors from the high-resolution model at near-surface (10 m) and deepwater (2580 m). The near-surface currents are dominated by quasi-regular formation of LC rings while deepwater is characterized by shorter timescales. A major discrepancy in simulation compared to the observation has been that the simulated LC sheds off rings at too regular intervals while the observations suggest more variable LC ring formation (Leben, 2005; Lugo-Fernandez, 2007). Perhaps, external influence such as rings migrating from the Caribbean Sea gives rise to more chaotic behavior of actual LC in the eastern GOM (Oey, 2004). Simulated currents from Years 9 and 10 yield mean currents of northeasterly direction (mean U = 17.3 cm s^{-1}, mean V = 13.6 cm s^{-1}) at 10 m and northwesterly direction (mean U = -2.8 cm s^{-1}, mean V = 1.1 cm s^{-1}) at 2580 m. These are comparable to what was observed (Table 2-4) except for significantly reduced energy level in the model deepwater, suggesting that the friction coefficients used in the model are still too high.

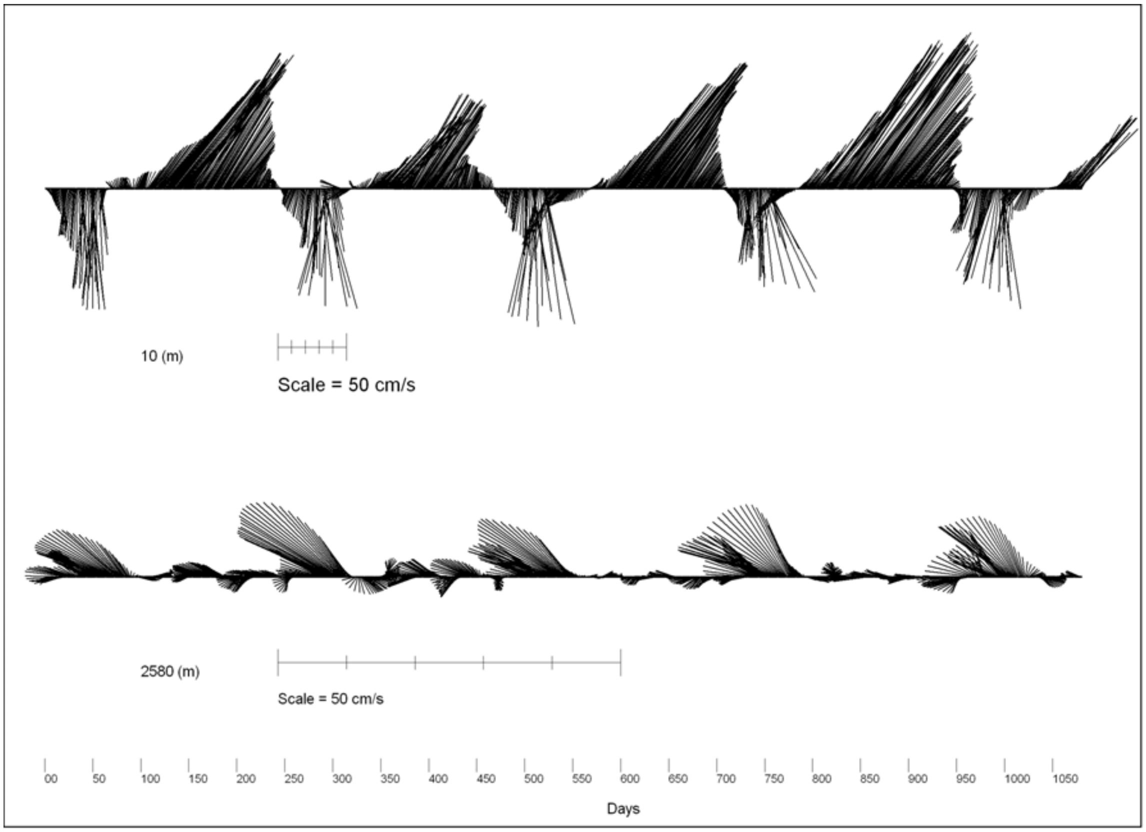

Figure 4-3. Simulated current vectors during Years 9-11 from the high-resolution model of GOM for the indicated depths.

Despite relatively homogenous water mass characteristics in deepwater in the eastern GOM, water mass properties measured at the mooring site displayed notable variations associated with energetic flow regimes observed. Model simulations suggest that eddy-like features that populate the model deepwater eastern GOM may be associated with horizontal advection of temperature and salinity gradients expected in the region. Figure 4-4 shows three-year average model temperature and salinity fields at 2200 m together with the average current velocity vectors at the same depth. Companion density field is shown in Figure 4-5. Deepwater on the Caribbean side of the Yucatan Channel is significantly saltier and colder, consequently heavier than deepwater on the GOM side. As this colder and saltier Caribbean deepwater flows into the eastern GOM, it immediately sinks. As this sinking Caribbean inflow begins to turn into the counterclockwise deepwater circulation noted by DeHaan and Sturges (2005), it mixes gradually with the surrounding deepwater in the eastern GOM. Consequent equilibration of density gives rise to saltier and warmer tongue of continuing Caribbean inflow which tends to hug the slope water off the Florida shelf. Superposition of eddy field on the resulting temperature and salinity gradients in the eastern GOM could give rise to notable temperature and salinity signal associated with energetic events observed at the mooring site. It should be noted that unlike temperature and salinity gradients that suggest westward penetration of the Caribbean inflow and gradual mixing with the surrounding deepwater in GOM, corresponding density gradients runs from north to south, i. e., deepwater becomes lighter as you move southward. This is consistent with the idea of counterclockwise deepwater circulation described by DeHaan and Sturges (2005).

Although a two-layer system is a good approximation for the eastern GOM, there are subtle but important differences in flow regime in deepwater above and below the sill depths in Yucatan Channel (~1900 m). Figure 4-6 shows three-year average model density field above (1800 m) and below (2200 m) the sill depths. Density field at 1800 m clearly indicates that it is dictated by the LC in the eastern GOM while at 2200 m, it reflects counterclockwise deepwater circulation.

4.3 Interpretation of Observations

In the light of deepwater circulation simulated in the model, an attempt is made here to interpret the observations at the mooring site. It appears that deepwater currents observed at the mooring site could be interpreted as manifestations of the simulated deepwater flow. The general northwestward deepwater mean flow pattern measured at the mooring site for each of the three deployments fits nicely into the similar northwestward flow simulated in deepwater in the model. The three most energetic events in deepwater observed could be interpreted as manifestation of anticyclones formed in deepwater as part of a modon pair underneath the LC rings. In particular the strong northward currents captured by the mooring could be associated with the anticyclonic circulation of the deep anticyclone. The dominance of these energetic northward flow events captured by the mooring results in the general northward mean currents observed in deepwater at the mooring site.

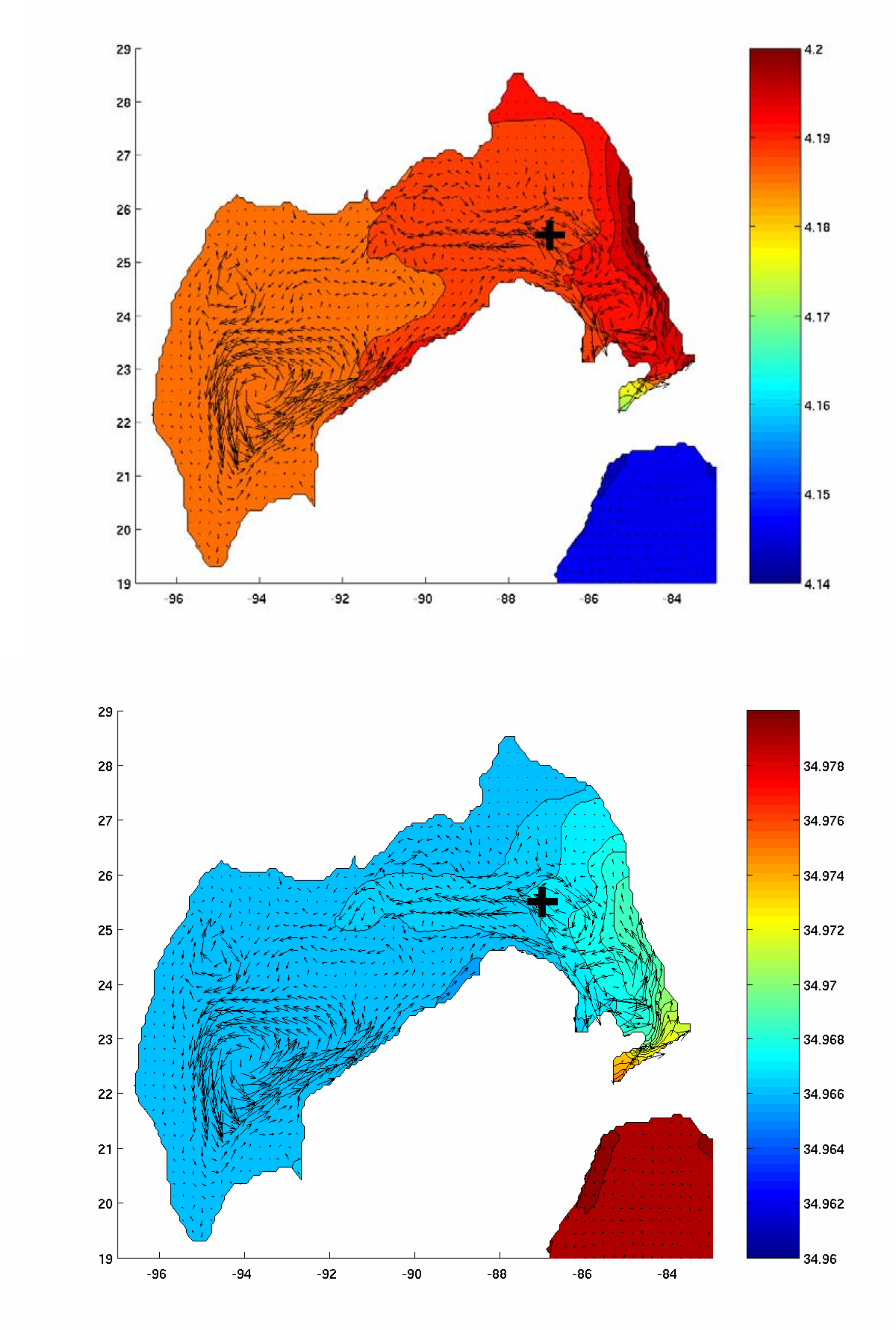

Figure 4-4. 3-year average model temperature (top) and salinity field (bottom) at 2200 m. The velocity vectors are drawn at every third grid point.

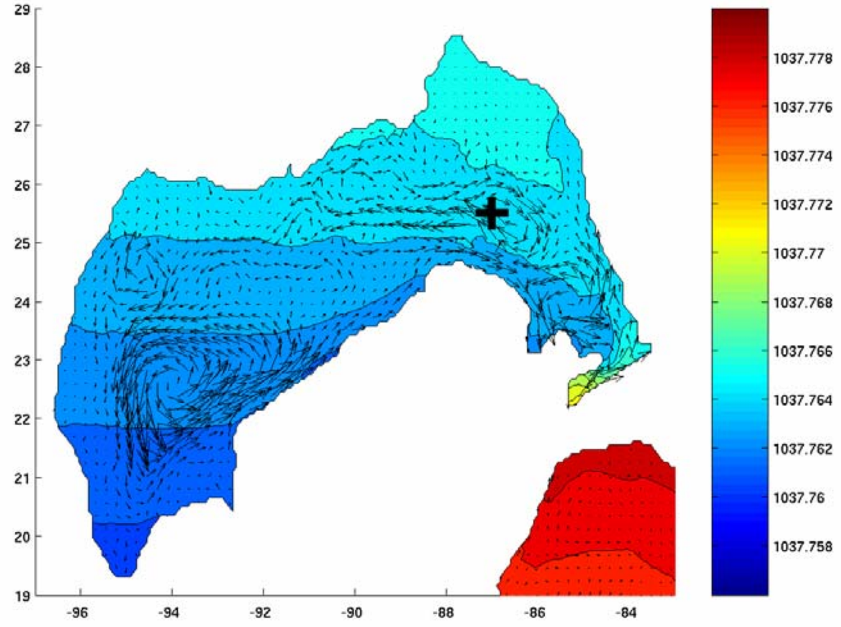

Figure 4-5. 3-year average model density field at 2200 m. The velocity vectors are drawn at every third grid point.

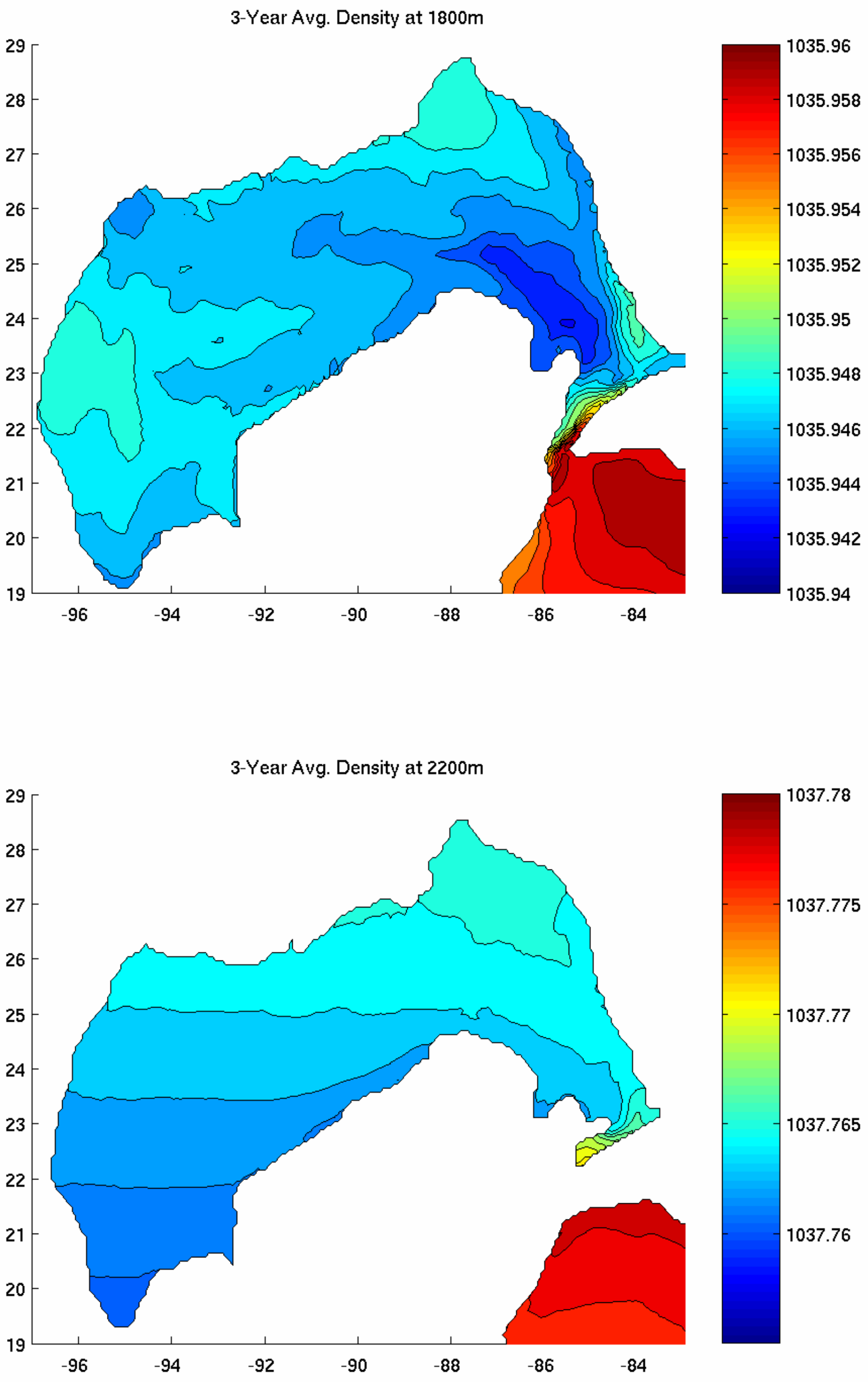

Figure 4-6. The 3-year average model density field at 1800 m (top) and 2200 m (bottom).

A question arises as to why the energetic northward flow was not always followed by southward flow as the deep anticyclone and the following cyclone pass by the mooring site as depicted by the model simulation. One explanation could be that as evident in Figures 4-2, relatively compact size of the deep anticyclone and the cyclone makes model representation of deepwater flow in the eastern GOM quite sensitive to the model representation (both horizontal as well as vertical) of bottom topography. This, in turn, impacts accurate simulation of deepwater flow at the mooring site in the model. Moreover, nearly regular formation of LC rings in the model compared to more chaotic eddy formation observed in the real eastern GOM (Leben 2005; Lugo-Fernandez, 2007), results in more regular deep eddy dynamics in the model. Also, the friction coefficients used in the high-resolution model are still too high leading to the subdued simulated model deepwater flow.

A major finding from the mooring data is a disparity in dominant time scales between the upper-layer and lower-layer flows. In analyzing model output from the high-resolution model, it became apparent that the bottom topographic constriction located between the eastern and central basins poses formidable challenge to any deepwater eddies migrating westward from the eastern GOM. Figure 4-7 shows a sequence of stream function which is a good indicator of the upper-layer flow and current velocity vectors at 2200 m from the high-resolution model. Narrowness of the bottom topographic constriction relative to the size of typical deepwater eddies formed underneath the LC in the eastern GOM gives rise to energetic eddy-topographic interaction as deepwater eddies try to squeeze through the bottom topographic constriction on their westward journey into the central gulf . Consequently, deformation, and even breakup of deepwater eddies are common. An end result is that size of deepwater eddies in the vicinity of the mooring site would be smaller than the case when there were no bottom topographic constriction.

In order to test this hypothesis, two additional model simulations were conducted using the coarse-resolution model, one with realistic bottom topography and the other with flat bottom topography (without the prominent bottom topographic constriction) (for details of the model setups, please refer to Appendix). Figure 4-8 shows simulated current vectors at 2800 m at the mooring site for the coarse-resolution model of GOM with the realistic bottom topography and with the flat bottom topography. It is evident that in flat-bottom case, deepwater currents exhibit more regular wave-like features reflective of a modon pair expected in deepwater. In contrast, in realistic-bottom case, deepwater currents are more irregular and less wave-like. Figure 4-9 shows current spectra in variance preserving form, for simulated current components at 2800 m at the mooring site for the coarse-resolution model with the flat bottom and with the realistic bottom topography. In the flat-bottom case, deepwater is much more energetic than the realistic-bottom case. Moreover, the primary peak is located near 80-day period, reflecting temporal scale of deepwater eddies (modon pairs) formed in the eastern GOM. There is a secondary peak near 30-40 day range. In the realistic-bottom case, the primary energy peak shifts to 30-40 day range, a characteristic time scale associated with smaller deepwater eddies generated by the deformation and breakup of deepwater eddies initially formed below the LC rings and perhaps TRWs noted previously by Oey and Lee (2002).

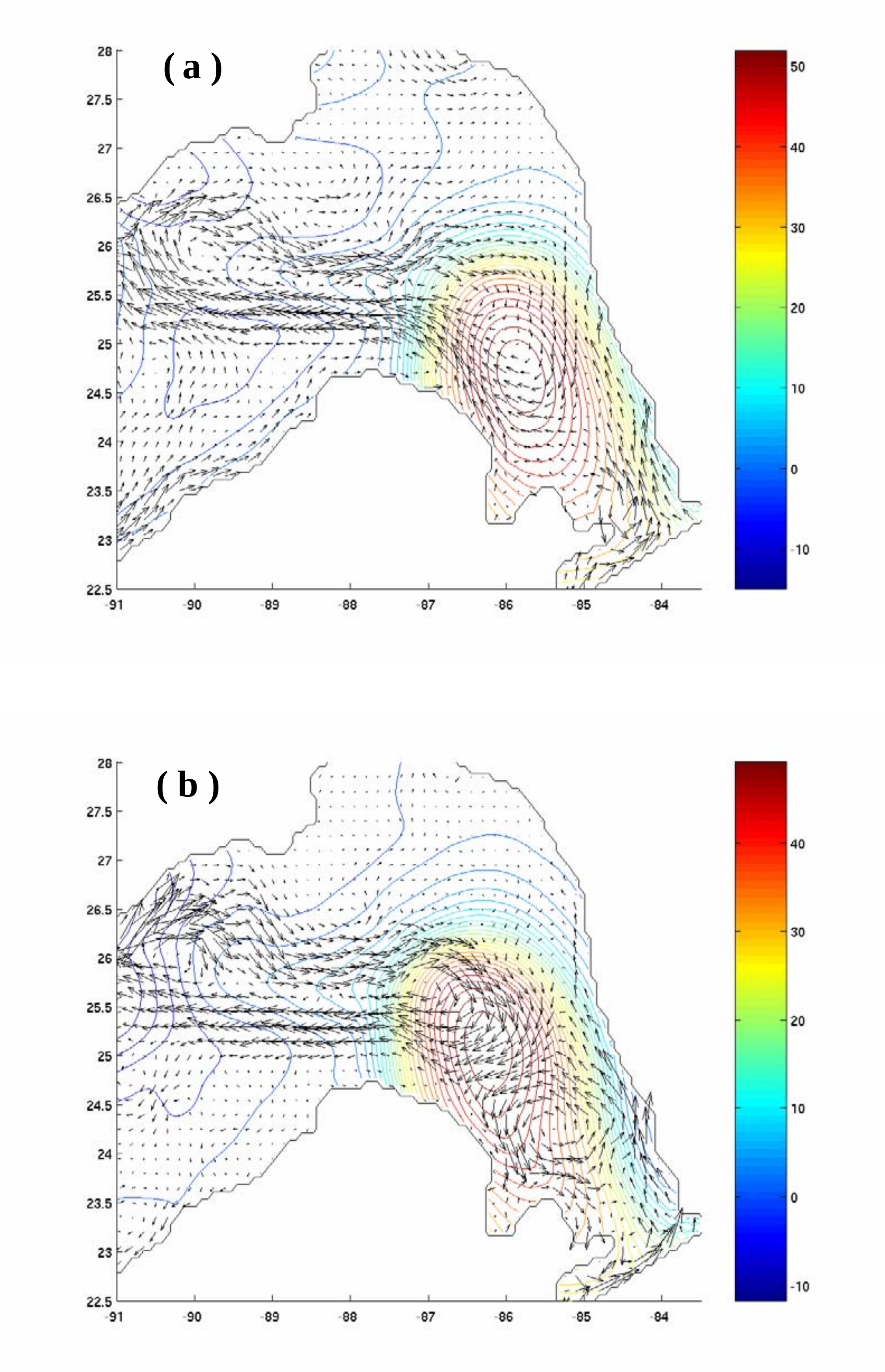

Figure 4-7. A sequence of stream function and velocity vectors at 2200 m from the high resolution model for days (a) 241, (b) 271, (c) 301, (d) 331, (e) 361, and (f) 391.

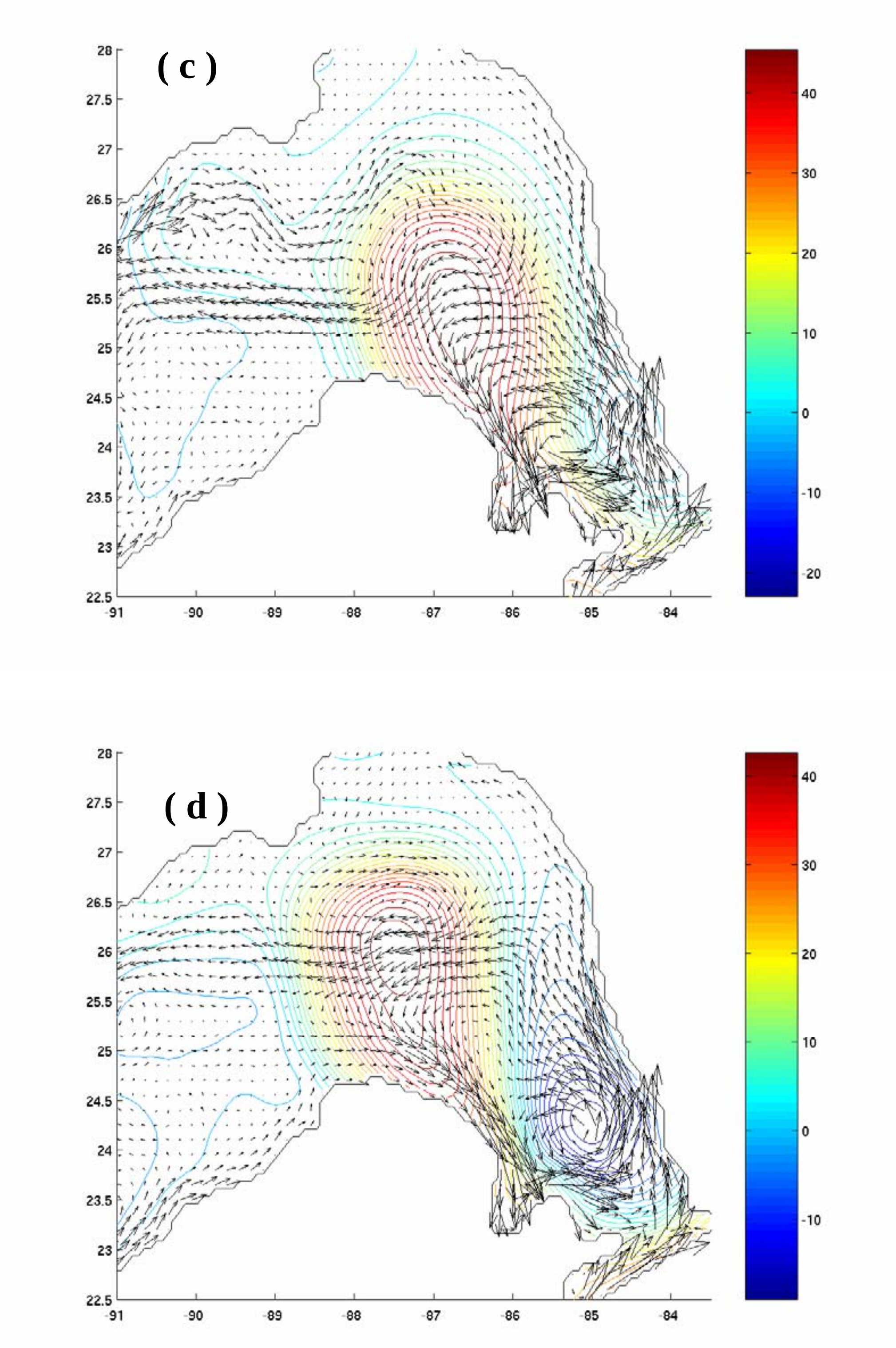

Figure 4-8. A sequence of stream function and velocity vectors at 2200 m from the high resolution model for days (a) 241, (b) 271, (c) 301, (d) 331, (e) 361, and (f) 391 (continued).

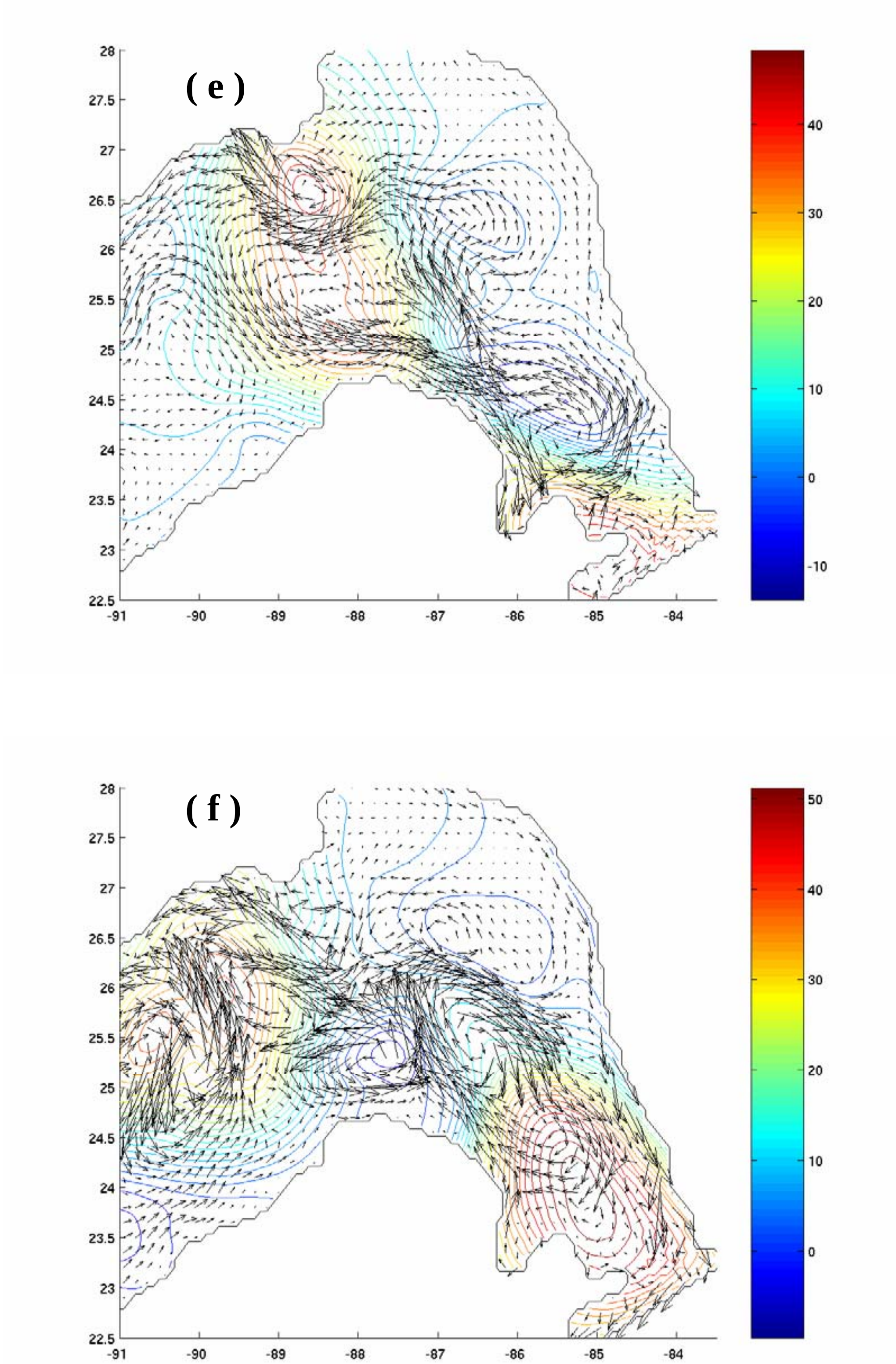

Figure 4-9. A sequence of stream function and velocity vectors at 2200 m from the high resolution model for days (a) 241, (b) 271, (c) 301, (d) 331, (e) 361, and (f) 391 (continued).

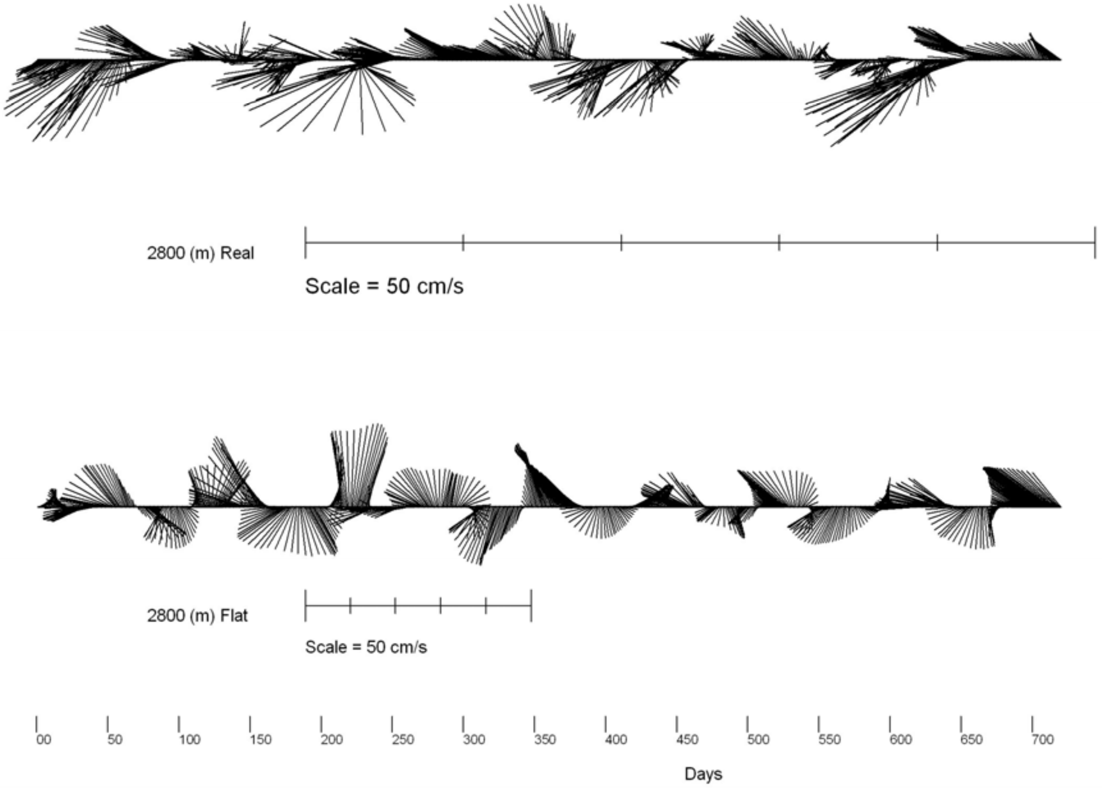

Figure 4-10. Simulated current vectors at 2800 m at the mooring site for the coarse-grid model of GOM with the realistic bottom topography (top) and with the flat bottom topography (bottom).

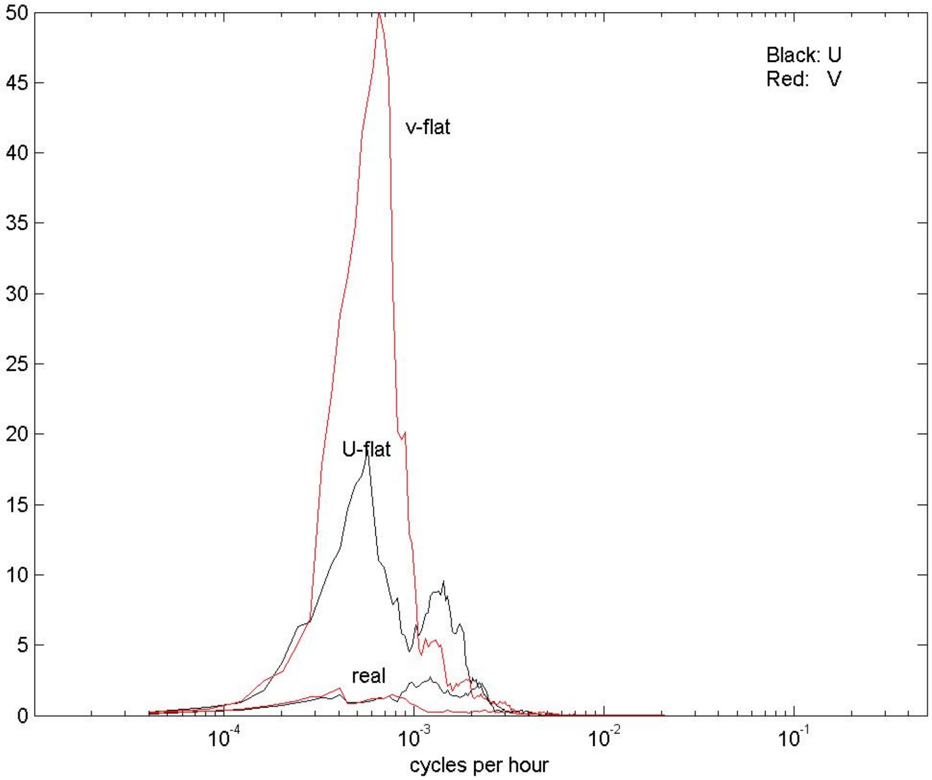

Figure 4-11. Current spectra in variance preserving form, for simulated (daily-sampled) current components at 2800 m at the mooring site for the coarse-grid model of GOM with flat bottom and with realistic bottom topography. For each case, two year records were used.

The presence of bottom topographic constriction reduces westward penetration of eddy kinetic energy into the central and western basins (Figure 4-10). Without this constriction, most of eddy kinetic energy could easily penetrate into the central and western basins. In contrast, in the realistic-bottom case, significant portion of eddy kinetic energy is trapped in the eastern GOM and a reduced amount of eddy kinetic energy ended up in the central and western basins. Distribution of eddy kinetic energy in the realistic-bottom case looks very similar to the lower-layer kinetic energy in the 20-100-day periods identified by Oey and Lee (2002) in their model study of GOM, because of the dominance of low-frequency variability in deepwater. In their analysis, Oey and Lee (2002) concluded that interaction of the LC and the bottom topography in the eastern gulf results in the generation of TRWs that propagate into the northern slope water region in the central GOM. There is no doubt that some of the kinetic energy trapped in the eastern gulf by the topographic constriction is converted into TRWs with some of the remaining kinetic energy is converted into smaller deepwater eddies that would propagate into the central and western basins. It is interesting that at the mooring site, kinetic energy levels in the lower layer remain nearly unchanged with depth, and do not appear to suggest bottom trapping of kinetic energy characteristic of TRWs (see Table 2-4).

4.4 Summary

The first observations of the upstream conditions in the middle of the eastern GOM with an emphasis on deepwater flow underneath the LC revealed that a two-layer approximation is a reasonable way to characterize currents at the mooring site with the interface located near 700-800 m. The upper-layer currents are dominated by the LC and LC rings while generally the upper- and lower-layer currents appear to be decoupled except occasional establishment of coupling between the two layers. Deepwater in the eastern GOM is energetic and barotopic throughout the lower layer, and it appears to be driven by the LC and LC rings. Deepwater at the mooring site appears to be relatively energetic characterized by 40-50 day variability with 10-30 cm s^{-1} currents. Short-duration energetic events lasting a few days could result in strong deepwater currents exceeding 1 knot all the way to the bottom. These energetic events in deepwater appear to take place when the LC makes notable northward extension preceding the formation of LC rings. Deepwater currents at the mooring site appear to be the manifestations of a modon pair which forms underneath a LC ring in the eastern GOM. Shorter time scales associated with deepwater flow at the mooring site is a reflection of smaller deepwater eddies resulting from deepwater eddies interacting with the bottom topographic constriction located between the eastern and the central gulf. Every one of the three deployments turned out to be unique, confirming the previous observation that every LC ring formation is unique and a long-term measurement is required in order to establish basic statistics of ocean dynamics in the eastern GOM.

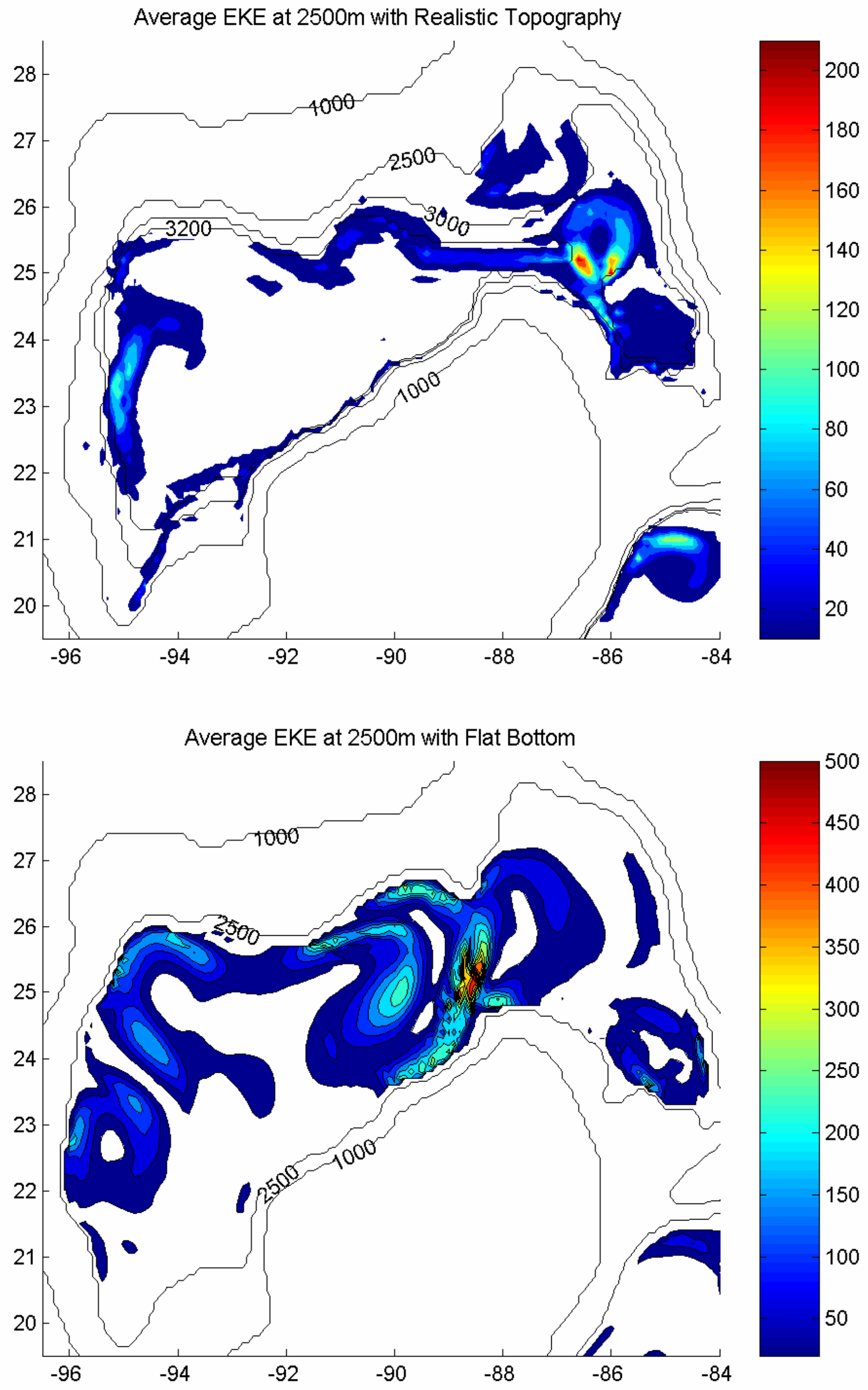
Average EKE at 2500m with Realistic Topography

Average EKE at 2500m with Flat Bottom

Figure 4-12. The average eddy kinetic energy computed with 3 years of daily model output at 2500 m depth for (top) the course grid model with realistic bottom topography and (bottom) the course grid model with a flat bottom. The labels for the bathymetric contours are in meters. See the appendix for details of the model configuration.

CHAPTER 5

REFERENCES

Bryan, K. 1969. A numerical model for the study of the world ocean. J. Comput. Phys., 4:347-376.

Buerkert, T.P. 1997. Barium in water and foraminiferal shells: Indicators of present and past oceanographic conditions in the Gulf of Mexico. Ph. D. dissertation. Louisiana State University, Baton Rouge, LA.

Bunge, L., J. Ochoa, A. Badan, J. Candela, and J. Sheinbaum. 2002. Deep flows in the Yucatan Channel and their relation to changes in the Loop Current extension. J. Geophys. Res., 107:3233, doi:10.1029/2001JC001256.

Carney, R.S. 1996. Addressing the ecological unknowns of deep water oil and gas development. Deepwater 1996 Information Transfer Meeting Presentations. U.S. Dept. of the Interior, Minerals Management Services, Gulf of Mexico OCS Region, New Orleans, LA.

Cherubin, L.M., W. Sturges, and E.P. Chassignet. 2005. Deep flow variability in the vicinity of thye Yucatan Straits from a high-resolution numerical simulation. J. Geophys. Res., 110: C04009, doi:10.1029/2004JC002280.

Conkright, M.E., S. Levitus, T. O'Brien, T.P. Boyer, C. Stephens, D. Johnson, L. Stathoplos, O. Baranova, J. Antonov, R. Gelfeld, J. Burney, J. Rochester, & C. Forgy. 1998. *World Ocean Database 1998* Documentation and Quality Control. National Oceanographic Data Center, Silver Spring, MD.

Cox, M.D. 1984. A primitive equation three-dimensional model of the ocean, Tech. Rep. 1, GFDL, NOAA, Princeton Univ., Princeton, N. J.

Cushman-Roisin, B., E.P. Chassignet, and B. Tang. 1990. Westward motion of mesoscale eddies. J. Phys. Oceanogr., 20:758-768.

DeHaan, C.J., and W. Sturges. 2005. Deep cyclonic circulation in the Gulf of Mexico. J. Phys. Oceanogr., 35:1801-1812.

Hamilton, P. 1990. Deep currents in the Gulf of Mexico. J. Phys. Oceanogr., 20:1087-1104.

Hamilton, P. and A. Lugo-Fernandez. 2001. Observations of high speed deep currents in the Northern Gulf of Mexico. Geophys. Res. Letters, 28:2,867-2,870.

Hamilton, P. 2007. Deep-current variability near the Sigsbee Escarpment in the Gulf of Mexico. J. Phys. Oceanogr., 37:708-726.

Hellerman, S., and M. Rosenstein. 1083. Normal monthly wind stress over the world ocean with error estimates, J. Phy. Oceangr., 13:1093-1104.

Hoffmann, E.E., and S.J. Worley. 1986. An investigation of the circulation of the Gulf of Mexico. J. Geophys. Res., 91:14,221-14,236.

Hurlburt, H.E., and J.D. Thompson. 1982. The dynamics of the Loop Current and shed eddies in a numerical model of the Gulf of Mexico. In: Nihoul, J.C.J., ed. Hydrodyanmics of Semi-enclosed Seas. New York: Elsevier Science. Pp.243-298.

Leben, R.R. 2005. Altimeter-derived Loop Current metrics. Circulation in the Gulf of Mexico: Observations and Models. In: Sturges, W. & A. Lugo-Fernandez, eds. Circulation in the Gulf of Mexico: Observations and Models. Geophys. Monogr., Vol. 161, Amer. Geophys. Union. Pp.181-201.

Lugo-Fernandez, A. 2007. Is the Loop Current a chaotic oscillator? J. Phys. Oceanogr., 37:1455-1469.

McLellan, H.J. and W.D. Nowlin. 1963. Some features of the deep water in the Gulf of Mexico. J. Mar. Res., 21:233-245.

Oey, L.-Y. 1996. Simulation of mesoscale variability in the Gulf of Mexico: Sensitivity studies, comparison with observations, and trapped wave propagation. J. Phys. Oceanogr., 26:145-175.

Oey, L.-Y. 2004. Vorticity flux through the Yucatan Channel and Loop Current variability in the Gulf of Mexico. J. Geophys. Res., 109:C10004, doi:10.1029/2004JC002400.

Oey, L.-Y., and H.-C. Lee. 2002. Deep eddy energy and topographic Rossby waves in the Gulf of Mexico. J. Phys. Oceanogr., 32:3499-3527.

Oey, L-Y., T. Exer, and H.-C. Lee. 2005. Loop current, rings and related circulation in the Gulf of Mexico: A review of numerical models and future challenges. In: Sturges, W. & A. Lugo-Fernandez, eds. Circulation in the Gulf of Mexico: Observations and Models, Geophys. Monogr., Vol. 161, Amer. Geophys. Union. Pp.31-56.

Pacanowski, R., K. Dixon, and A. Rosati. 1991. The GFDL Modular Ocean Model users guide version 1.0, GFDL Ocean Group Tech. Rep. 2, Princeton, NJ.

Romanou, A., E.P. Chassignet. 2004. Gulf of Mexico circulation within a high-resolution numerical simulation of the North Atlantic Ocean. J. Geophys. Res., 109:C01003, doi:10.1029/2003JC001770.

Smith, W.H.F., and D.T. Sandwell. 1997. Global sea floor topography from satellite altimetry and ship depth soundings, Science, 277:1956-1962.

Sturges, W. and R. Leben. 2000. Frequency of ring separation from the Loop Current in the Gulf of Mexico: A revised estimate. J. Phys. Oceanogr., 30:1814-1819.

Sturges, W., J.C. Evans, S. Welsh, and W. Holland. 1993. Separation of warm-core rings in the Gulf of Mexico. J. Phys. Oceanogr., 23:250-268.

Vukovich, F.M. and B.W. Crissman. 1986. Aspects of warm rings in the Gulf of Mexico. J. Geophys. Res., 91:2645-2660.

Vukovich, F.M. 2007. Climatology of ocean features in the Gulf of Mexico using satellite remote sensing data. J. Phys. Oceanogr., 37:689-707.

Weatherly, G.L., N. Wienders, and A. Romanou. 2005. Intermediate-depth circulation in the Gulf of Mexico estimated from direct measurements. In: Sturges, W. & A. Lugo-Fernandez, eds. Circulation in the Gulf of Mexico: Observations and Models. Geophys. Monogr., Vol. 161, Amer. Geophys. Union. Pp.315-324.

Welsh, S.E. 1996. A numerical modeling study of the Gulf of Mexico during present and past environmental conditions. Ph. D. dissertation, Louisiana State University, Baton Rouge, LA.

Welsh, S.E., and M. Inoue. 2000. Loop Current rings and the deep circulation in the Gulf of Mexico. J. Geophys. Res., 105(C7):16,951-16,959.

Welsh, S.E., and M. Inoue. 2002. Lagrangian study of the circulation, transport, and vertical exchange in the Gulf of Mexico: Final report. U.S. Dept. of the Interior, Minerals Management Service, Gulf of Mexico OCS Region, New Orleans, LA. OCS Study MMS 2002-064.51 pp.

CHAPTER 6

APPENDIX

DESCRIPTION OF MODEL USED

The numerical model employed in both the coarse grid and the fine grid simulations is MOM1 (Pacanowski et al. 1991), which was introduced by Bryan (1969) and programmed by Cox (1984). This model has also been referred to as the "Bryan-Cox Model" and the GFDL model. MOM1 has been used previously to simulate circulation in the GOM (Sturges et al., 1993; Welsh, 1996; Welsh and Inoue, 2000).

In this study, all model simulations are initialized with the annual averages of the 3-D temperature and salinity fields derived from the Global Ocean Temperature and Salinity Data (Conkright et al. 1998). Level 1 temperature and salinity fields are restored to seasonal climatology with a relaxation time scale of 6 weeks in the coarse resolution case and 13 weeks in the fine resolution case. This surface boundary condition allows for surface heat and moisture fluxes, which should be close to real surface fluxes. An internal boundary condition is used to simulate the seasonally varying geostrophic flow through the Caribbean Sea, thus forcing the inflow to the GOM. The desired vertical density structure is produced by relaxing the temperature and salinity to climatology at all grid points along a N-S transect in the Caribbean. The location of the N-S transect is farther to the east in the fine grid case, which has a much larger domain. A constant is added to the u-component of velocity at every grid point along this same transect to reach a target value of 28 Sv for the annual-mean volume transport through the Yucatan Channel. The surface wind stress field is derived from the Hellerman and Rosenstein (1983) normal monthly wind stress climatology. Wind stress is applied over the entire GOM and in the Caribbean to the west of the geostrophic forcing region.

A.1 Coarse Resolution Simulations

A.1.1 Realistic Bathymetry

The coarse resolution grid is derived from the ETOP05 world topography data set. The bathymetric values are linearly interpolated to 0.1° and smoothed to prevent topographically induced $2\Delta x$ noise in the numerical solution. The model domain extends from 98.0°W to 72.0°W and from 15.0°N to 31.0°N (top figure in Figure A-1). The model grid has lateral dimensions of 280 by 161. There are 20 levels in the vertical with a maximum depth of 3850 m. The use of evenly spaced vertical levels is preferred to reduce the error in the finite difference formulation of the vertical velocity. Greater resolution is needed near the surface for more accurate representation of the shelf bathymetry and to resolve the thermocline. Therefore, the thickness of each of the upper 3 levels is 25 m, while the lowest 10 levels are each 300-m thick, and the transition region from level 4 through 10 gradually increases in thickness. The model domain extends outside the GOM into a synthetic return flow region that links the Straits of

Florida with the western Caribbean. The bathymetry in the return flow region is altered to allow flow exiting the GOM to re-circulate around Cuba and enter the GOM through the western Caribbean.

A.1.2 Flat Bottom

There is a constriction in the bottom bathymetric contours centered at approximately 88°W and 25.5°N that divides the deep eastern basin from the central and western basins. Animations of the deep circulation from the coarse grid simulations indicate that this constriction has a profound impact on the westward propagation of deep cyclones and anticyclones, although the impact differs for the two different classes of deep eddies. There is a transformation in the shape of the deep eddies as they pass through the constriction. Although it was obvious that propagation of eddies would be considerably different without the constriction, what was the control of the constriction on the upper layer circulation? An experiment was designed to determine the effect of removing the constriction on both the deep circulation and the formation and propagation of Loop Current rings in the surface layer.

The constriction extends zonally from 88.5˚W to 86.5˚W and is constrained on the south side by the base of the escarpment near 26˚and by the 3200 m isobath on the northern side (Figure A-2). The grid was altered in order to remove the constriction as objectively as possible without changing the general shape of the deep basins (bottom figure in Figure A-1). The two bottommost levels were removed, thereby reducing the total number of levels to 18 and the maximum depth to 3250 m. Vertical levels 16 and 17 were set equal to 18, which further reduced the effect of the constriction. A side effect of this latter change was to artificially create straight walls from 2350 m to 3250 m.

The flat bottom simulations were initialized identically to the realistic bathymetry case and all of the model parameters remain unchanged. The surface forcing and the internal forcing were also treated identically. There was a difference in the number of years of spin-up between the realistic bathymetry cases and the flat bottom cases. The realistic bathymetry case was spun-up for 19 years, during which time adjustments were continuously being made to the model parameters. Then the model was spun-up for another 4 years without any changes to the model parameters and the production runs began with year 24. The flat bottom model was spun-up for 8 years using the same parameters as were selected for the production runs of the realistic bathymetry case and then the model was run for another 3 years for analysis (years 9, 10 and 11). The mean transport through the Yucatan Channel for the realistic bathymetry simulations for years 24 through 27 was 28.0 Sv, whereas the mean transport for the flat bottom simulations for years 9 through 11 was 28.3 Sv. The difference of 1% in the 3-year mean transports should have had negligible impact on the behavior of the LC system.

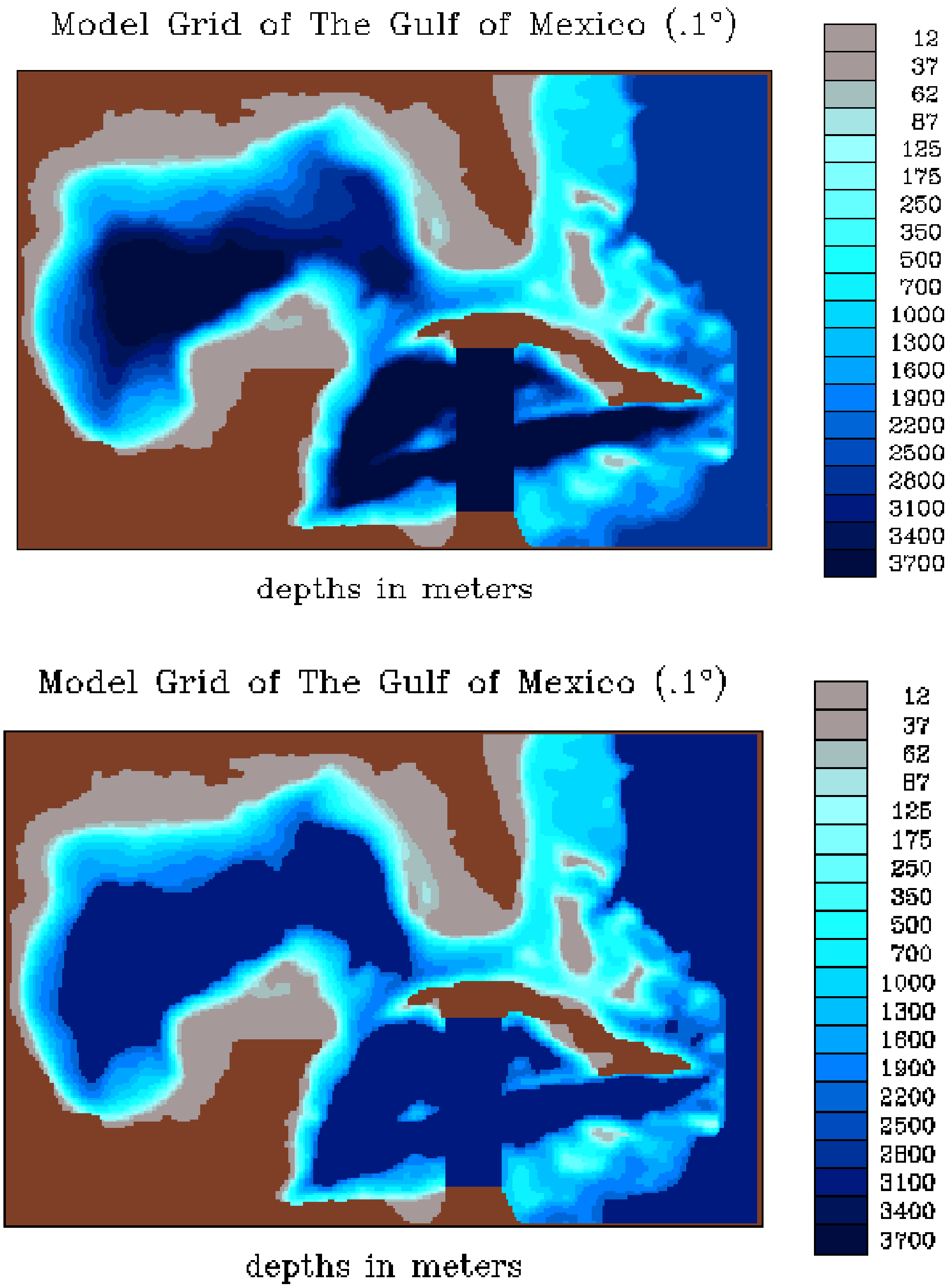

Figure A-1. Coarse resolution model grids of the Gulf of Mexico and Caribbean using 0.1° grid spacing in the horizontal. The realistic bathymetry grid features 20 vertical levels (top) and the flat bottom grid features 18 vertical levels (bottom). The depths of each vertical levels corresponds to the colorbars on the right.

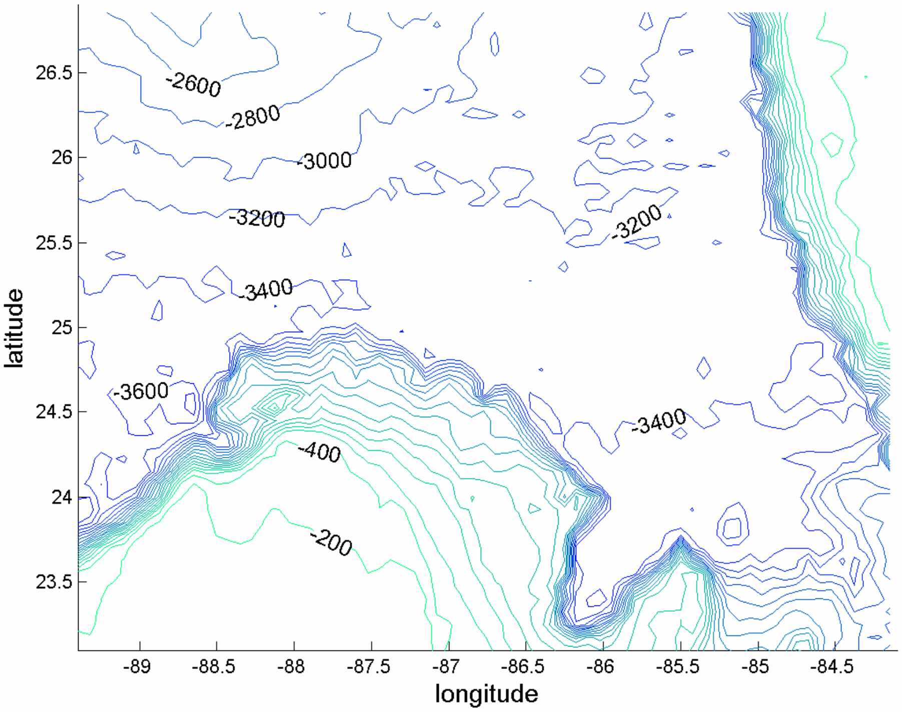

Figure A-2. Bathymetry of the deep eastern GOM in meters using the Etopo2 2-minute horizontal resolution bathymetric data set.

A.2 High Resolution Simulations

The coarse grid model was able to simulate realistic upper level circulation features with temporal and spatial scales which are comparable to observations. Great attention was given to correctly reproducing the observed physical characteristics and behavior of the model LC, as well as the shedding and westward migration of LC rings. The model deep circulation was strongly coherent in the vertical below the interface, as observed in deep current meters records and other numerical models of the GOM. Analysis of the deep model circulation indicated that the bottom bathymetry was strongly influencing the behavior of the deep eddies. Consequently, in order to better understand the current-topographic interactions in the deep, a model was developed with a much higher vertical and horizontal resolution and a larger domain. We were especially interested in resolving small-scale bottom topographic features, such as a narrow deep constriction separating the eastern and the central basins.

The high resolution grid was derived from the Global Sea Floor Topography featuring 2 minute horizontal spacing (Smith and Sandwell 1997). The model grid has 0.075° horizontal resolution and 100 vertical levels. In the upper 200 m, the vertical levels are 20-m thick and the remaining 90 levels are each 40-m thick. The geographic boundaries of the model domain are 97.7°W:58.1°W and 9.1°N:30.85°N, which includes the entire Caribbean (Figure A-3). The geostrophic forcing region, which was moved farther east, is centered at 66°W, and accounts for all total transport through the Greater and Lesser Antilles. Southward flow is also forced at the Windward Passage and the Anegada-Jungfern Passages to account for inflow to the Caribbean from the north. The purpose of moving the geostrophic forcing region to the east, forcing inflow through the northern passages, and applying the wind forcing over a larger area is to enable the generation of mesoscales eddies that form south of Hispaniola. These eddies contribute to the vorticity of the Yucatan and Loop Current system and may play a role in the separation and reattachment of Loop Current Rings.

Although very fine horizontal and vertical resolutions should allow for lower friction, the optimum values for viscosity and diffusivity in the fine resolution simulations are 65 m^2s^{-1}, which is in fact slightly higher than the coarse grid simulations, which used 55 m^2s^{-1}. The need for slightly higher values for the frictional coefficients arose when the model velocity field became unstable below the LC on the west Florida slope at 1600 m depth in model year 8. The instability appeared to result from topographically-induced numerical noise at a time when the maximum speed in the surface layer directly above exceed 140 $cm \cdot s^{-1}$. Year 8 was restarted at the beginning with the higher values for viscosity and diffusivity and then run for 4 years without producing any model instabilities.

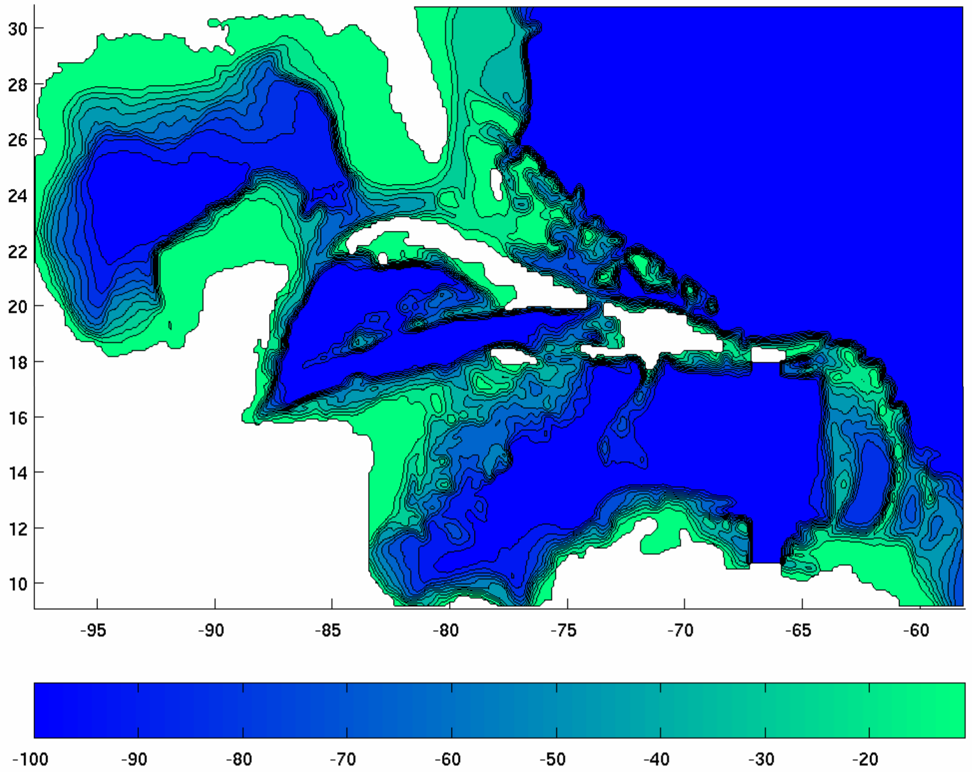

Figure A-3. High resolution model grid of the Gulf of Mexico and Caribbean using 0.075° grid spacing in the horizontal and 100 levels in the vertical. The 10 solid contour lines excluding the coastline represents every 10th vertical grid level.

The Department of the Interior Mission

As the Nation's principal conservation agency, the Department of the Interior has responsibility for most of our nationally owned public lands and natural resources. This includes fostering sound use of our land and water resources; protecting our fish, wildlife, and biological diversity; preserving the environmental and cultural values of our national parks and historical places; and providing for the enjoyment of life through outdoor recreation. The Department assesses our energy and mineral resources and works to ensure that their development is in the best interests of all our people by encouraging stewardship and citizen participation in their care. The Department also has a major responsibility for American Indian reservation communities and for people who live in island territories under U.S. administration.

The Minerals Management Service Mission

As a bureau of the Department of the Interior, the Minerals Management Service's (MMS) primary responsibilities are to manage the mineral resources located on the Nation's Outer Continental Shelf (OCS), collect revenue from the Federal OCS and onshore Federal and Indian lands, and distribute those revenues.

Moreover, in working to meet its responsibilities, the **Offshore Minerals Management Program** administers the OCS competitive leasing program and oversees the safe and environmentally sound exploration and production of our Nation's offshore natural gas, oil and other mineral resources. The MMS **Minerals Revenue Management** meets its responsibilities by ensuring the efficient, timely and accurate collection and disbursement of revenue from mineral leasing and production due to Indian tribes and allottees, States and the U.S. Treasury.

The MMS strives to fulfill its responsibilities through the general guiding principles of: (1) being responsive to the public's concerns and interests by maintaining a dialogue with all potentially affected parties and (2) carrying out its programs with an emphasis on working to enhance the quality of life for all Americans by lending MMS assistance and expertise to economic development and environmental protection.